Politecnico di Torino

Master's degree in Environmental Engineering
"Tutela Ambientale" curricula

July 2025 graduation session

Simulating the atmospheric dispersion of microplastics with a Lagrangian particle numerical model

Supervisor:
Eng. Marco Ravina
External supervisor:
Doctor Silvia Trini Castelli

Candidate:
Elena Brandi

A.Y. 2024/2025

Summary

Abstract

This thesis work aims to simulate and investigate the dispersion of microplastics (MPs) in the atmosphere with the application of a Lagrangian particle numerical model. In particular, this study examine the long-range transport of this emerging pollutant and, for this reason, the first chosen area of investigation is a remote region such as the Tibetan Plateau. Another goal of this work is to study areas characterised by different topographical features, and so the Pacific Ocean is chosen as a second region of investigation. In both cases, some reference articles that investigated these areas and found the presence of MPs in such places are studied and taken as starting points for this work. Several simulations were carried out in the backward mode in order to study the possible origin of the pollutant under consideration in the two mentioned zones. In the case of the Tibetan Plateau, it was possible to verify the atmospheric provenience of air masses both in the pre-monsoon period and monsoon period and to define in which case the long-range transport of pollutants was more likely to be the responsible factor for MPs presence, compared to the short-range transport. In the case of the Pacific Ocean, instead, it was noticed that, investigating the Oceanic area close to China and Japan, only the coastal zone was influenced by masses of air coming from the continent. In contrast, the areas of the ocean farther from the coast were found to be influenced by air masses coming from the east and so travelling over the Ocean. Considering another reference article that assumed the Ocean as a possible source of MPs emission to the atmosphere, backward and forward simulations were performed to investigate the circulation of air masses above the North Pacific Ocean and the possible transport of MPs inside them. Besides addressing the specific case studies, this study also provides the assessment, with related examples, of the potential of Lagrangian particle numerical models in application to the investigation of MPs transport in the atmosphere and regarding different topographical areas of the planet. This, even if the obtained results can be at present mostly qualitative because of the emerging nature of the topic of the MPs atmospheric transport, given that still little is known and few data are available up to now.

1. Introduction

The problem of plastic pollution is one of the most discussed environmental topics since nowadays the plastic waste is ubiquitous and is found in every environmental compartment, representing a risk both for human health and for the environment. Plastic was invented at the end of the nineteenth century, but it started to spread on a large scale in the second half of the twentieth century, and the quantities produced are still increasing year by year. In particular, suffice it to say that half of all the plastic produced was generated in the last fifteen years. Due to the fact that plastic is composed of synthetic chains, it is not biodegradable, and once it is released in the environment and not disposed of properly, it does not degrade naturally in it. On the contrary, it can be fragmented during its transport through the environment by natural agents such as sunlight, wind or sea waves, in smaller particles known as microplastics (MPs), where with this term particles of plastic with dimensions between 1 μm and 5 mm are indicated, and precisely for their small size the microplastics results as more impactful. While speaking about microplastics one must consider that in addition to the phenomena of fragmentation of plastic in smaller particles, MPs can be also generated by different processes such as the tyres abrasion, the release from synthetic fibres from textiles and the industrial emissions, and in general by human activities involving plastic materials that can release these small particles and which can end up in the environment. In general, the MPs are indicated as "primary microplastics" when produced already with the dimensions of a microplastic, for example, in cosmetics, toothpastes, and household products, while MPs that originate from the fragmentation of bigger plastic materials are known as "secondary microplastics". Also, it has to be pointed out that different kinds of MPs polymers and morphologies exist (see Appendix 1). Even the subject of MPs pollution is a current and well-known problem and a central theme in the environmental debate, and a lot of information and studies about microplastics in terrestrial, marine, and aquatic environments and about their impact on the ecosystems are present in the literature. On the contrary, less is known about their faith in the atmosphere, and only recently, the focus has also been placed on this environmental matrix, as a possible way of transport for MPs. This, both in terms of short and long-range transport, and so considering the atmospheric transport at a local scale, up to several hundreds of kilometres, and at a synoptic scale, from several hundred to thousands of kilometres. At present, the atmospheric transport of microplastics is an emerging topic and different studies about the presence of these pollutants in remote places like Arctic, Antarctica, Alps, Tibetan Plateau exist and prove the evidence of long-range transport, even if the information about the atmospheric transport of microplastics are still few and further investigations are undoubtedly necessary. The study of the presence and transport of MPs through the atmosphere is relevant for the global investigation of plastic pollution because it allows to consider the fact that MPs long-range atmospheric transport can carry these particles also to remote places affecting negatively areas that would be considered pristine, and because as recent studies have highlighted, these particles in the atmosphere may have an impact on the weather and the climate changes. In particular, for example, it has been demonstrated that MPs in snow or ice can reduce the albedo effect leading to a faster melting of them (Bergmann et al., 2022), that MPs in the atmosphere can act as nucleation seeds in clouds promoting the ice formation in cloud droplets (Seifried et al., 2024), and that their presence in the atmosphere may be related to climate changes for their role in trapping the infrared radiation coming from the Earth surface (Bergmann et al., 2022) and for their release of greenhouse gases during their degradation due to UV light.

2. Scientific background

2.1. Pollutant dispersion in the atmosphere

The Earth's atmosphere can be described by layers characterized by different features and thicknesses: troposphere, stratosphere, mesosphere, thermosphere, and exosphere. The troposphere is the part of the atmosphere extending from the Earth's surface up to about 10 km of altitude, the stratosphere is the layer between 10-50 km, the mesosphere is between 50 and 80-90 km, and the thermosphere extends up to 500 km. The exosphere is the outermost region of the atmosphere. It starts at an altitude of about 500 km and is extended to approximately 10000 km. In this layer, the molecules with sufficient energy that reach the so-called escape velocity of 11.2 km/s can evade from the Earth's gravitational attraction, scattering in space.

As the aim of this thesis concerns the investigation of the dispersion of microplastics, intended as a particular type of emerging pollutant in the atmosphere, the layer that is of our interest is the first one, since weather processes and pollutant transport characterise it. Specifically, the troposphere can be divided into the "Planetary Boundary Layer" (PBL) that corresponds to the lower part of the troposphere and is influenced by the presence of the Earth's surface, and in the "Free Atmosphere" (FA), that is the portion of the Earth's atmosphere above the planetary boundary layer. Between them, a transition zone is present and described afterwards.

The PBL is affected by turbulent processes that are mainly related to the Earth's surface friction and the thermal gradients in it. Also, these processes determine the PBL structure and can lead to the vertical and horizontal dispersion of pollutants and to their deposition on the soil. On the contrary, the FA is interested by a motion of the masses of air that can be approximated as mostly laminar. For this reason, pollutants in the FA are often associated with the long-range transport since the masses of air can travel undisturbed in it for long distances.

The dispersion of the traces in the PBL is due to wind transport (advection) and turbulent dispersion (mixing). Specifically, the turbulent dispersion can be related to vertical temperature gradients or wind velocity profiles. In the first case, the turbulence phenomenon is called "convective turbulence" and in the second one "mechanical turbulence".

In fluid dynamics, the main parameter used to describe a turbulent flow is the Reynolds number (R_e), which allows one to distinguish between a laminar and a turbulent flow. It consists of a dimensionless number that represents the relationship between inertial and viscous forces. It is defined as follows:

$$R_e = \frac{U*L}{\nu}.$$

In the expression, U is the flow speed, L is a characteristic length, and ν is the kinematic viscosity of the fluid. Typically, for values higher than 4000, the motion is considered turbulent, while for values lower than 2000-2500, it is considered laminar. The PBL is typically characterised by high values of the Reynolds number.

Some of the main features of the turbulence are:

- Irregularity: a turbulent phenomenon varies unevenly in space and time
- Diffusivity: mass, momentum, and heat transfer
- Three-dimensionality
- Dissipative: conversion of mechanical energy into internal energy due to viscous forces
- Continuous phenomenon: macroscopic phenomenon for which it is intended that it is not affected by the molecular structure of the matter.

The meteorological variables describing the PBL (as wind, turbulent sensible and latent heat flux, friction velocity, temperature) are characterized by turbulent fluctuations and are studied following

Reynolds' hypothesis. Reynolds' hypothesis states that a turbulent variable (u) can be determined as the sum of an average term ($\bar{u}$) and a term due to the turbulent fluctuation (u'), as follows:

$$u = \bar{u} + u'.$$

In this description, the average values are predictable and can be known with the use of specific laws, while the turbulent fluctuations are treated as stochastic phenomena.
The PBL daily development and thickness are variable and depend on many features such as the latitude, the season, and the time of day. The width of the PBL can reach a maximum of about 2-3 km, and it is usually higher over land than overseas. This is because its depth is strictly related to the thermal energy emitted by the Earth's surface that is transmitted to the above air as heat and to the complexity of the surface the PBL is in contact with. So, since the ground undergoes higher daily temperature changes than the sea surface, and since the sea surface is usually uniform, it results in a wider layer in the first case.
The characteristics and the width of the PBL evolve during the day, and this is important to know as they influence the dispersion of pollutants in it. Here is a brief description of the development of the different layers of the planetary boundary layer during the day and their main features:

- Convective layer (or Mixed layer): it develops between sunrise and sunset. After sunrise, the sun starts to warm the surface of the Earth and consequently the air above. This results in the formation of a convective and turbulent layer due to the upward movement of heated air particles and the downward movement of the cold one. This is the case in which the PBL has the greatest thickness. Because of these conditions of air mixing, the pollutants can be spread to large volumes and can easily reach the ground.

- Residual layer: it develops after sunset. In this period of the day, the vertical temperature gradient tends to annul, as well as the convective movements of the air and the related convective turbulence. Consequently, the only turbulence present is the mechanical one, which is related to the wind velocity profiles and is isotropic. The transport of pollutants is therefore determined by the average wind, and since the stable layer acts as a barrier between the residual layer and the surface of the Earth, long horizontal distances can be travelled, and the pollutants are able to reach the ground only when convective movement starts again the morning after.
- Stable layer: this layer develops during nighttime. It is in direct contact with the Earth's surface, which is cold, and this leads to a thermal inversion (i.e., the temperature of the air increases with altitude). No vertical movement of the air is present, and so eventual contaminants emitted in this layer do not diffuse in any direction. Contaminants emitted in the above residual layer can move downward but are not able to pass through the stable layer once they meet it.
- Surface layer: this expression is used to indicate the part of the PBL that is nearest to the Earth's surface, usually with a maximum height that corresponds to around 1/10 the PBL height, and that is affected by the turbulence caused by friction phenomena. It coexists with the layers just described above, and so, during the daytime the surface layer is characterized by the features of the convective layer and during nighttime by the ones of the stable layer.

The Figure 2.1 sums up the information about the daily development of the PBL just described.

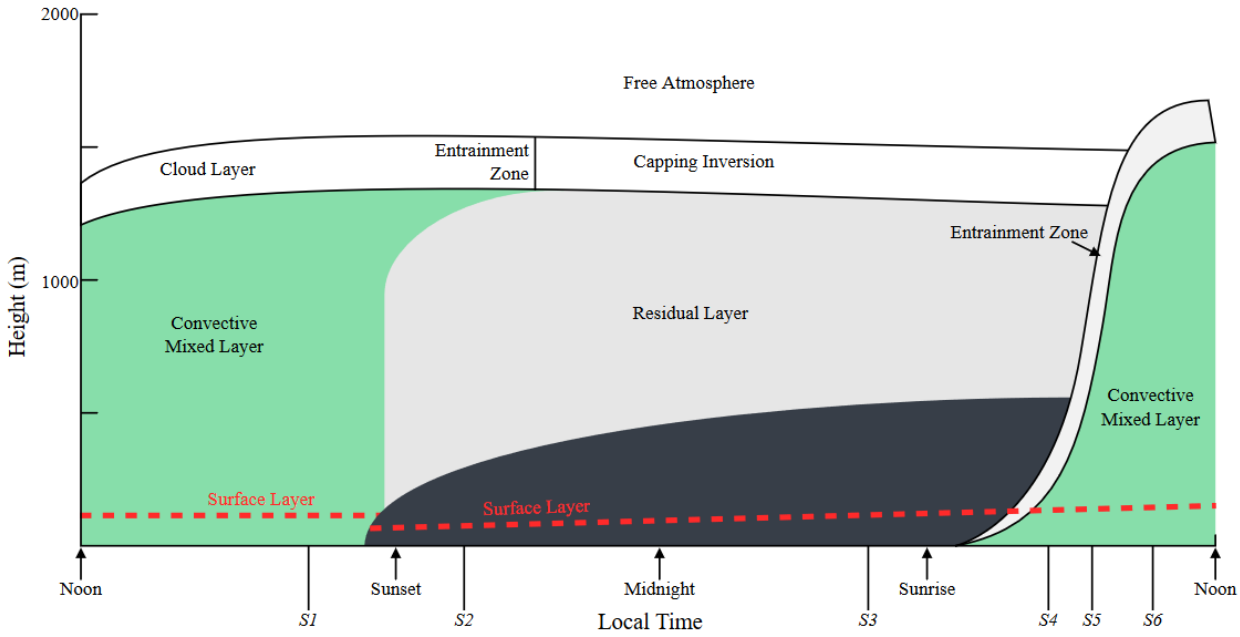

Figure 2.1 Development of planetary boundary layer during the day (Source: Planetary boundary layer - Wikipedia).

In Figure 2.1, in addition to the layers previously introduced, the entrainment zone and the capping inversion are reported. These two layers represent the transition zone between the PBL and the FA. In particular, the entrainment zone develops during daytime and because of the entrainment of the non-turbulent flow of the free atmosphere by the turbulent flow of the convective mixed layer. The capping inversion, instead, is a layer of temperature inversion that develops during nighttime and above the residual layer.

2.2. Lagrangian Particles Dispersion Models (LPDM)

The Lagrangian particle dispersion models are numerical models used for the study of the dispersion of pollutants in the atmosphere. Two types of approaches in dispersion modelling exist: the Eulerian and the Lagrangian ones. In Eulerian models, the reference system is fixed in space and stationary in time, while in Lagrangian models, the reference system moves solidly with the particles. This means that, in the first case, the values of a variable $\varphi(t)$ are calculated at a fixed point in space, whereas in the second case, the values assumed by the variable $\varphi(t; x, y, z)$ are calculated at the position of the particle at each time step. In terms of equations, for the Eulerian and Lagrangian case respectively, it results:

$$\frac{\partial \varphi}{\partial t} = u * \nabla \varphi = S,$$

$$\frac{d\varphi}{dt} = S,$$

where t is the time, S represents the source term and u is the velocity. In the first equation, the term $\frac{\partial \varphi}{\partial t}$ represents the variation of the generic variable with time and at a specific position, and $u * \nabla \varphi$ is a non-linear advection term where ∇ represents the spatial gradient at the same position. In the second equation, $\frac{d\varphi}{dt}$ represents the variation of the generic variable following the particles of air. As regards numerical modelling it means that in the Eulerian case the equation is solved at each point of a 3D grid, while in the Lagrangian case, being the model "grid-free" for definition, the trajectory of a parcel

is solved in a 3D domain through the interpolation of the meteorological variables at each position assumed by the particle.

In the case of this work, the particle is an air parcel that contains a tracer, and following Trini Castelli (2021), it is defined as a portion of the atmosphere that is:

- Large enough to contain several molecules and to have well defined physical properties (temperature, density, humidity, pollutant concentration)
- Small enough to be considered infinitesimal, a «unit».

In other words, following Anfossi and Physick (2004), these fictitious particles are small enough to be affected by the motion of the smallest eddies of turbulence and big enough to contain a significant number of molecules of pollutants.
The Lagrangian particle dispersion models are the most advanced among the Lagrangian models, but other types exist such as the mean trajectory models, the box models, and the puff models.
The mean trajectory models are the simplest among those mentioned. These kinds of models calculate the trajectory of the particle of air only considering the mean velocity $\bar{u}$ and neglecting the turbulent contribution u'. A description of the atmosphere based on these simplified assumptions would be representative in a case of laminar flow or low turbulence, as it happens in the stratosphere. On the contrary, the PBL is strongly characterised by the turbulent motion, so the mean trajectories are not suitable for its description (Lin, 2012). In the box model computation, the particles of air are considered grouped and represented by a box of varying size depending on the degree of mixing. The motion of the boxes can be described by single or multiple mean wind trajectories, and this last one allow to better represent the effects of the dispersion. Anyway, being this type of model still based on mean wind trajectories, its simulations do not account for wind shear, and so they give a representation that is too simplified of the atmospheric boundary layer. The Lagrangian Puff models describe a cloud of pollutant by representing the air parcels as puffs of growing size. The transport is determined by the mean wind, while the diffusion is given based on a Gaussian distribution. These kinds of models can be applied in situations when the mean wind and turbulence are relatively constant, but otherwise, they are not very accurate. At last, in the Particles models, the ones used for this thesis work and the most diffused type nowadays, every particle of air has the same defined mass, and its motion, described as a Markov process, is calculated by considering both the mean wind and the diffusion component. In this case, the turbulent effects are represented. In Figure 2.2, a representation of the different models taken by Lin (2012) is reported.

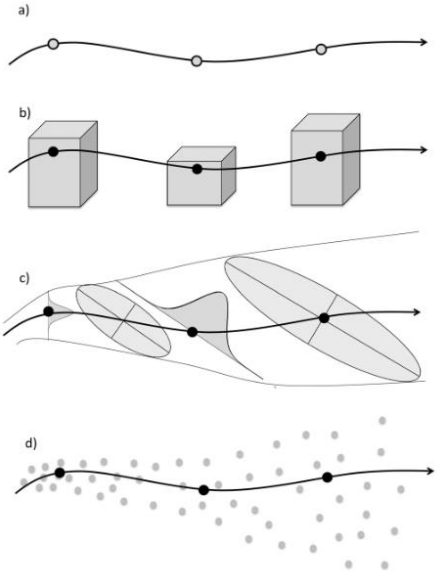

Figure 2.2 Image from Lin (2012) representing the scheme of the four Lagrangian models: a) mean trajectories, b) box models, c) Gaussian puff, d) Lagrangian particle dispersion models.

From a historical point of view, the Lagrangian particle models rely on the generalised Langevin equation for particles velocity that results from the study of Brownian motion. As described in the work of Anfossi and Physick (2004), in 1905, Einstein published a paper about the Brownian motion, where the concept of stochastic modelling of natural phenomena was introduced for the first time. In 1908, Langevin proposed a new way to interpret the Brownian motion, suggesting that each particle is subjected to a deterministic force and a stochastic force. The first one is related to the viscous drag, while the second one considers the random impacts with other particles found in the fluid where the particles are moving. The original Langevin equation is reported here:

$$\frac{dv}{dt} = -\beta * v + \lambda * \mu(t),$$

where v is the velocity, t is the time, μ is a random function, and β and λ are two constants. In the case of atmospheric turbulent dispersion, the first term of the equation represents the friction force exerted by the flow on the particle (the deterministic term), and the second term represents the accelerations caused by pressure fluctuations (the stochastic term). Over the years, many scientists have made significant contributions to the development of this topic. Of particular relevance, is here cited the work of the mathematician Obukhov, who in 1959 first proposed the description of the evolution of the motion of an air parcel in the atmosphere as a Markov process. A central problem of this topic was the fact that the proposed equations (for example the one proposed by Smith, 1968) were not able to take into account the non-homogeneous turbulence, which, considering the atmospheric matrix, is fundamental given that the vertical turbulence conditions in the PBL are never homogeneous. Up to now, the final formulation is due to Thomson (1987). He demonstrated that the physical consistency in Lagrangian dispersion models can be ensured using the “well-mixed condition", for which particles initially uniformly distributed in space must remain so and should exhibit the same velocity distribution as the fluid, and developed an advanced formulation of the Langevin equation, allowing for the representation of non-Gaussian and inhomogeneous turbulence without requiring ad hoc corrections.

The Lagrangian particle models are widely used for the study of pollutants dispersion in the atmosphere since they allow to obtain a realistic description of atmospheric flows and diffusion processes, considering the air masses moving as Lagrangian parcels. Specifically, by comparing the Lagrangian models with the Eulerian ones, some advantages and disadvantages can be pointed out. Referring to Lin (2012) and Trini Castelli (2021), the main advantages are:

- Availability of trajectory information: information about particles trajectories can be obtained with Lagrangian simulations but not with Eulerian simulations.
- Physical realism: the air parcels are simulated more realistically with the Lagrangian simulations since the atmosphere can be considered as Lagrangian for the fact that air is made up of molecules and atmospheric flows consist of the motion of these molecules.
- Capability of describing non-diffusive near-field to sources: Lagrangian models can describe the non-diffusive near-field to sources.
- Numerical stability: the Eulerian equation has a nonlinear advection term $u * \nabla\varphi$ that is not contained in the Lagrangian equation, making the latter one numerically stable and allowing to obtain more accurate results.
- Resolving subgrid scale variability: the results of Eulerian simulations are tied to a grid, while this does not happen for the Lagrangian ones. So, in this second case, the air particles bring with them some subgrid-scale information and resolve a finer-scale heterogeneity that would not be solved with a Eulerian approach.

On the contrary, some disadvantages are:

- Computational cost: in general, Lagrangian models are cheaper to run than the Eulerian ones, but it is also true that in cases of simulations with a particularly high number of particles or small time steps, the computational cost could be significant.
- Irregularity of “grids”: being the Lagrangian parcels positions “grid-free”, additional procedures will be required for their count and concentration/deposition field representation.
- Inconsistencies with Eulerian driving meteorological fields: in many cases the Lagrangian models use Eulerian output to simulate the atmospheric dynamics, and this could lead to some inconsistencies between the two models.
- Troubles on the resolution of the chemistry: the description of the interaction between particles is difficult since the distance between air parcels changes continuously. Also, in general, LPDM cannot solve chemical reactions of the second order.

3. Articles review and case studies selection

3.1. Research papers

The first part of this thesis work consisted of the study of scientific articles to frame the state of the art regarding the atmospheric transport of microplastics and their presence in remote places on Earth. Articles about different remote areas were selected to study various scenarios, and in order to have a global idea about the studies conducted up to now about this topic. The aim is to investigate the role of atmospheric long-range transport of MPs in remote places where no local sources are detectable or significant.
All the articles reported below, except for the last one introduced hereinafter, present similar procedures to analyse this subject. In all these cases, a remote place is considered, and some samplings are done to verify the presence of MPs. Then, possible particles found in the samples are studied and classified based on the polymer type, the morphology and the abundance. In most cases, some backward simulations are performed with the HYSPLIT model (see Section 3.3) to investigate the possible provenience of the microplastics found.
This is of particular interest to make a comparison with the MILORD model, here used to perform simulations in the same areas investigated in the selected articles. This enables to evaluate whether MILORD simulations are consistent with those obtained by the authors of the articles, assessing the accuracy of its output as first step, then applying it to investigate the long-range MP transport in all cases. Here is the list and a brief description of the articles studied.

- Bergmann, M., Mützel, S., Primpke, S., Tekman, M. B., Trachsel, J., Gerdts, G., (2019). *White and wonderful? Microplastics prevail in snow from the Alps to the Arctic*. Sci. Adv. 5, eaax1157. https://doi.org/10.1126/sciadv.aax1157

About the study: the study investigates the presence of MPs in the Arctic, and to do this snow samples are collected from ice floes in the Fram Strait and in Svalbard and then analysed. To evaluate the MP pollution degree of the area, a comparison is made between the values of MP concentration found in the Arctic zone and the values obtained from the analysis of snow samples collected in the Swiss Alps and in European sites, in order to represent both remote and populated regions.
Model: no model simulations are done.
Results: the obtained values of MP concentration in the ice floes in the Fram Strait and in Svalbard are considered significant, even if those concentrations are lower than the ones found in European sites. Consequently, the snow of the Arctic is considered contaminated by MP presence. In particular, the authors of this article underline the role of the scavenging process through which the snow passing through the atmosphere binds the MP particles and they estimate the annual MP deposition in the Fram Strait and in Svalbard, starting from annual snowfall data.

- Liu, K., Wu, T., Wang, X., Song, Z., Zong, C., Wei, N., Li, D., (2019). *Consistent transport of terrestrial microplastics to the ocean through atmosphere*, Environ. Sci. Technol., 53, 10612–10619. https://doi.org/10.1021/acs.est.9b03427

About the study: in this article, the role of pollutant terrestrial transport to the ocean is studied. In this case, a sampling cruise is done in order to collect samples of air concentration in three areas of the Pacific Ocean that represent the nearshore zone, the pelagic zone, and the remote zone. These areas include the East coast of China and the area of the North Pacif Ocean between Japan and the Philippines (see Figure 3.2).
Model: in the article, three backward simulations of the duration of 48 h are done with the HYSPLIT model. Each one is performed with a starting point chosen to represent one of the three zones of investigation.

Results: the presence of MPs in the air over the ocean and its spatial distribution are obtained in this study. Also, the difference between the values of MP abundance relative to daytime and nighttime suggests, following the idea of the authors, that the relative humidity could play a role in the deposition of MP particles, which is supposed to be higher at night, and would explain the lower values of MP concentration in air detected during the night.

- Zhang, Y., Gao, T., Kang, S., Allen, S., Luo, X., Allen, D., (2021). *Microplastics in glaciers of the Tibetan Plateau: Evidence for the long-range transport of microplastics*. Science of The Total Environment 758, 143634. https://doi.org/10.1016/j.scitotenv.2020.143634.

About the study: the aim of the study is to evaluate the presence of MPs in the Tibetan Plateau and demonstrate the role of the atmospheric long-range transport of these pollutants. For this purpose, snow samples are collected from two glaciers on the Tibetan plateau and studied. The two glaciers of the study are the Laohugou glacier and the Qiangyong glacier. The first is in the northern part of the Tibetan Plateau, while the second is in the southern part.
Model: backward simulations starting from the sampling points on the two glaciers are performed with the HYSPLIT model.
Results: the backward simulations show that the provenience of microplastics depends on the season and help to identify the possible source areas. The evidence of long-range transport to remote areas where local sources could hardly be responsible for contamination is here proved. Also, another phenomenon that is considered in the article is the fact that in the summer the Tibetan Plateau is affected by the presence of the South Asian monsoon, and this involves more precipitation and consequently the so-called "plastic rains" which may bring bigger quantities of MPs on the studied glaciers.

- Aves, A. R., Revell, L. E., Gaw, S., Ruffell, H., Schuddeboom, A., Wotherspoon, N. E., LaRue, M., and McDonald, A. J., (2022). *First evidence of microplastics in Antarctic snow*, The Cryosphere, 16, 2127–2145. https://doi.org/10.5194/tc-16-2127-2022.

About the study: the aim of the study is to estimate the presence of airborne MPs in Antarctica. The area of the sampling is the Ross Island region, and 19 samples are collected both close and far from the two base sites situated there. To be sure of studying the microplastics transported by the atmosphere, the samples were collected during or shortly after a snowfall event.
Model: backward simulations are performed with the HYSPLIT model and from the starting points corresponding to each sampling site.
Results: with this article, the presence of MPs in Antarctica is confirmed and both possible local and far sources are identified. Local sources are represented by the presence of the two research stations and by open-water regions such as Ross Sea polynya and McMurdo Sound polynya. The long-range transport can be represented by ocean currents, sea spray, and atmospheric transport. As regards the atmospheric transport, the trajectories obtained with the application of the HYSPLIT model show, for most of the samples, the influence of a Ross air stream event. For these cases, it is found that microplastics may come from the Amundsen or Ross seas. A different result is obtained in one site (site 19) where the trajectories calculated show a different path coming from the Weddell Sea.

- Wang, Z., Kang, S., Zhang, Y., Luo, X., Kang, Q., Chen, P., Guo, J., Hu, Z., Yang, Z., Zheng, H., Gao, T., Yang, W., (2024). *Microplastics in glaciers of Tibetan Plateau: Characteristics and potential sources*. Science of The Total Environment 954, 176370. https://doi.org/10.1016/j.scitotenv.2024.176370

About the study: this study investigates the presence and provenience of MPs in the Tibetan Plateau area. To do this, samples of snow are collected from six different glaciers on the Tibetan Plateau and

analysed. To represent the atmospheric transport of the region, the periods of investigation are divided into monsoon and pre-monsoon, and for the areas that are not affected by the monsoon, the atmospheric transport is described through the spring and summer seasons.
Model: backward simulations are performed with the HYSPLIT model and starting from the sampling point of each glacier.
Results: the presence of MPs in the Tibetan Plateau area is confirmed, and potential short-range and long-range sources are identified with the use of the HYSPLIT model. The seasonal atmospheric transport is investigated, and the differences in the results due to the different positions of the glaciers in the Tibetan Plateau and to their proximity or not to populated areas are described.

- Shaw, D. B., Li, Q., Nunes, J. K., Deike, L. (2023). *Ocean emission of microplastic*. PNAS Nexus, 2 (10). https://doi.org/10.1093/pnasnexus/pgad296

In addition to the articles just mentioned, one more study (Shaw et al. 2023) is considered. This study is about the MP presence in the Ocean and their possible transfer to the atmosphere through the phenomenon of bubble bursting (Deike et al. 2022). Unlike what is done in the previous mentioned articles, in this work no direct measures are done. On the contrary, measures previously done about MP mass concentration in the Ocean (Kaandorp et al. 2023) are elaborated to obtain an estimation of possible values of annual mass concentration of MPs emitted by the Ocean itself. In this case, this paper is kept in account because, considering the Ocean as a possible source of MPs for the atmosphere, we can identify the areas with higher microplastic emissions and use them to perform a forward analysis. In this case, our work aim is to perform a forward simulation with the MILORD model to study the possible fate of MPs coming from the ocean.

3.2. Case studies selection

From the list of the studied articles done in the previous paragraph, three papers are chosen for the work of this thesis. The first article chosen is the one by Wang et al. (2024) about the Tibetan Plateau (TP) area. It is chosen to consider an orographic complex area, and among the two articles studied about the TP it is evaluated as the most complete since it considers more glaciers than the article of Zhang et al. (2021). The second chosen paper is the paper of Liu et al. (2019), about the Pacific Ocean. In this case, the aim is to investigate a different geographical and topographical area since here the area of interest is over the sea. The last chosen article is the article of Shaw et al. (2023). In this case, the choice is made to perform a different kind of modelling analysis, moving from the backward mode of the two earlier cases to the forward mode, since in this work a possible source area of MPs is identified. In particular, from the study of the research papers, it has been noticed that the articles of Liu et al. (2019) and Shaw et al. (2023) could be linked, since they concern two close areas of the North Pacific Ocean, where the first one is intended as a receptor, and the second one as a source of MPs in the Ocean.
For eventual future work, considering other different case studies would give additional information about further geographical areas.

Tibetan Plateau

Three glaciers of the Tibetan Plateau area are considered (Figure 3.1): the Dongkemadi glacier (DKMD), the Anglong glacier (AL), and the Kuoqiongangri glacier (KQGR).
The Dongkemadi glacier is in the central part of the TP, in particular in the Tanggula Mountain region. It is quite isolated with no big cities close to it, and just the National Highway 109 (G109) 10 km away from it. The AL Glacier is situated in the Western part of the Tibetan Plateau, and it belongs to the Ngari Prefecture. Even the AL glacier is quite isolated but, precisely for its western position, the influence of overpopulated cities of neighbouring India cannot be excluded *a priori* as a possible

source of microplastics. At last, the Kuoqiongangri glacier belongs to the Southern part of the TP and in this case, during the analysis it must be taken into account that it is close to the city of Lhasa, which is about a hundred kilometres eastward from the glacier.
These simulations aim to perform some tests for the case of the DKMD glacier in May 2022, and to investigate the atmospheric transport over the pre-monsoon and monsoon periods, here represented respectively with April and June, for all three glaciers in the TP area. The choice of investigating these two periods of the year is because, as mentioned in the reference article of this case study, it has been demonstrated in a previous study (Chen et al., 2020) that the pre-monsoon period results to be the most relevant period of the year as regard the pollutants atmospheric transport. The years in which the simulations are performed are chosen starting from the simulations done in the article, in order to investigate the same month and the same year and make a further comparison between our results and the results obtained in the article. This, considering that few details are given in the reference article about the setup of their HYSPLIT simulations, and therefore that a rigorous and thorough comparison with MILORD simulations cannot be pursued. The coordinates of the chosen glaciers correspond to the ones provided in the reference article and all the simulations about the area of the Tibetan plateau are performed in backward mode.

The main data of the chosen sites for the simulations in this area are reported in Table 1.

Table 1. Main data about the chosen sites for the backward simulations on the Tibetan Plateau area.

Reference	**Simulation domain**	**Sites**	**Receptor**	**Sampling date**	**Duration of the simulation of the article**	**Duration of the simulation of this work**	**Simulation period**
Wang et al. 2024	15 - 45°N, 60 - 120°E	Tibet, DKMD: Dongkemadi glacier	33.099°N, 92.04°E, 5550 m a.s.l.	20 May 2022	Monthly	1 month	May 2022 – April 2022 and June 2021
		Tibet, KQGR: Kuoqiongangri glacier	29.859°N, 90.191°E, 5781 m a.s.l.	17 May 2022	Monthly	1 month	April 2022 and June 2021
		Tibet, AL: Anglong glacier	32.84°N, 80.921°E, 5950 m a.s.l.	14 May 2022	Monthly	1 month	April 2022 and June 2021

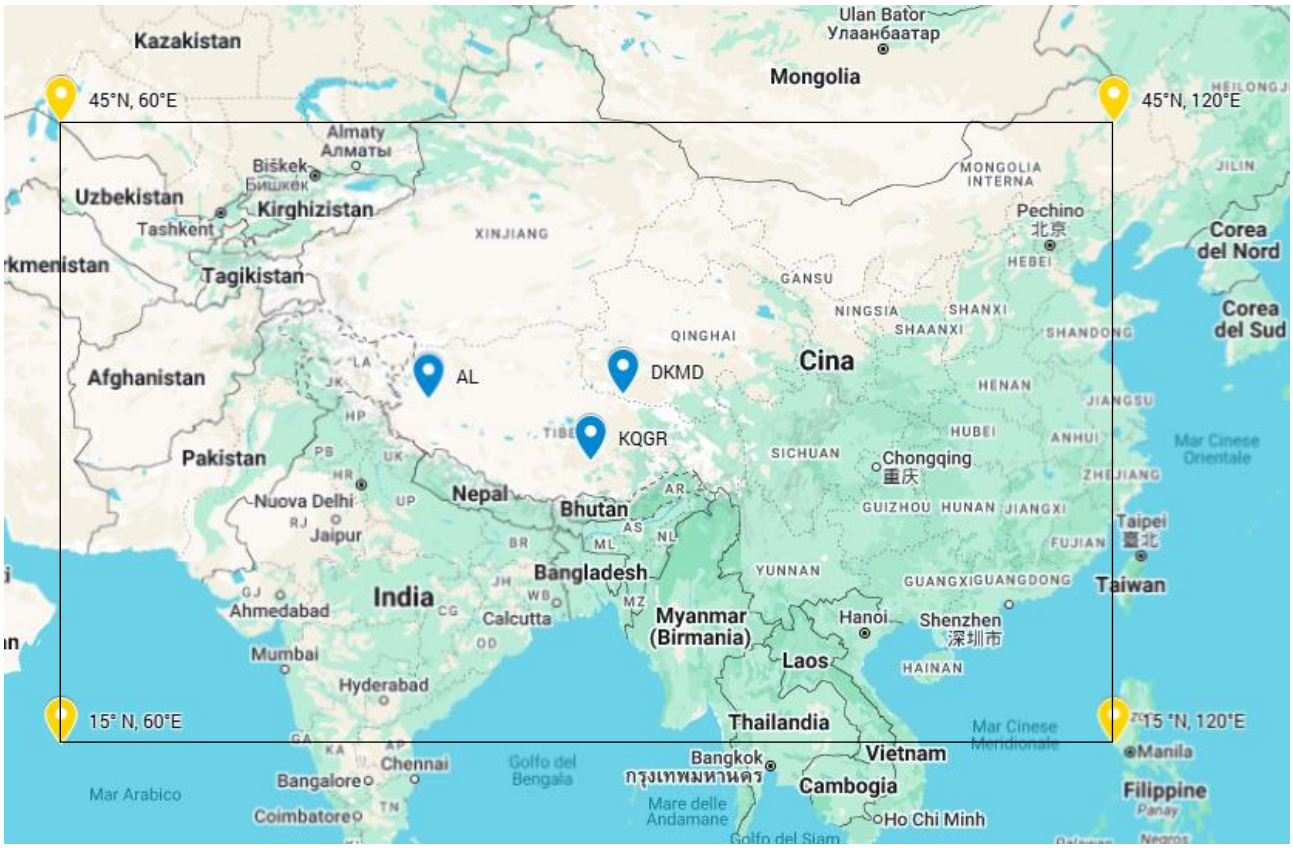

Figure 3.1 The image reports the geographical domain for the backward simulations on the TP delimited by the yellow markers, and the positions of the three glaciers chosen represented by the blue markers (Source: Google – My Maps).

Pacific Ocean

In this case, three locations of the North Pacific Ocean are chosen to represent the nearshore, the pelagic and the remote zone of it. These points are taken considering the path followed by the sampling cruise done during the experimental campaign relative to the reference article. Specifically, a continuous sampling is made, and in the additional material each sampling stop and its duration are provided. For this study, one point for each area of investigation is chosen (Figure 3.2), taking the coordinates from the list of the samplings done, while the starting points for the backward analysis performed by the authors are chosen to represent the three areas (nearshore, pelagic, remote), but they do not belong to the path followed by the cruise. In the case of this work, it results that the point representing the pelagic zone is about 1200 km from the one representing the nearshore zone, and that the point representing the pelagic zone is about 1700 km far from the one representing the pelagic zone. Also, the backward analyses performed in the reference paper have a duration of two days. Here, the choice is to perform the simulation for 2 days, one week and one month to investigate the provenience of the particles of MPs found in the chosen sampling points and also to have an idea of the atmospheric flow of that area with a larger temporal scale. All the simulations are performed in backward mode, and the altitude of the receptor is chosen to represent the quota of the sea, intended as level of pressure and approximated to 1013 hPa (corresponding to about 2 m height a.s.l.). The simulations are performed from the last day of sampling in backward mode for the three durations indicated in the table.

The main data of the chosen sites for the simulations in this area are reported in Table 2.

Table 2. Main data about the chosen sites for the backward simulations on the North Pacific Ocean area.

Reference	Simulation domain	Sites	Receptor	Sampling date	Duration of the simulation of the article	Duration of the simulation of this work	Simulation period
Liu et al. 2019	0 - 45°N, 110 - 165°E	Ocean - nearshore zone	28.2405°N, 121.999°E, ~ 2 m a.s.l.	27-28 Nov 2018	48 h	2 days,1 week, 1 month	November 2018
		Ocean - pelagic zone	22.3078°N, 130.828°E, ~ 2 m a.s.l.	4-5 Dec 2018	48 h	2 days, 1 week, 1 month	December/ November 2018
		Ocean - remote zone	11.328°N, 142.201°E, ~ 2 m a.s.l.	13-14 Dec 2018	48 h	2 days, 1 week, 1 month	December/ November 2018

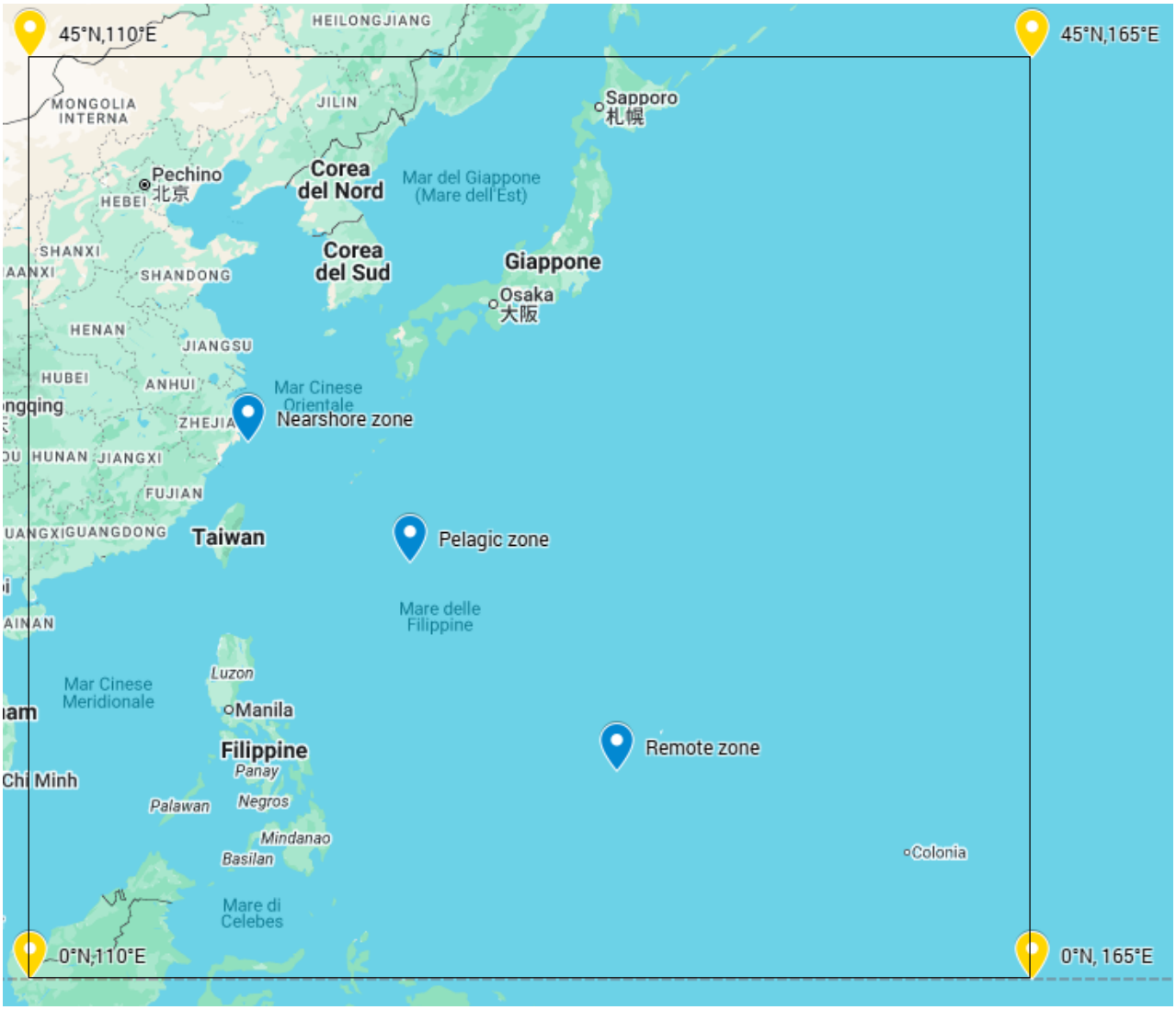

Figure 3.2 The image reports the geographical domain for the backward simulations on the North Pacific Ocean delimited by the yellow markers, and the positions of the points representing the three area of investigation represented by the blue markers (Source: Google – My Maps).

Pacific Ocean (forward modelling)

This article (Shaw et al. 2023) aims to estimate the possible MP emissions from the Ocean to the atmosphere above, and from its results, two areas of the Pacific Ocean are identified as characterised by particularly high emissions. Between the two areas, the one in the North Pacific Ocean is chosen for this study and to perform the forward analysis (Figure 3.3). This area is represented by the coordinates reported in Table 3, and it is noticed that it is found in the surrounding area identified as the "Pacific Trash Vortex", a floating waste accumulation region, in particular of plastic waste, located indicatively between 35º-42º N and 135º-155º W[1]. The altitude of the source is chosen to represent the quota of the sea intended as level of pressure and approximated to 1013 hPa.

Table 3. Main data about the chosen site for the forward simulations on the North Pacific Ocean area.

Reference	**Simulation domain**	**Site**	**Source**	**Duration of the simulation of this work**	**Simulation mode**
Shaw et al. 2023	0 - 56°N, 103 - 240°E	Pacific Ocean	30°N, 220°E (= 140°W), ~ 2 m a.s.l.	From the 2^{th} of November to the 14^{th} of December	Forward

During the investigation and during the performance of the simulations for the case study of Liu et al. (2019), it has been noticed that there could be a possible link between the remote zone of the Pacific Ocean indicated in that article, and the area of MPs emission estimated by Shaw et al. (2023). For better investigating this possible relation, the duration of the simulation is made to last around one month and a half, so to investigate a period of time considered sufficient for the air masses to travel from the point indicated as source (Table 3) to the point indicated as receptor (Table 4). Also, the backward simulation as regards the point representing the remote zone of the article of Liu et al. (2019), is here repeated extending the simulation domain to the one used in this paragraph (Table 3 and Table 4), and for the same duration of simulation of the forward case. This is done to compare the results of the forward and backward analyses done for the same duration and in the same spatial domain.

Table 4. Main data about the site representing the remote zone of Pacific Ocean taken from the article of Liu et al. (2019) here used to perform again the backward simulation but in the spatial domain and for the duration of the forward simulation described in Table 3 for Shaw at al. (2023).

Reference	**Simulation domain**	**Site**	**Receptor**	**Duration of the simulation of this work**	**Simulation mode**
Liu et al. 2019	0 - 56°N, 103 - 240°E	Ocean - remote zone	11.328°N, 142.201°E, ~ 2 m a.s.l.	From the 14^{th} of December to the 2^{nd} of November	Backward

The dates of the two simulations of this paragraph are chosen considering the sampling dates relative to the point chosen to represent the remote area of the Ocean from the article of Liu et al. (2019) (see Figure 3.4).

[1] Pacific Trash Vortex - Wikipedia

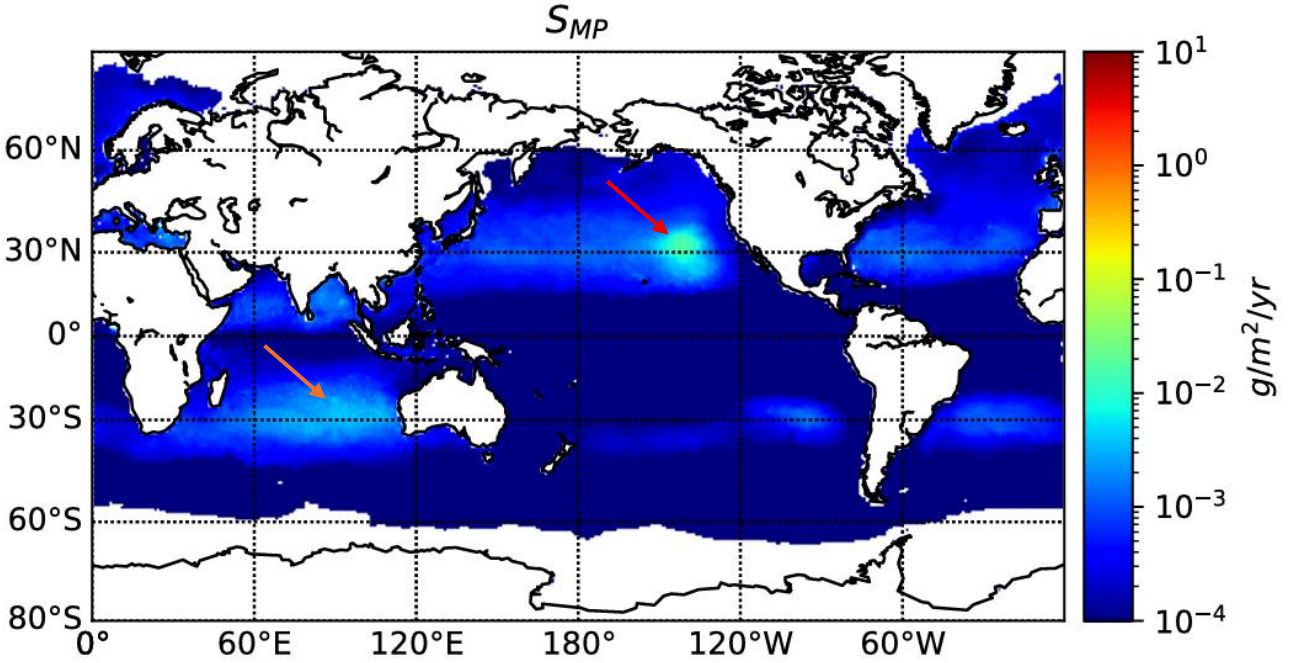

Figure 3.3 The orange and red arrows indicate the two areas of the Pacific Ocean identified as characterised by particularly high emissions, and the red arrow represents the one chosen for our work. The legend of the image reports the concentration of MP emitted by the ocean expressed as $g/m^2/yr$ (Source: Shaw et al. 2023).

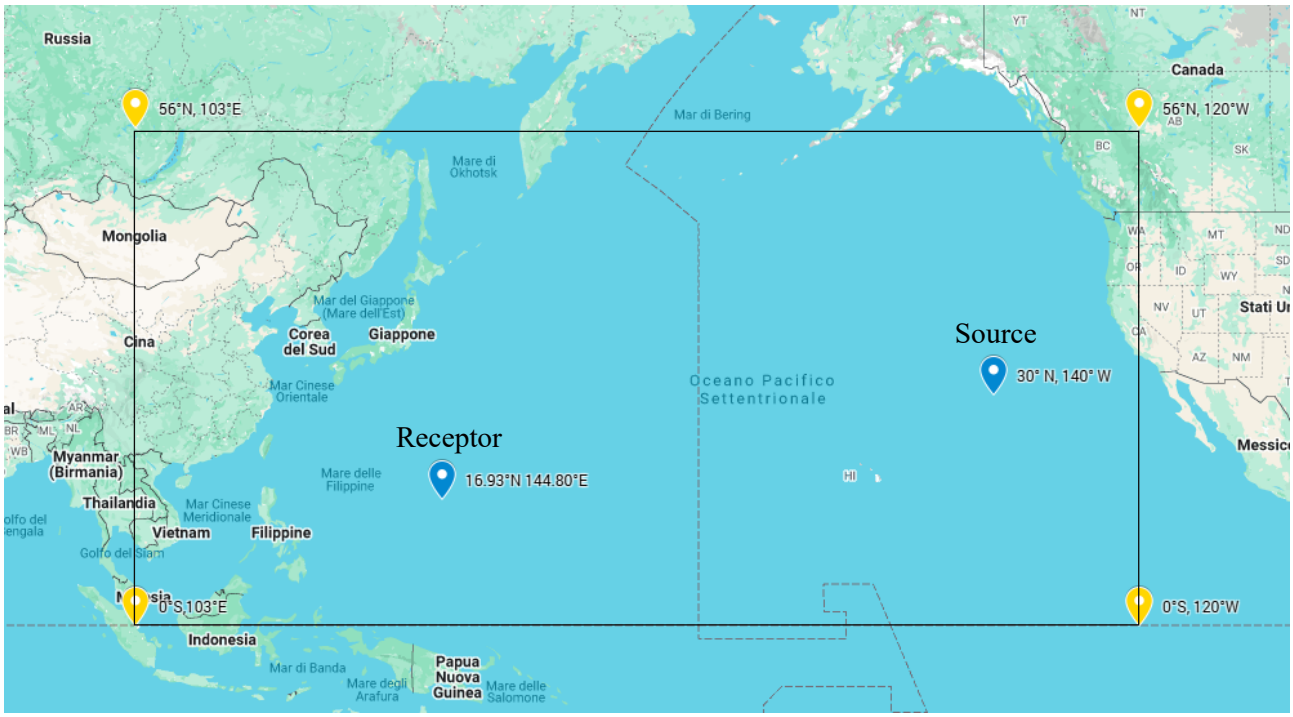

Figure 3.4 The image reports the geographical domain for the forward and backward simulations on the North Pacific Ocean delimited by the yellow markers, and the positions of the source and receptor points represented by the blue markers (Source: Google – My Maps).

3.3. Modelling

In the articles mentioned in paragraph 3.2 in which backward trajectory simulations are performed, the model used is the HYSPLIT model (Stein et al., 2015). For this reason, the model is briefly introduced here. The model's name was initially meant as an acronym standing for Hybrid Single-Particle Lagrangian Integrated Trajectory, and suggesting his hybrid computational approach. The

model calculation method is a hybrid between the Lagrangian methodology, which considers a reference system that moves following the single particle, and the Eulerian one, which instead considers a fixed 3D grid as a reference system. The first approach is used for the advection and diffusion calculations, while the second one is used to compute pollutant air concentrations. It was developed by the National Oceanic and Atmospheric Administration (NOAA) and Air Resources Laboratory and the Australian Bureau of Meteorology Research Center, to simulate the transport in the atmosphere of air parcels, and to represent the dispersion of contaminants and hazardous materials, their chemical transformation and deposition. Through the years the model has been applied to different case studies and to investigate the atmospheric transport of different substances such as radioactive materials, wildfire smoke, dust, and volcanic ashes. In the case studies considered in this work, it has been used to investigate the atmospheric transport of MPs. This is done by performing backward analyses to investigate possible source-receptor relationships, as one of the most common applications of the model. The first version of the model was developed in the early 1980s (HYSPLIT1). With HYSPLIT1, segmented pollutant puffs were released close to the surface and their trajectories were followed for several days. The calculation of the transport was based on rawinsonde data of wind taken twice daily, without interpolation. HYSPLIT2 version, developed in 1988, worked with interpolated rawinsonde or any other measured data for the estimation of vertical mixing coefficients, but only with HYSPLIT3 gridded output from meteorological models started to be used. In HYSPLIT3, the calculation of trajectories, transport, and dispersion of pollutants was made with cylindrical puffs that grow and split when reaching the size of the meteorological data grid. This third version of the model also represented the first attempt to include chemistry in the modelling system. In 1998, the fourth version of the HYSPLIT model was developed (Draxler and Hess, 1998), representing the basis for the current model version. It allows to represent the air masses with different Lagrangian representations (trajectories, puff and 3D particles) and it can use multiple meteorological grids, with fine or coarse resolution, and calculate the dispersion of pollutants starting from data of vertical diffusivity profile, wind shear, and horizontal deformation of the wind field. To date, the HYSPLIT model can be run interactively on the READY website or installed on a PC or LINUX workstation and continues to be one of the Lagrangian models most used by the science community for the study of the atmospheric transport and diffusion.

4. Simulations

4.1. MILORD model

The numerical model used to perform the simulations reported in this thesis work is the MILORD model (Model for the Investigation of LOng Range Dispersion). The MILORD model is a Lagrangian particle dispersion model (LPDM) and was created in 1992-1993 at the Istituto di Cosmogeofisica to simulate the long-range transport and the dispersion of particles in the atmosphere related to accidental releases (Anfossi et al., 1995). It was validated on the case study concerning the release of Cs-137 as a consequence of the Chernobyl accident, based on the relative recorded data over Europe by the ATMES project, and also on the case study of the ETEX I field experiment. The model is under continuous application and development at the Institute of Atmospheric Sciences and Climate (CNR-ISAC). In 2017, an article regarding the use of the MILORD model for the investigation of the release of Cs-137 from Fukushima Daichi nuclear plant caused by the earthquake and the subsequent tsunami in March 2011 was published (Boetti et al., 2017), to evaluate and improve the model. In 2019, the model was applied for the first time in the backward mode to study the possible provenience of peaks of CO_2 concentration observed at Plateau Rosa in the Italian Alps, by a station for the measurement of greenhouse gases (Ferrarese and Trini Castelli, 2019). More recently, it has also started to be applied to the study of atmospheric MP transport. Several zones have been investigated, such as the French Pyrenees (Martina and Trini Castelli, 2023), Madrid city (Musso, 2025), and Canada (Musso, 2025; Ziero, 2025). With the present work, the aim is to continue the study of the MP atmospheric transport with the MILORD model, investigating even more remote zones of the Earth, such as the Tibetan Plateau and the North Pacific Ocean, thus highlighting its long-range contribution.

As a Lagrangian model, the dispersion of the pollutants is simulated through the description of trajectories of fictitious particles that represent a finite mass that contains a certain concentration of the contaminant, in a three-dimensional wind field (Trini Castelli, 2012). The reference system is not fixed and follows the movement of these particles. Also, these particles are intended to be both small enough to follow the motion of the smallest turbulence eddies present in the atmosphere and big enough to contain several molecules sufficient to allow neglecting the effect of the single one (Anfossi and Trini Castelli, 2009). So, the diffusion in the atmosphere of the contaminant in exam and its possible deposition on the soil is studied by reconstructing the trajectories followed by these Lagrangian particles, with the possibility of obtaining them both in the forward and backward mode. Hereinafter, the main features reported about the MILORD model and useful for the comprehension of the work done in this document are taken from the articles of Anfossi et al. (1995) and Trini Castelli (2012).

Particles position computation

The transport of the particles in air is intended as the result of two components of dispersion: advective transport (horizontal and vertical motions) and turbulent diffusion (stochastic displacement).

The advective term is computed following an algorithm suggested by Reap (1972), while the stochastic component is described starting from the generalised Langevin equation for the horizontal and over PBL vertical displacements. The vertical displacements inside the PBL are instead evaluated by a uniform distribution, considering a full mixed layer.

The model can describe the behavior of a tracer or a pollutant in the atmosphere considering the following variables: dry and wet deposition, radioactive decay, and chemical transformations.

It works starting with topographical and meteorological data (topography, 3-D wind, and precipitation) and calculates the PBL height or takes a fixed value of it depending on how the calculation process is set up.

The model calculates the position of the particles at each time step and follows the iterative process reported here:

$$x_i(t+\Delta t) = x_i(t) + \bar{u}_i(t)\Delta t + u_i'(t)\Delta t,$$

$$x_{2i}(t+\Delta t) = x_{1i}(t) + \bar{u}_{1i}(t)\Delta t,$$

$$x_{3i}(t+\Delta t) = x_{1i}(t) + 0.5[\bar{u}_{1i}(t) + \bar{u}_{2i}(t)]\Delta t\ .$$

In the previous equations $x_i(t)$ is the *i-th* (*i*=1,2,3) component of particle position, $\bar{u}_i(t)$ is the transport due to the mean wind and $u_i'(t)$ refers to the atmospheric turbulence contribution. The term $x_{2i}(t+\Delta t)$ represents the first guess of the position at $t+\Delta t$ that is obtained by entering in the first equation the positions and the wind velocity at the time *t* as $x_{1i}(t)$ and $\bar{u}_{1i}(t)$ respectively. Then, the term $x_{3i}(t+\Delta t)$ refers to a third iteration. This is done up to the calculated position converges within the prescribed limit. The term $u_i'(t)$ represents the turbulent motion and is computed differently if regarding the horizontal displacement or the vertical one. The horizontal displacement due to turbulence is computed by:

$$u_i'(t)\Delta t = \sqrt{2K_i\Delta t}\,\mu_i,$$

for *i*=1,2 and where K_i are the horizontal diffusion coefficients and μ_i are random numbers picked up from a Gaussian distribution having mean value and standard deviation equal to 0 and 1 respectively. The vertical displacement due to turbulence is computed by distinguishing between two situations:

1) the particle moves above the mixing layer, i.e. $x_{3i}(t) > Z_g + H$ (Z_g is the height of the orography below and *H* is the mixing height): $u_3'(t)\Delta t = \sqrt{2K_3\Delta t}\,\mu_3$,
2) the particle moves within the mixing layer: $u_3'(t)\Delta t = (\mathrm{H} - Z_g)\nu$. In this case, the vertical position is randomly re-assigned within *H,* justifying this choice by considering that the time step, typically 30-60 minutes in these models, is larger than the eddy turnover time. ν represents a uniformly distributed random number.

PBL height

Another important feature for the computation of the simulations is the height *H* of the planetary boundary layer. The MILORD model foresees three possible choices for the setting of the PBL height:

1- The variation of the PBL height is calculated based on a simple algorithm reproducing a standard daily cycle (Desiato, 1992)
2- The mixing height is fixed as a constant value in space and time
3- The mixing height is read from an external file

Specifically, in the case of PBL height calculation, a constant value is set for the mechanical mixing height $h_m(x,y,z)$, which corresponds to the value of mixing height over the sea for all 24 hours of a day and over land during the night. This interval of time is defined considering the nighttime as between two hours before sunset (t_s-2) and two hours after the dawn (t_d+2). A value representative of the mixing height at 12 G.M.T., $h_c(t)$, is then fixed. The diurnal variation of the PBL mixing height $h_c(t)$ is therefore calculated by linearly interpolating the value of h_m at h_d+2 and $h_c(12)$ at 12 GMT. This calculation results in a growing trend from t_d+2 to t_s-4 where it is stopped and kept constant up to t_s-2. For the remaining part of the day the mixing height $h_c(t)$ is set as equal to h_m. The final value of the PBL height $H(x,y,z)$ is chosen as the highest value between h_m and $h_c(t)$.

The value of mixing height is also relevant in the operation of the model as it represents one of the three vertical boundaries of the model. It has to be taken into account that the particles are not allowed to cross these vertical boundaries. The only case for which the particles can pass from the mixing layer to the free atmosphere, and viceversa, is the variation of the height of the mixing layer during their path. In other words, if at time *t* a particle is within (over of) the mixing layer, at time *t+Δt* it may pass to the other layer only if, during the *Δt*, *H* has become lower (higher) than the particle height. The other two vertical boundaries are the top and bottom of the computational domain.

Source and emission

The coordinates and the height of the source must be provided. As regards the emission, the information needed for the simulations is the emission rate, the number of Lagrangian particles generated, and the duration of the emission. The duration of the emission may not correspond to the duration of the simulations. The model works by generating at each defined time step the given number of Lagrangian particles and moving them at the following instant. The flow rate is associated with each single Lagrangian particle.

Deposition

The MILORD model was thought to simulate both the dry and wet processes of deposition. A particle with radioactivity *A(t)* contributes to the dry deposition a portion of its radioactivity D_{dry}, and to the wet deposition a portion D_{wet}:

$$D_{dry} = A(t)[1 - \exp(-\lambda_d(t)\Delta t)],$$
$$D_{wet} = A(t)[1 - \exp(-\lambda_w(t)\Delta t)].$$

A(t) represents the mass or radioactivity of the particle and $\lambda_d(t)$ and $\lambda_w(t)$ are described by the following equations:

$$\lambda_d(t) = \frac{v_d}{H(x,y,t)},$$
$$\lambda_w(t) = \lambda_{w0}(P(t))^{\alpha}.$$

In the last expression, v_d is the deposition velocity, *P(t)* is the precipitation intensity, and λ_{w0} and α are empirical coefficients.
The radioactive decay is computed as follows:

$$A(t) = A_0 \exp(-\lambda t),$$

where A_0 is the initial activity and λ is the radioactive decay rate.
The model can also compute first order chemical reactions with appropriate relationships implemented in the code. An example can be found in the work of Anfossi and Sacchetti (1994) as regards the transport of Volcano Etna emissions and about mass-balance equations for sulphur dioxide and particulate sulphate. For the present work regarding the MPs, only the dry deposition is considered, the pollutant in exam is intended as non-radioactive, and it is assumed that no chemical reactions happen.

Configuration

The input data required by the model are:

- Meteorology: 3D wind fields at standard pressure levels
- Topography

- Boundary conditions:
  1) Ground particle reflection
  2) Particles crossing the top of the domain or lateral boundaries are lost
  3) Particles are allowed to pass from inside the PBL to the free atmosphere only if the PBL height changes during the path of the particles
- Emission
- Other configuration parameters (values of the diffusivities, dry and wet deposition coefficients, location and dimension of the source)

Also, being a Lagrangian model, it is characterized by a grid-free approach and no spatial resolution determines the particle motion. The only dependency on the resolution is related to the meteorological and topographical grid spacing of the data used as input. As regards the temporal resolution, a fixed time step must be set.

Output

The model generates as output a file where the information about each particle's age and coordinates, its residual mass or activity and dry and wet deposition rates are saved. Then, with a process of post-processing, the time averaged three-dimensional concentration fields over specific locations or over a grid are returned, where the averaging time and the option between specific location or grid is chosen by the user.

4.2. Model configuration and graphical presentation of the results

As introduced in the previous paragraph, the model needs to be configured by defining some parameters used for the run of the simulations. In the present paragraph, the parameters used for the simulations of this work are listed in Table 5.

Table 5. Parameters set for the MILORD simulations

Time steps	
Number of time steps per day	40 or 80
Duration of each time step	2160 s or 1080 s
ECMWF data (weather and orography)	
ECMWF data domain resolution	0.5°x0.5° or 0.25°x0.25°
Interval time between the surveys	6 h
Vertical levels considered (hPa)	1000, 950, 925, 900, 850, 800, 700, 600, 500, 400, 300, 250, 200
PBL	
Setting of PBL height	Parameterized, local daily cycle at particle position, calculated by the model.
PBL height for mechanical turbulence	300 m
PBL mixing height at 12 hours	1500 m
Others	
Diffusivity coefficients (horizontal and vertical)	1500 m^2/s, 50 m^2/s
Resolution of the output grid	0.1°x0.1°
Number of Lagrangian particles generated for each simulation	100 000 (ca.)

The emission type of the simulations done in this work is always continuous. The model foresees the possibility to insert the values of the mass contained in each Lagrangian particle and emitted at each time step, but, in the present case, no computation is made on the mass since the aim is to study the trajectories of the particles. The values of masses inserted in the simulations have been chosen relating to the concentration of MPs found in the samples collected in the reference articles but are not reported since they do not affect these simulations. Other parameters as regards the specific case studies have already been described in chapter 3.2 and the choice of the spatial resolution for the meteorological and topographical input data and of the temporal resolution is described in chapter 5, for each simulation performed.

Graphical presentation of the results

The output files obtained with the MILORD model simulations are elaborated with R codes to generate graphs that allow the user to visualize the achieved results. Specifically, for each simulation that is performed in this work, four graphs are produced: three of them, from now on referred as contour plots, give a qualitative information about the geographical provenience of the MPs and allow to have a first idea of the travelled distance by most of the particles. The three contour plots display respectively the trajectories of the particles travelling above the PBL, inside the PBL, and both above and inside the PBL. For each of these three cases, the relative frequency of the number of trajectories for each single cell is calculated as the number of the trajectories passing through that cell (above the PBL, below it, or both respectively) and divided for the total number of trajectories counted in all the cells for the whole period of the simulation (both above and below the PBL). Here it is important to specify for clarity, that in the count of the number of trajectories, if a particle passes through a single cell more than one time, a new trajectory is seen by the single cell every time, since the count is done on the number of trajectories and not on the number of particles. The number resulting from this calculation is then multiplied for a factor of 100 for a better visualisation of the results in the legend of the graph. The fourth graph is a distribution graph and gives a more quantitative information about the distance travelled by the particles. The same calculation for the relative frequency of the trajectory number is done, but without the multiplication for the factor 100. For the graphical representation of the contour plots, the values of relative frequency are divided in levels, chosen by the user to ensure a significant and readable graphic output, and to which one is associated a specific colour. In the distribution graph, the relative frequency of the trajectory number is plotted on the y-axis and as a function of distance that is reported on the x-axis and expressed in kilometres.
The information given by the contour plots coupled with the one emerging from the distribution graph provide indications about the displacement of the masses of air in the investigated area and for the possible research of emission sources. In addition, plots of time frames of the distribution of the particles in the investigated area are reported when useful for the discussion. Animations in time of the particle plume development are also produced.

5. Results

5.1. Tibet

Some test simulations are initially performed to gain confidence with the model and to verify its robustness in application to such highly complex topography. For this aim, for the simulations, the DKMD glacier is chosen as starting point, and the selected month is May 2022, the month in which the authors of the reference article (Wang et al, 2024) made their samplings of MP concentrations. The first test simulations are performed using both 0.5°x0.5° and 0.25°x025° resolutions for the meteorological and orographical data used as input, to verify if there is a significant difference between the output obtained in the two cases. A previous study demonstrated that there is not a significant difference between the results of the simulations performed using 0.5°x0.5° or 0.25°x025° resolutions, in a case of a flat area in the Great Lake region in Canada (Ziero, 2025). It is assumed that in this case the complexity of the orography of the Tibetan Plateau could play a different role. For this test, both the resolutions were associated to a time step of 2160 *s* (corresponding to 40 time steps per day). Moving from 0.5°x0.5° grid resolution to the 0.25°x0.25° one, also the temporal resolution could be changed, moving to a time step of 1080 *s* (80 temporal steps in a day). Therefore, a second test is performed to verify if this change on the time step would lead to significant difference in the output. The third and last test simulation is done to study how the distribution of the particles evolve with the distance, when running some simulations of different durations, over the same glacier and over the same month. So, three simulations of two days, one week and one month respectively, and characterised by a continuous emission, are performed in the month of May 2022 and on the DKMD glacier. As output of this third test, the distribution curves representing the particles travelling both above and inside the PBL of the three cases are reported on the same plot to better compare the results obtained. Then, also the relative contour plots are presented.
After these preliminary analyses, simulations to study the atmospheric transport of MPs in the Tibetan region are performed. The simulations are done for DKMD, AL and KQGR glaciers and for the months of June 2021 and April 2022, with the aim of representing the monsoon and pre-monsoon periods, in the three different areas of the TP. The month and year of investigation are chosen to perform the analysis in the same month and year of the simulations performed in the reference article. A comparison with the results obtained in the reference article is then made to verify if there is a correspondence between our simulations done with MILORD model, and the ones of the article done with HYSPLIT model.

5.1.1. DKMD glacier, May 2022 – test simulations

For the first test simulation the backward trajectories are calculated using the meteorological and orographical data at the two mentioned grid spacings, and the graphical plot (Figure 5.2) is done by considering the difference between the values of frequency of the trajectories passing through each cell of the calculation domain obtained with 0.25°x0.25° resolution (Figure 5.1b) to the ones obtained with 0.5°x0.5° resolution (Figure 5.1a). This calculation is done for all particles, travelling both inside and above the PBL. It can be noticed that the values of the differences in the relative frequency are not significant, since their highest values found close to the receptor take absolute value of the order of 10^{-3}, whereas the correspondent relative frequency values calculated for the two grid resolutions (Figure 5.1) are of one or two order of magnitude higher. Most of the difference lies in ranges close to zero in the rest of the domain. The results show that even in this case of very complex orography there is not a significant difference in the results obtained in the two cases. So, it can be stated that the use of both the grid resolutions returns consistent results.

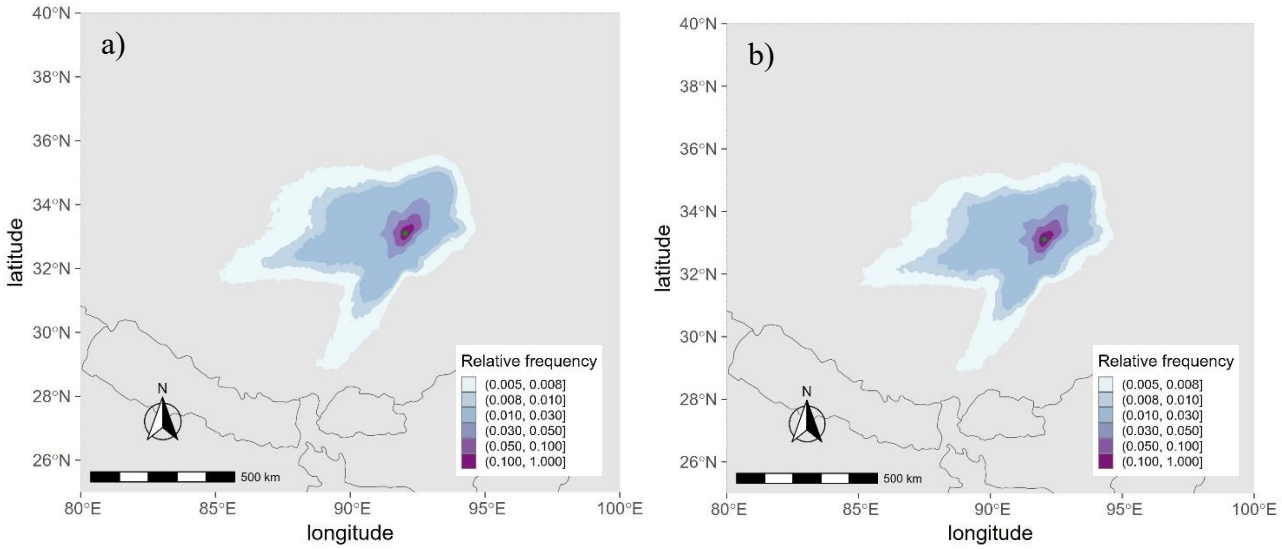

Figure 5.1 Simulations about all the particles travelling both inside and above the PBL for the month of May 2022 and for DKMD glacier. a) 0.5°x0.5° grid resolution, b) 0.25°x0.25° grid resolution.

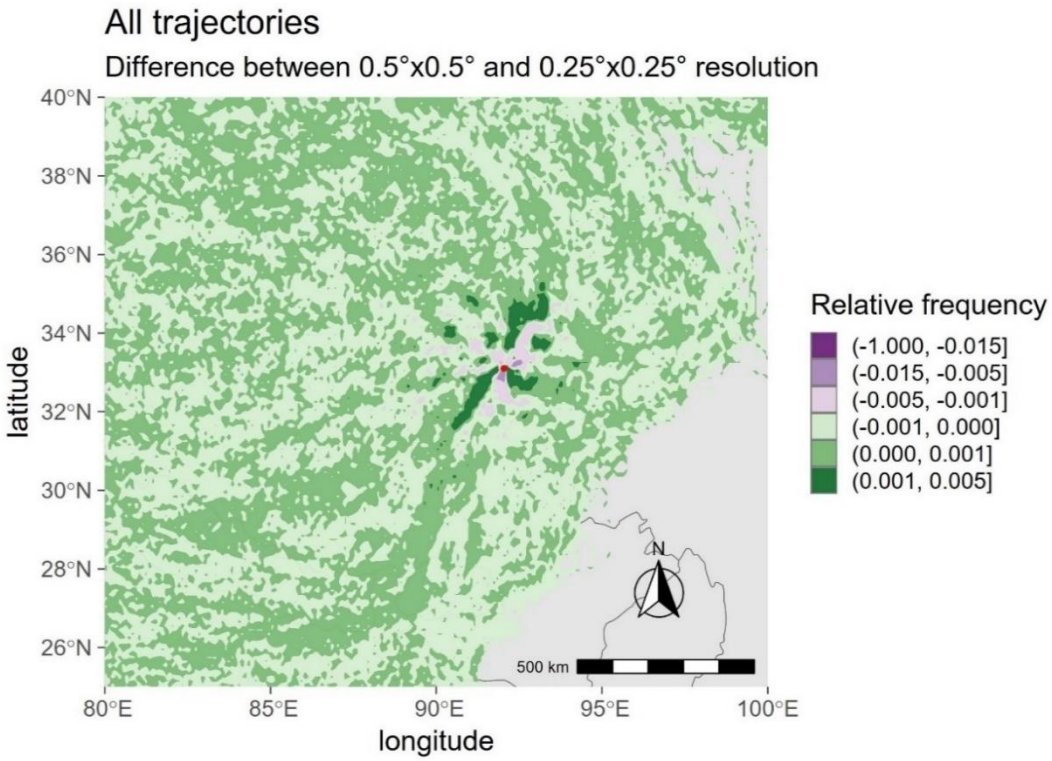

Figure 5.2 First test simulation output image representing the difference between the values of the relative frequency of the trajectory number obtained with 0.5°x0.5° grid resolution and 0.25°x0.25° grid resolution, for the month of May 2022, and for DKMD glacier.

From now on, for the simulations performed in the Tibetan Plateau area, it is chosen to use the resolution of 0.25°x0.25° for the meteorological and topographical input data, to better consider the complex orography of the area.

For the second test, the simulation with 0.25°x0.25° resolution is also performed changing the temporal resolution from 2160 *s* to 1080 *s* for the single time step. The resulting output is reported in Figure 5.3.

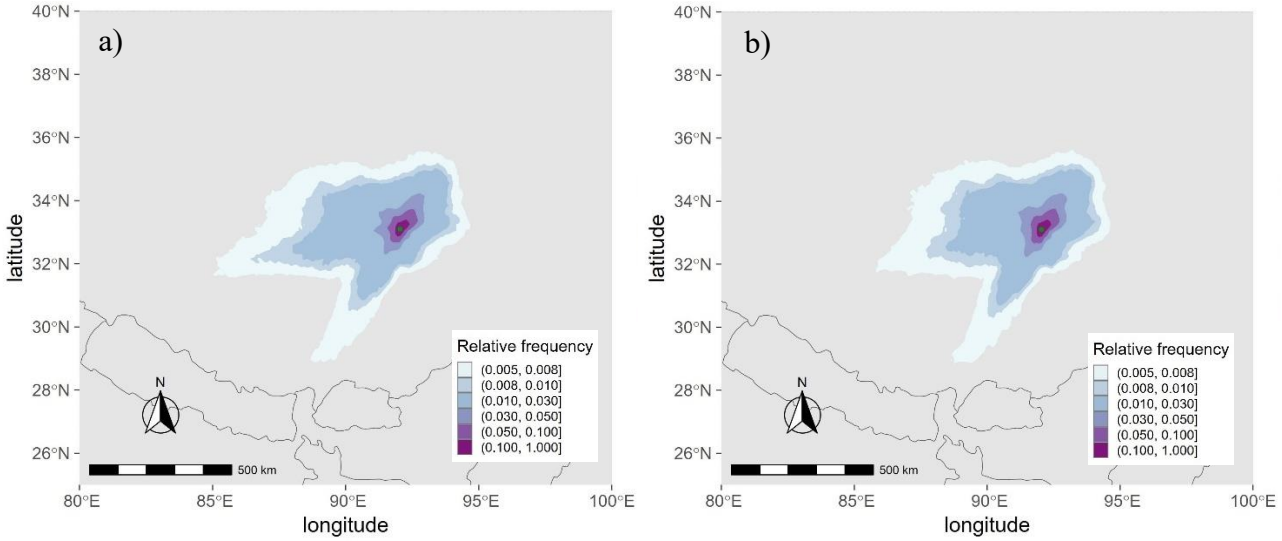

Figure 5.3 Second test simulation output images representing the simulations performed for the month of May 2022 and for DKMD glacier with 0.25°x0.25° grid resolution. a) temporal resolution of 40 time steps (2160 s), b) temporal resolution of 80 time steps (1080 s).

As it can be noticed, the two images do not show significant differences and so, also in this case, it can be stated that using both the two different time steps consistent results are obtained. For the following simulations relative to the Tibetan Plateau, it is chosen to keep the time step of 2160 *s*.
As regards the third test simulation, the output is reported in Figure 5.4.

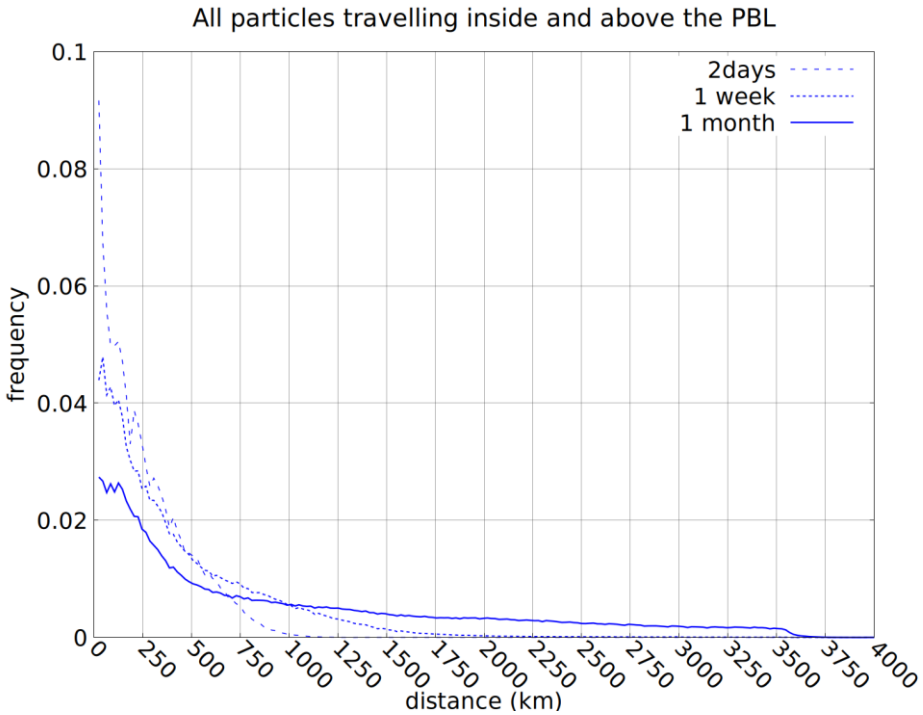

Figure 5.4 Third test simulation output image representing the three distribution curves of the relative frequency of the trajectory number obtained for the simulations of two days (dashed line), one week (dotted line) and one month (solid line), during the month of May 2022, and for DKMD glacier.

The graph shows the distribution of the relative frequency of the trajectory number for the particles travelling both inside and above the PBL (Figure 5.4). As it might be expected, the three curves differ for the fact that for shorter simulations the particles have less time to travel and to disperse, graphically translating in a curve with higher value of relative frequency close to the receptor and depicting shorter distances if compared to longer simulations. For increasing simulation time, clearly a different distribution of the relative frequency is found, given how they are calculated by

normalizing the number of trajectories in the cell over their total number in the domain. For longer simulation time, the particles travel for longer distances and the distribution spread over a large range. Thus, proportionally a lower frequency is found at shorter distance with respect to simulations run for shorter time. The graph provides an indication of the potential distance of the MP source areas, depending on atmospheric circulation and the correspondent travel time of the air masses. This is highlighted in Figure 5.5, Figure 5.6 and Figure 5.7, where the contour plots calculated directly from the number of trajectories are reported.

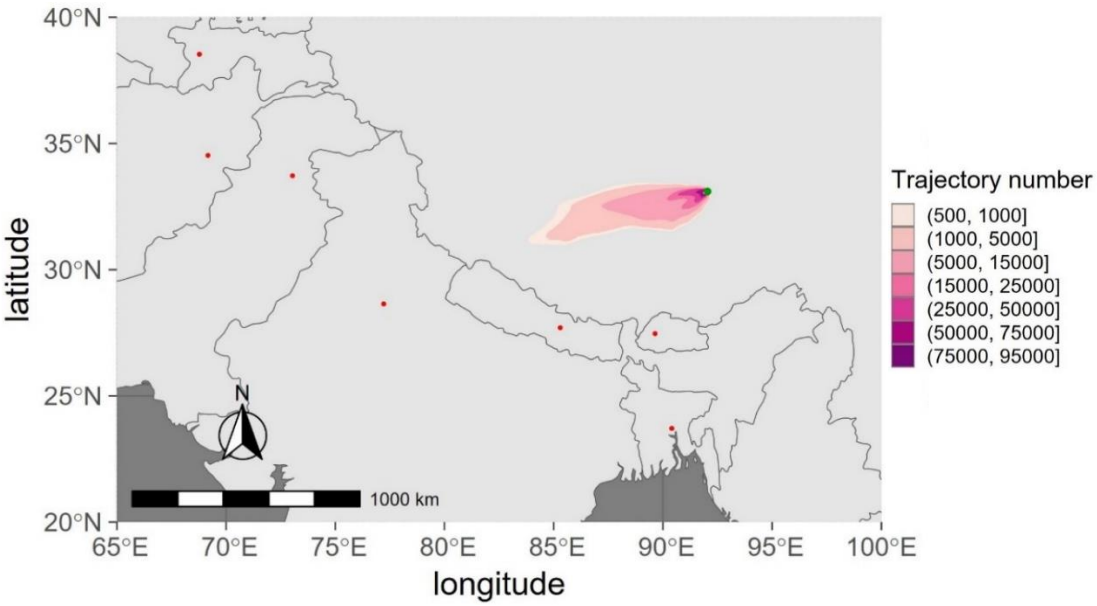

Figure 5.5 Contour plot of the trajectory number of particles travelling both above and inside the PBL and relative to the third test simulation. Two days simulation on the DKMD glacier and for May 2022. Zoomed image with respect the simulation domain.

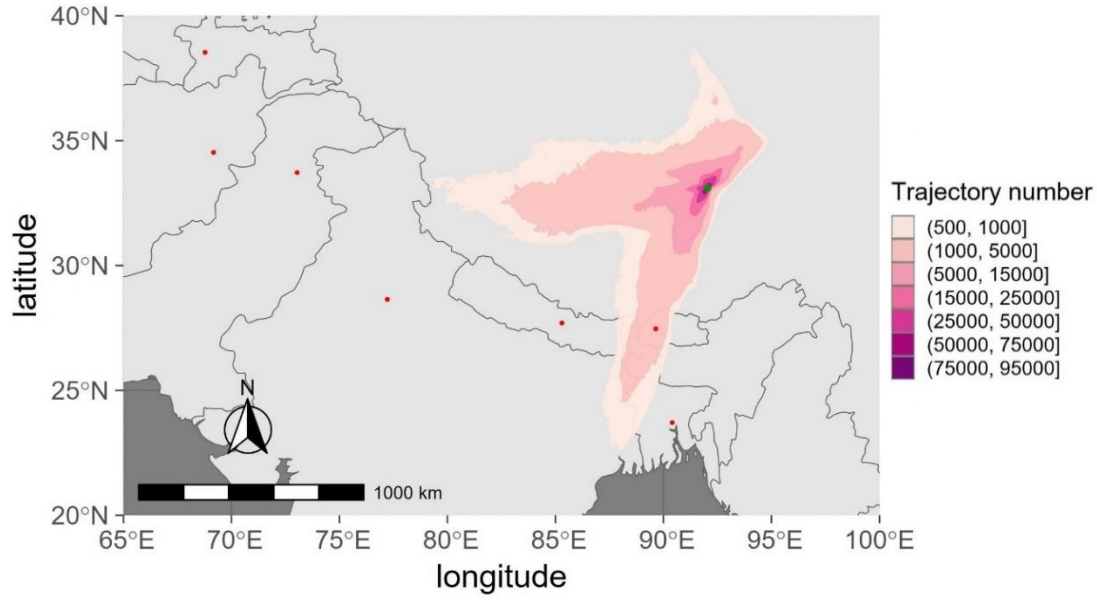

Figure 5.6 Contour plot of the trajectory number of particles travelling both above and inside the PBL and relative to the third test simulation. One week simulation on the DKMD glacier and for May 2022. Zoomed image with respect the simulation domain.

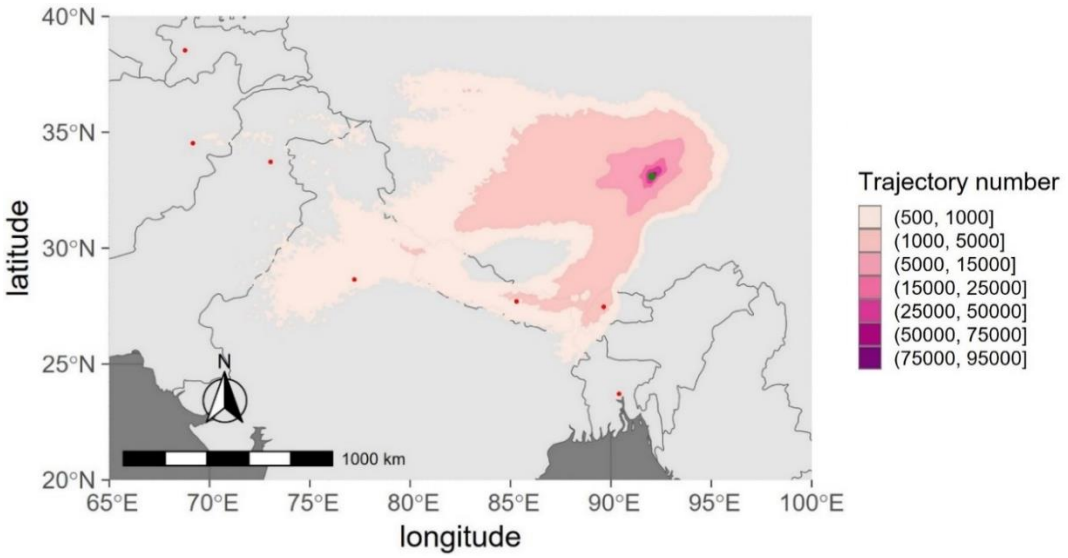

Figure 5.7 Contour plot of the trajectory number of particles travelling both above and inside the PBL and relative to the third test simulation. One month simulation on the DKMD glacier and for May 2022. Zoomed image with respect the simulation domain.

For the simulation of two days, it is noticed that the particles come from the West direction, for the simulation of one week the particles come from the South and South-West direction and pass over the city of Thimphu, capital of Bhutan. For the one-month simulation the particles come from the South and South-West direction, and the signal meets different populated regions, with a particular focus for the capitals Thimphu, Kathmandu (capital of Nepal) and New Delhi (capital of India).

5.1.2. All glaciers, pre-monsoon and monsoon simulations

After these test simulations, the output relative to the simulations performed for the study of the atmospheric transport of MPs in the Tibetan region is here reported for the three glaciers, in the following order: DKMD, KQGR and AL glacier. For each of them, the monsoon and pre-monsoon periods are investigated, representing these periods respectively with the months of June 2021 and April 2022. The three contour plots and the distribution graphs about the relative frequency of the trajectory number are reported for each case.

DKMD glacier

DKMD glacier, June 2021

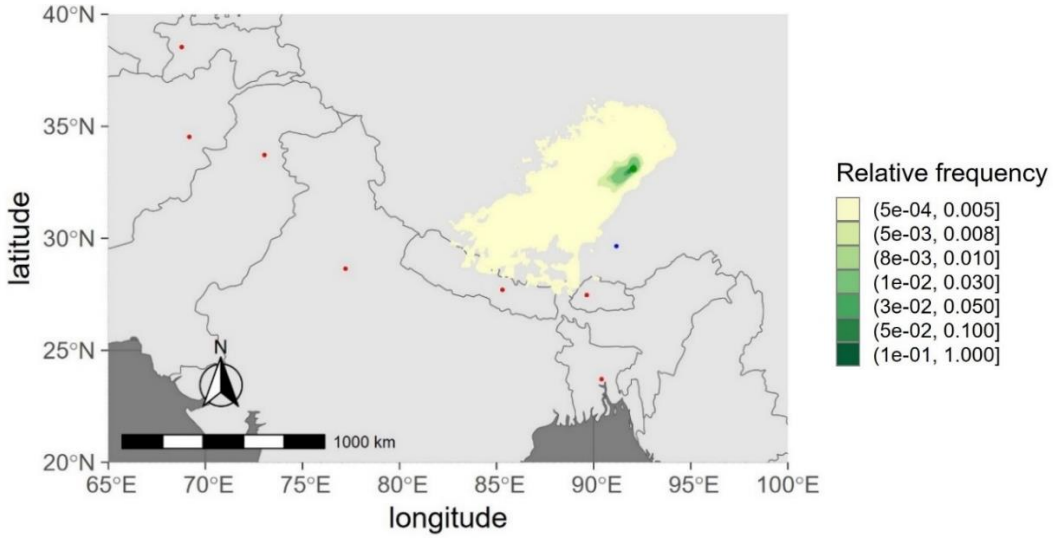

Figure 5.8 DKMD glacier contour plot of the trajectories relative frequency: particles travelling inside the PBL (June 2021). The green point represents the receptor, the blue point represents the city of Lhasa, the red points represent the capitals of the States of the area. Zoomed image with respect the simulation domain.

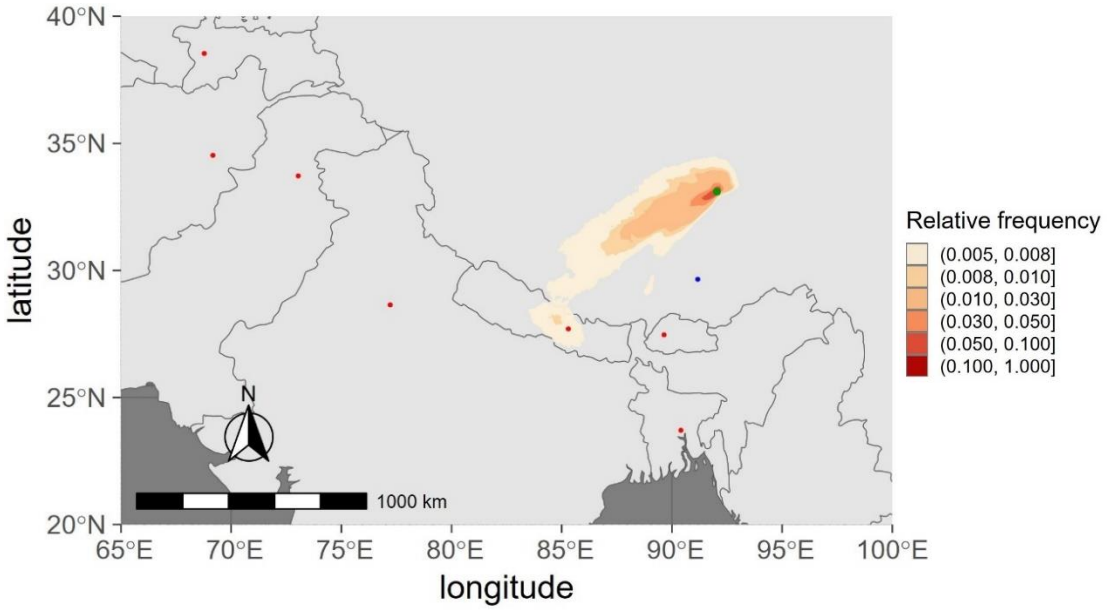

Figure 5.9 DKMD glacier contour plot of the trajectories relative frequency: particles travelling above the PBL (June 2021). The green point represents the receptor, the blue point represents the city of Lhasa, the red points represent the capitals of the States of the area. Zoomed image with respect the simulation domain.

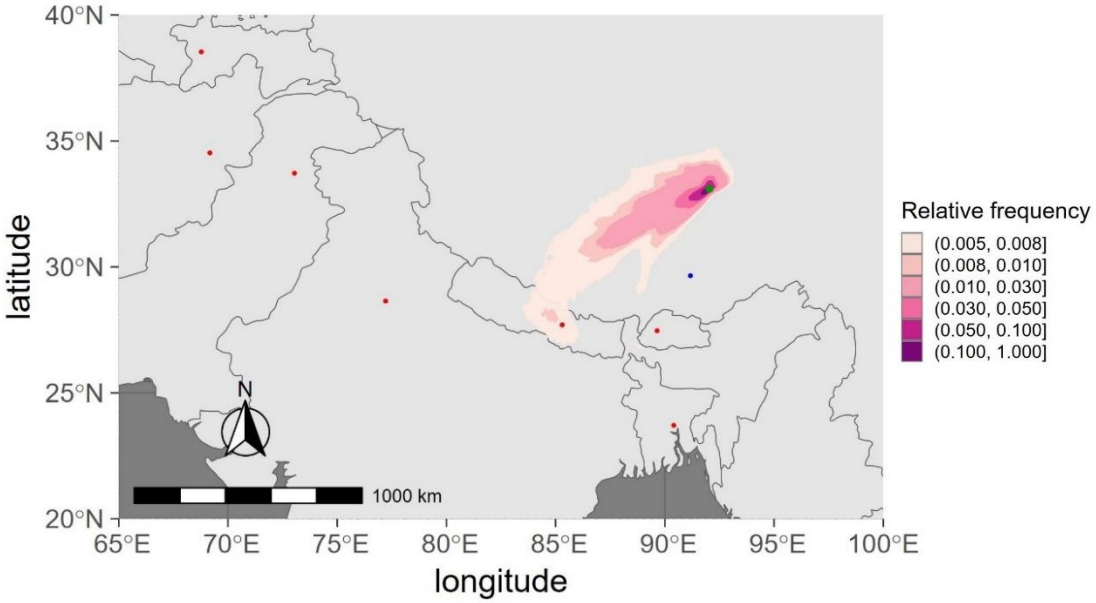

Figure 5.10 DKMD glacier contour plot of the trajectories relative frequency: all particles (June 2021). The green point represents the receptor, the blue point represents the city of Lhasa, the red points represent the capitals of the States of the area. Zoomed image with respect the simulation domain.

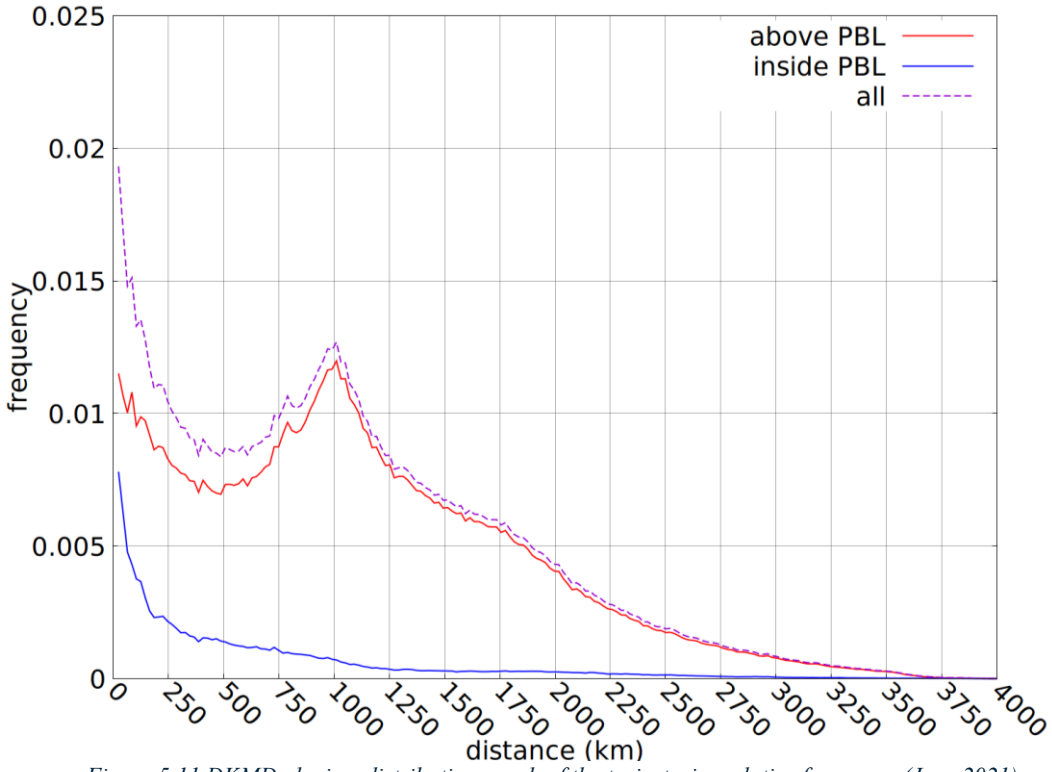

Figure 5.11 DKMD glacier: distribution graph of the trajectories relative frequency (June 2021).

For the DKMD glacier, and for the month of June 2021, the contour plots (Figure 5.8, Figure 5.9, Figure 5.10) show that the main signal comes from South-West direction, as it is found in the original article. In the distribution graph (Figure 5.11) it can be seen that most of the particles inside the PBL travel from a distance of about 500 km, and a maximum of 1000 km, while particles travelling above the PBL travel from a distance of about 3000 km. As regards the possible short-range sources that can be detected in the area of interest, in the provenience direction shown by the contour plot, and for the travelled distance of 500 km, the only sensible and potential source could be the National Highway 109 (see Figure 5.24a), as it is estimated that during the touristic season (from May to September) more than 10000 vehicles[2] travel through it. The Prefectures of Nagqu and Shannan belong to the area indicated in Figure 5.24a, but they do not intercept the signal, as they are found eastward from it. Also, these prefectures have a low population density of about 1 ab./km^2[3] and 4 ab./km^2[4] respectively. For these two reasons, they are not considered as possible short-range sources of MPs for the DKMD glacier. The city of Lhasa is found in the same region and it has a more significant density population of about 5266 inhabitants/km^2[5]. Also, it is a touristic city, and so it is probable that this would lead to an increase in the traffic and in the number of people present on the territory during the tourist season, with possible consequent increase of MP release. Again, its east position with respect to the signal, as it can be noticed in Figure 5.8, Figure 5.9, and Figure 5.10, suggests that it could hardly be a source of MPs for this case. On the contrary, the prefecture of Shigatse is in the same direction of provenience of the air masses for the specific case of DKMD glacier and June 2021, but also in this case, given its minimal density population of about 4 inhabitants/km^2[6], it is reasonable to exclude it as possible MP source. As regards the long-range transport, referring to the particles

[2] National Highway 109 (India) - Wikipedia
[3] Prefettura di Nagqu - Wikipedia
[4] Prefettura di Shannan - Wikipedia
[5] Lhasa - Wikipedia
[6] Prefettura di Shigatse - Wikipedia

travelling in the free atmosphere, it is noticed that the main part of the trajectories is seen in the range of about 1000 km, and come from the Nepal region (Figure 5.21 and see Figure 5.24b).
From the distribution graph an interesting trend can be pointed out as regards the particles that travel above the PBL. At around 1000 km distance from the receptor, it is found a positive peak in the values of relative frequency, indicating that a such distance a particularly high number of trajectories is counted. The geographical area corresponding to the peak of frequency is the Nepal region, a flat area delimited by the Tibetan Plateau (Figure 5.12 and Figure 5.13). This first geographical information may suggest that the high number of trajectories here detected can be related to a particular circulation in the area, constraining the passage of the air masses, thus of the particles, from the plane over the mountain ridge.

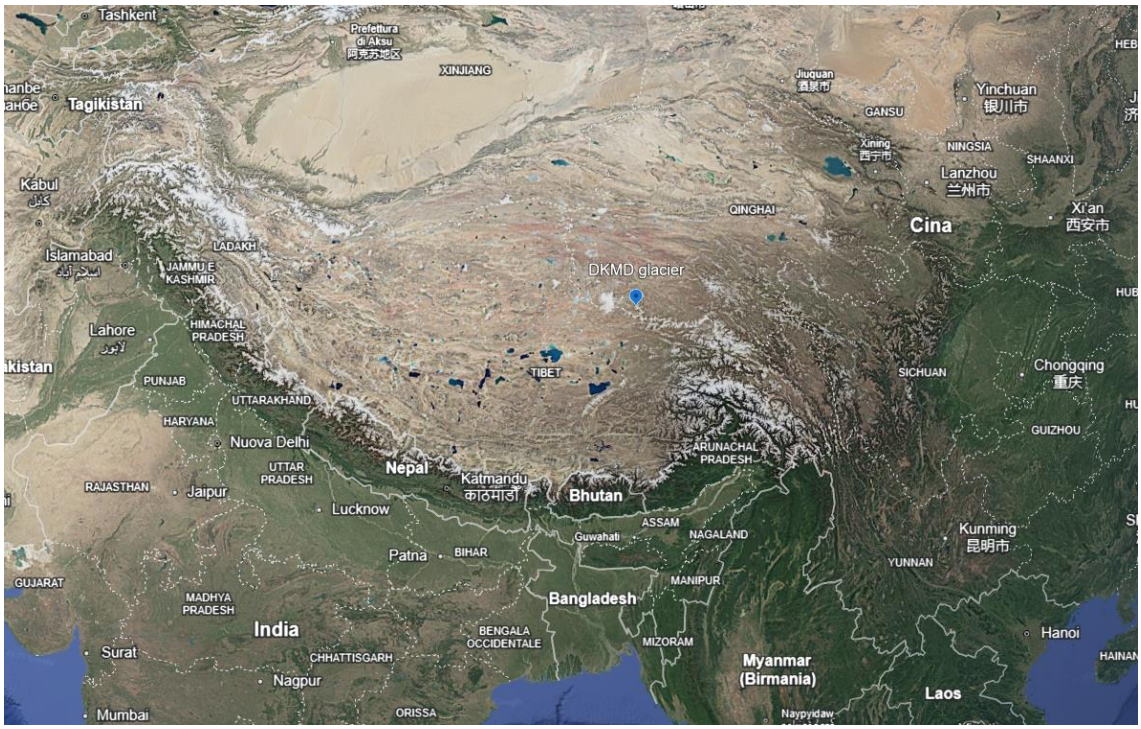

Figure 5.12 Area of investigation for the DKMD glacier (Source: Google Earth).

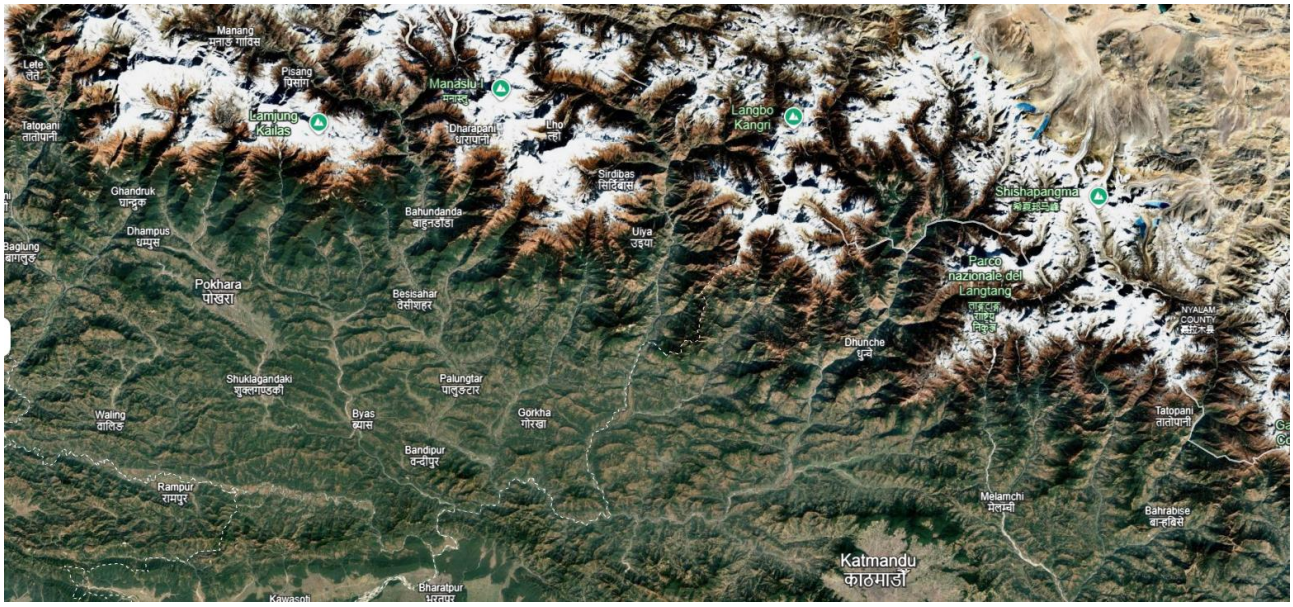

Figure 5.13 Zoom of the area of Nepal interested by the positive spike of the relative frequency of the particles travelling above the PBL (Source: Google Earth).

To verify the occurrence of such a condition, a check on the ECMWF wind field on that area and for the month of June 2021 is done. The wind field is investigated at both 850 and 950 hPa to represents the altitudes of that passage region in Nepal, from the plane area over the mountain, ranging from about 500 to 1500 m. Below, the relative images for three different days to represent the month of June 2021, specifically the 2^{nd} of June, 15^{th} of June and 30^{th} of June, are reported (from Figure 5.14 to Figure 5.19).

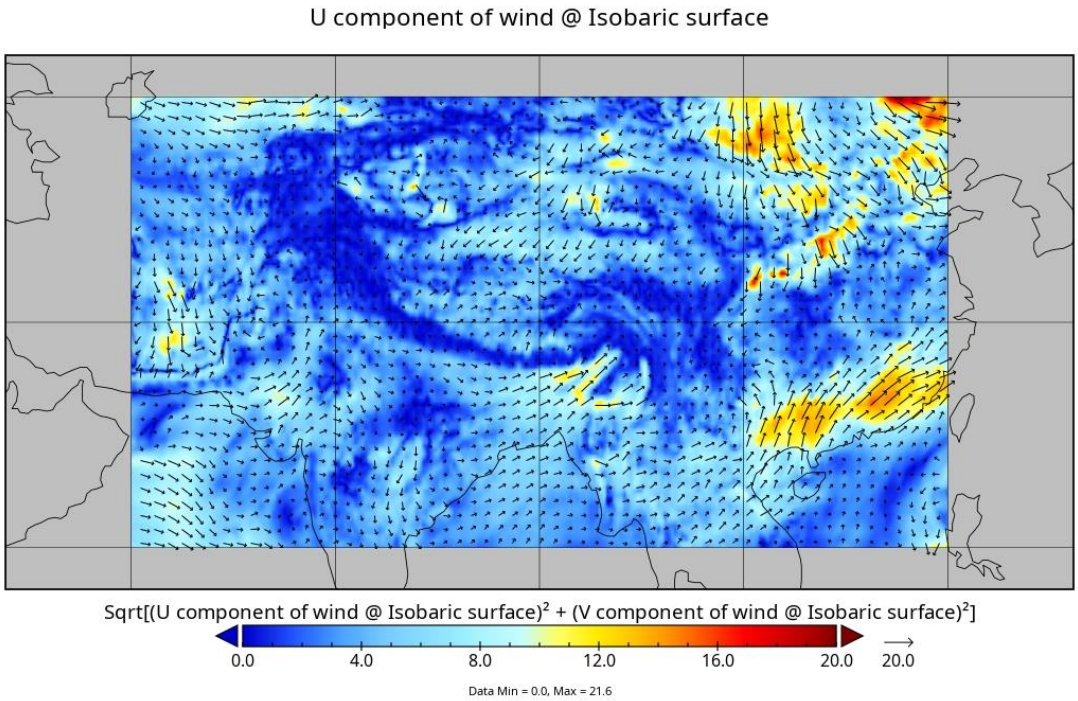

Figure 5.14 Image representing the wind field velocity at 850 hPa and for the 2^{nd} of June at 12:00 a.m. The image is centred at the coordinates of 30°N and 90°E (Source: ECMWF).

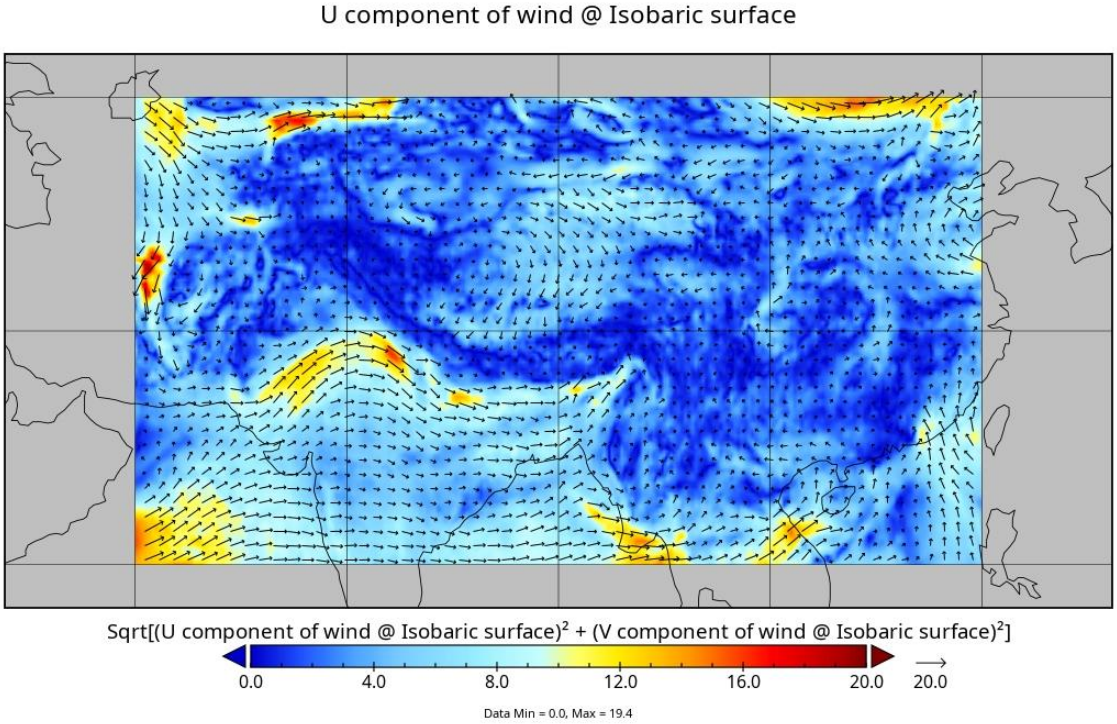

Figure 5.15 Same of Figure 5.14 at 950 hPa and for the 2^{nd} of June at 12:00 a.m.

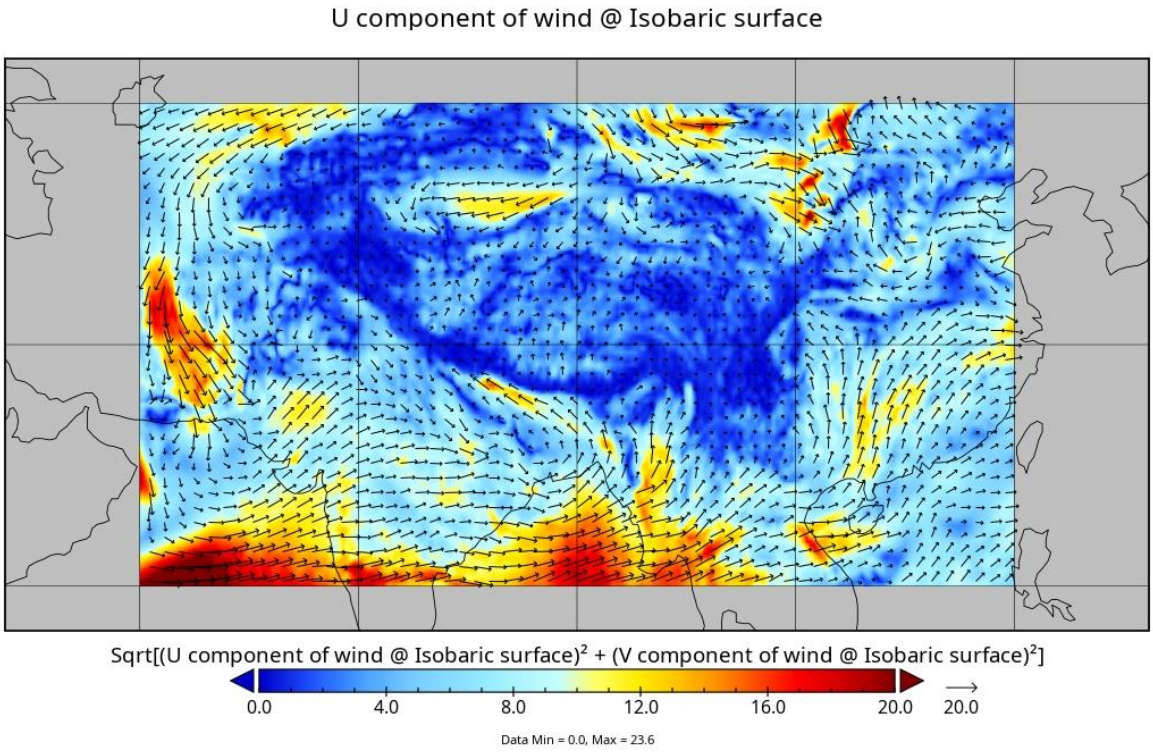

Figure 5.16 Same of Figure 5.14 for 850 hPa and for the 15^{th} *June at 12:00 a.m.*

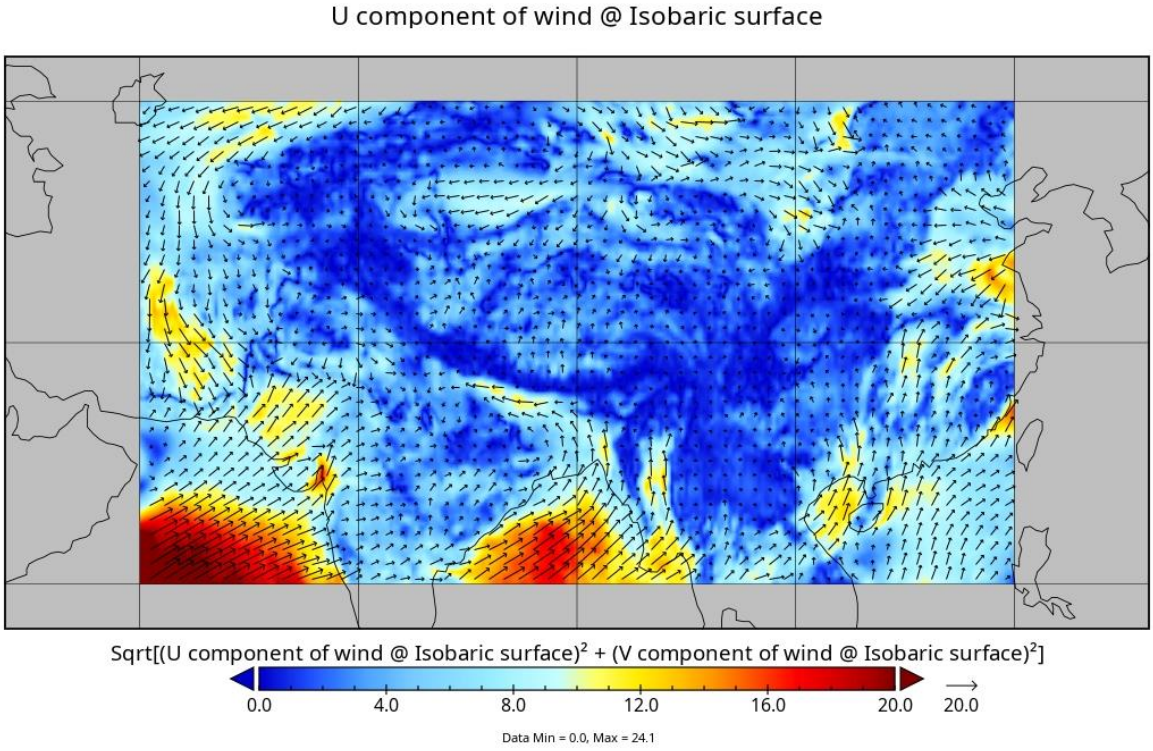

Figure 5.17 Same of Figure 5.14 at 950 hPa and for the 15^{th} *of June at 12:00 a.m.*

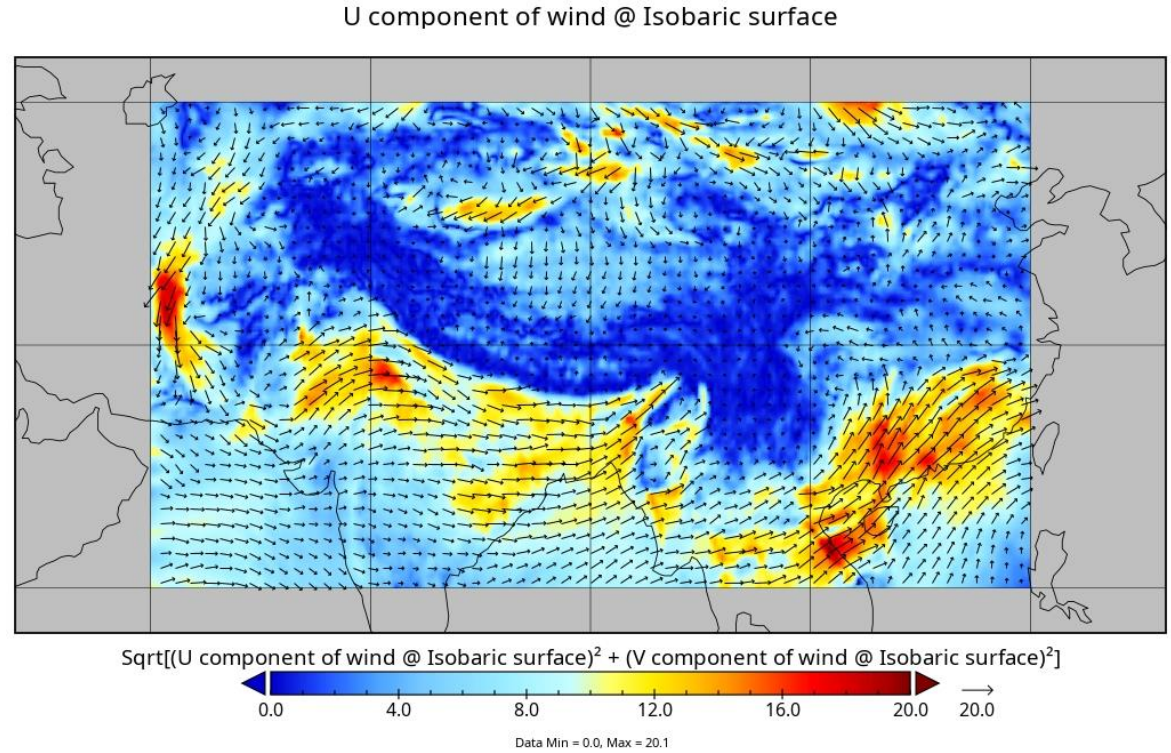

Figure 5.18 Same of Figure 5.14 at 850 hPa and for the 30^{th} of June at 00:00 a.m.

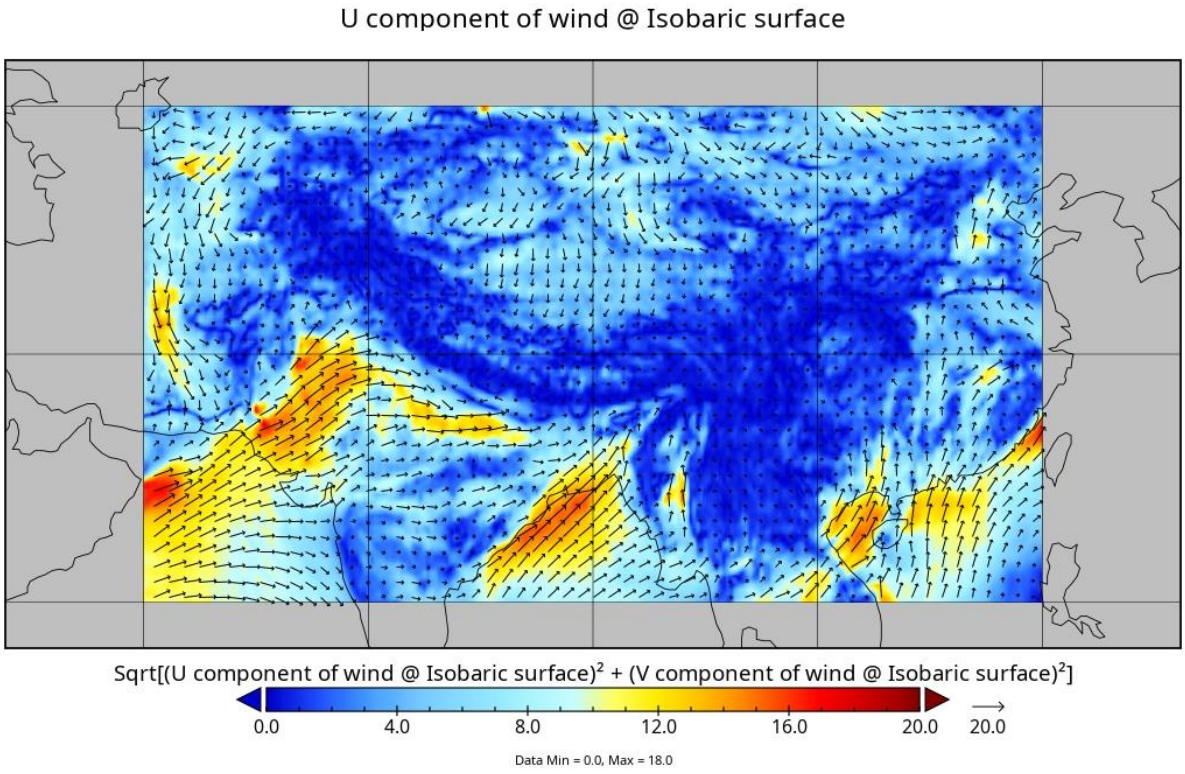

Figure 5.19 Same of Figure 5.14 at 950 hPa and for the 30^{th} of June at 00:00 a.m.

From the reported images, the investigated area in Nepal, is characterised by the dark blue colour and very small arrows, indicating low values of wind velocity. This is true for the whole month in exam and supports the hypothesis for which the peak of relative frequency is related to the fact that in such area the particles tend to accumulate and take more time to disperse, both for a geographical and meteorological reason.

DKMD glacier, April 2022

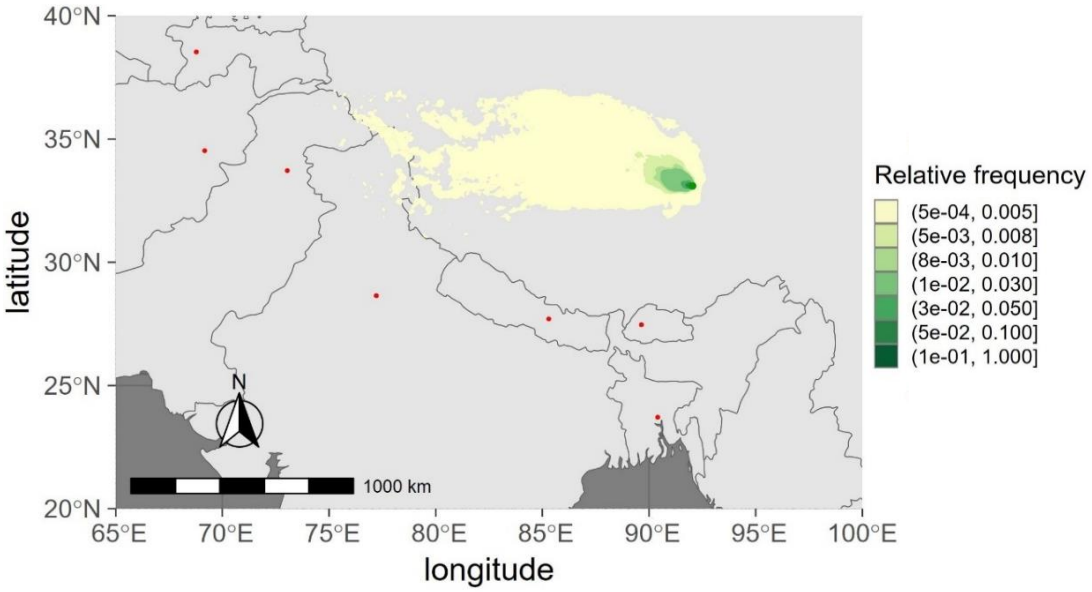

Figure 5.20 DKMD glacier contour plot of the trajectories relative frequency: particles travelling inside the PBL (April 2022). The green point represents the receptor, the red points represent the capitals of the States of the area. Zoomed image with respect the simulation domain.

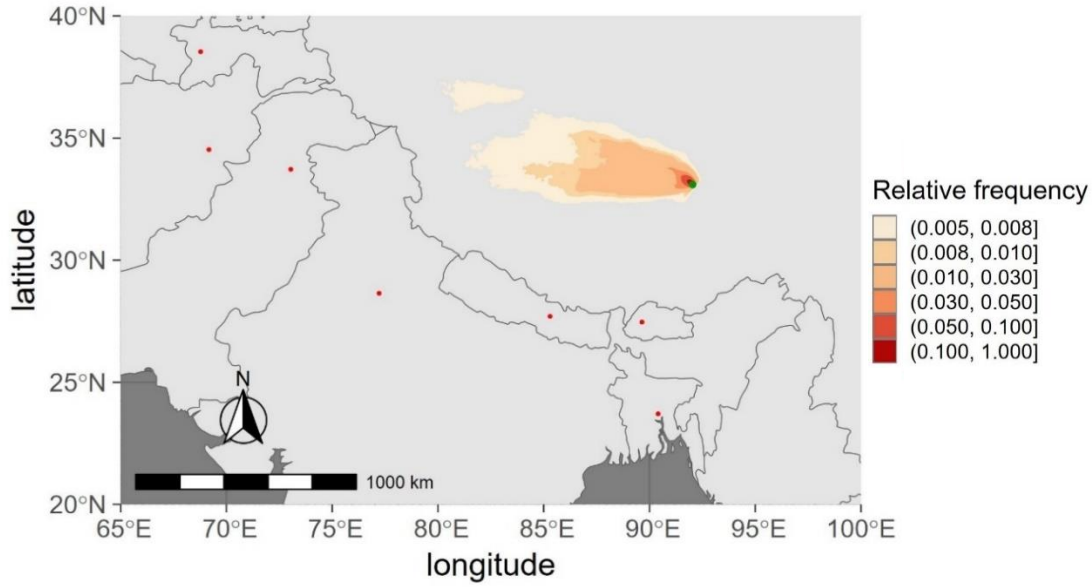

Figure 5.21 DKMD glacier contour plot of the trajectories relative frequency: particles travelling above the PBL (April 2022). The green point represents the receptor, the red points represent the capitals of the States of the area. Zoomed image with respect the simulation domain.

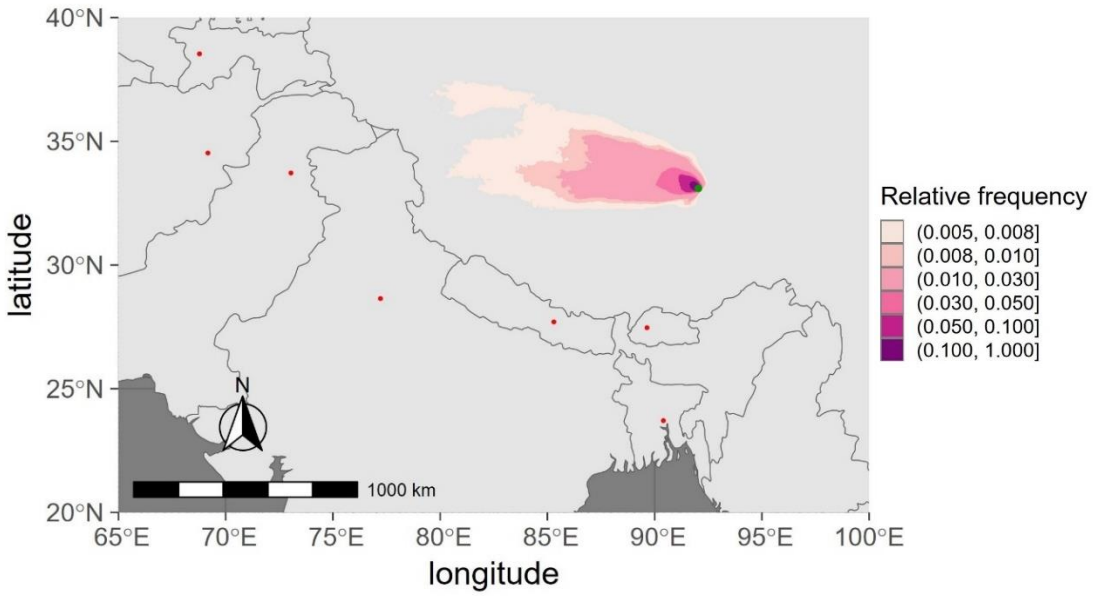

Figure 5.22 DKMD glacier contour plot of the trajectories relative frequency: all particles (April 2022). The green point represents the receptor, the red points represent the capitals of the States of the area. Zoomed image with respect the simulation domain.

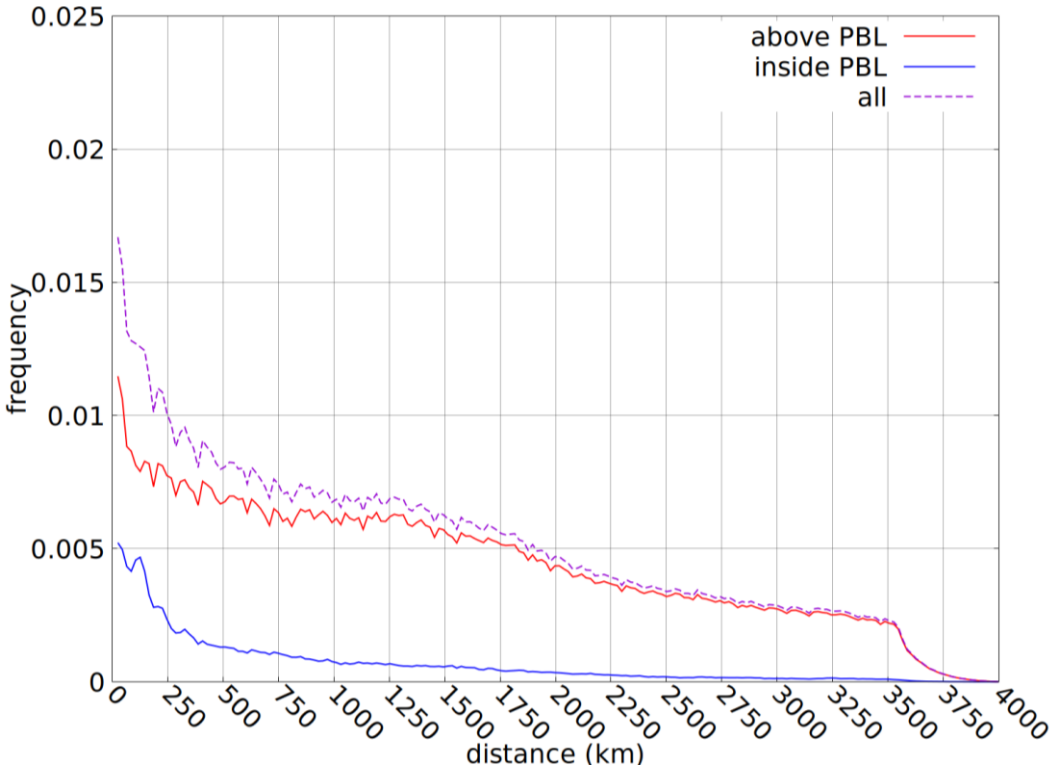

Figure 5.23 DKMD glacier: distribution graph of the trajectories relative frequency (April 2022).

For the DKMD glacier, and for the month of April 2022, the contour plots (Figure 5.20, Figure 5.21, Figure 5.22) show a signal that originates mainly from the West, and also in this case this result meets the one found in the reference article. From the distribution graph (Figure 5.23) it can be noticed that most of the particles inside the PBL travel up to about 500 km, while the particles travelling above the PBL arrive from distances up to 3500 km. Also in this case, the only possible short-range source of MPs in the range of 500 km and in the West direction is the National Highway that is 10 km from the glacier (Figure 5.24a). As regards the long-range transport it is seen from Figure 5.21 that the

main part of the trajectories is seen in the range of 1000 km, and travelling over an area without any significant cause of MP emission (Figure 5.24b).

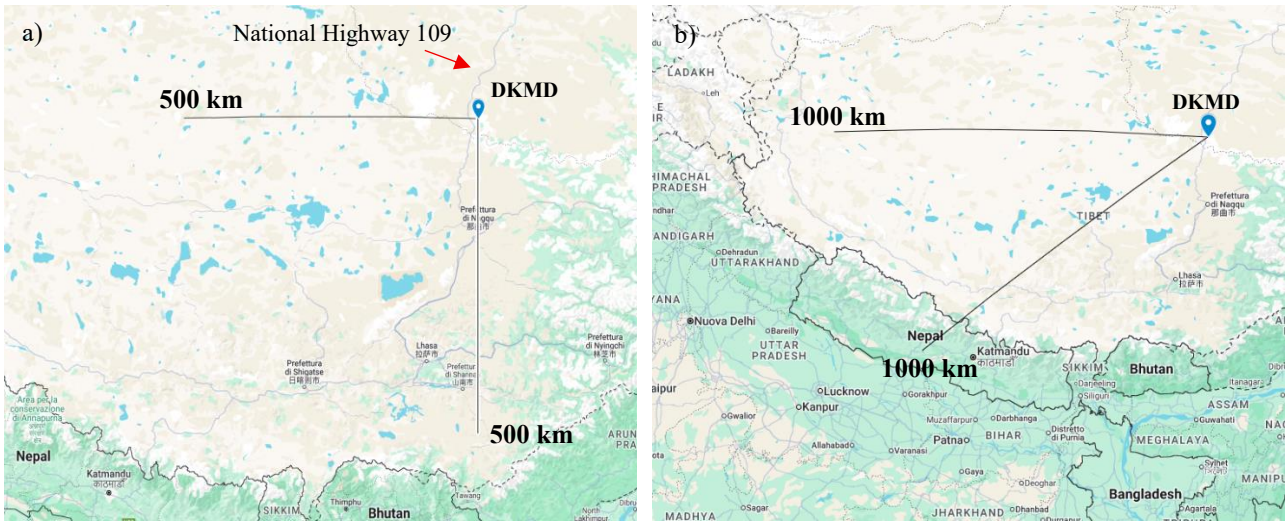

Figure 5.24 DKMD glacier: a) Area of impact of a possible short-range source given a travelling distance for the particles travelling inside the PBL and the direction of provenience read in the relative contour plot, b) area of provenience of the particles travelling above the PBL in the range of 1000 km (Source: Google – My Maps).

KQGR glacier

KQGR glacier, June 2021

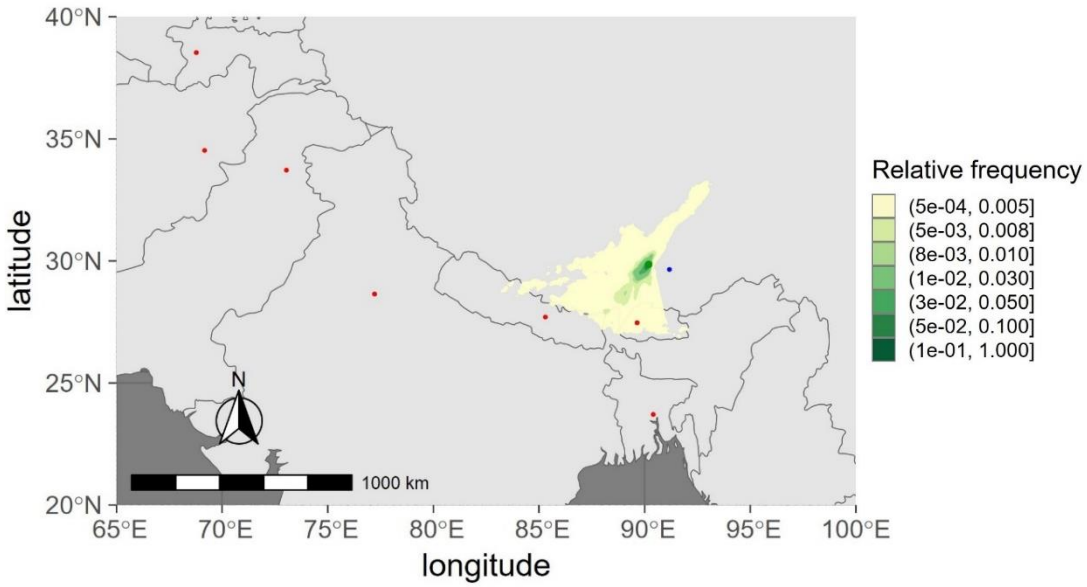

Figure 5.25 KQGR glacier contour plot of the trajectories relative frequency: particles travelling inside the PBL (June 2021). The green point represents the receptor, the blue point represents the city of Lhasa, the red points represent the capitals of the States of the area. Zoomed image with respect the simulation domain.

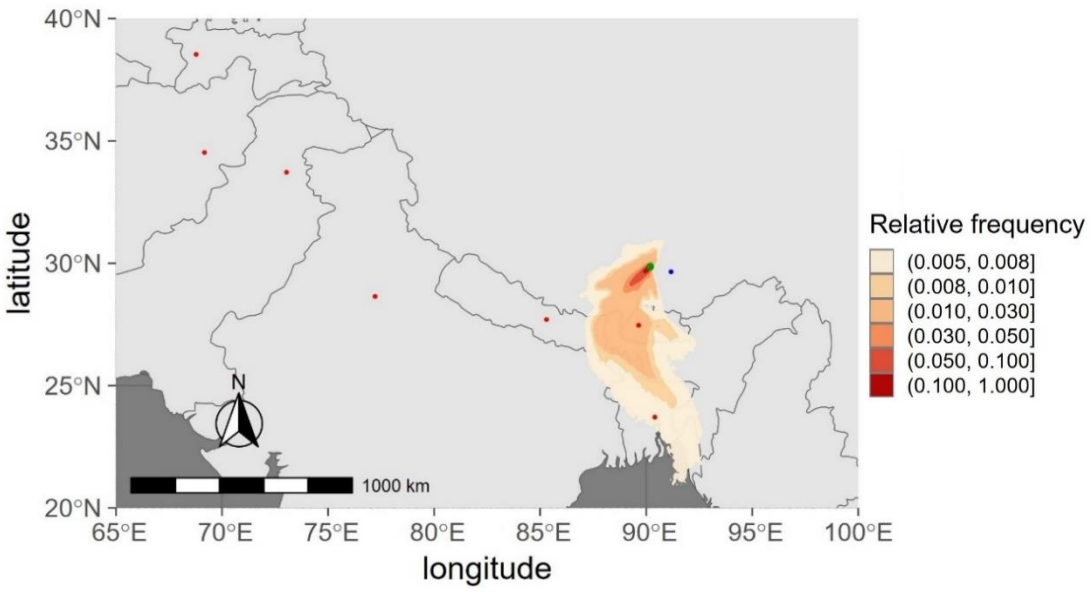

Figure 5.26 KQGR glacier contour plot of the trajectories relative frequency: particles travelling above the PBL (June 2021). The green point represents the receptor, the blue point represents the city of Lhasa, the red points represent the capitals of the States of the area. Zoomed image with respect the simulation domain.

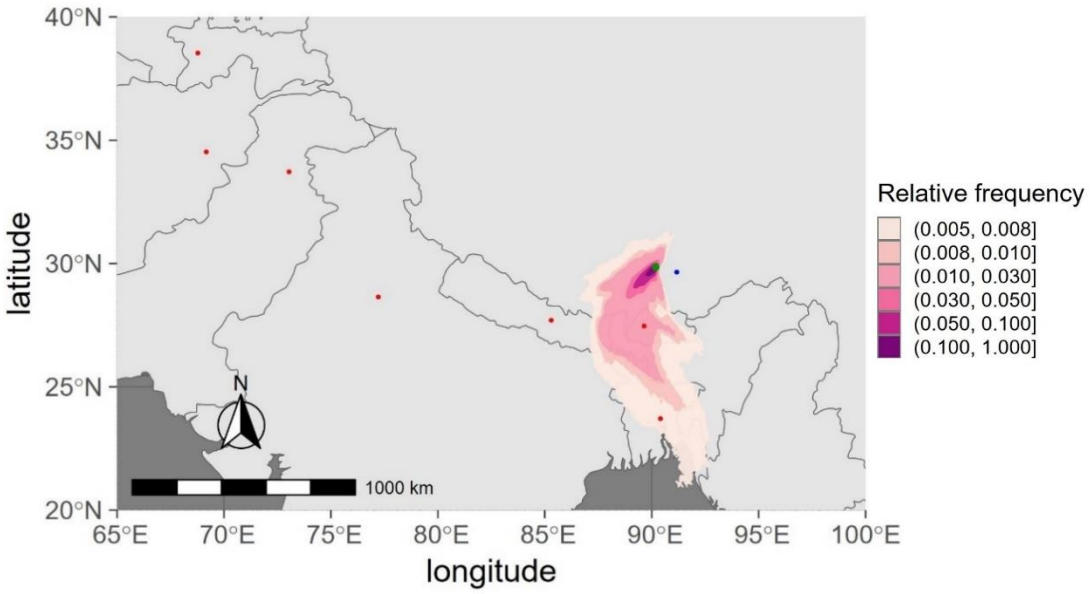

Figure 5.27 KQGR glacier contour plot of the trajectories relative frequency: all particles (June 2021). The green point represents the receptor, the blue point represents the city of Lhasa, the red points represent the capitals of the States of the area. Zoomed image with respect the simulation domain.

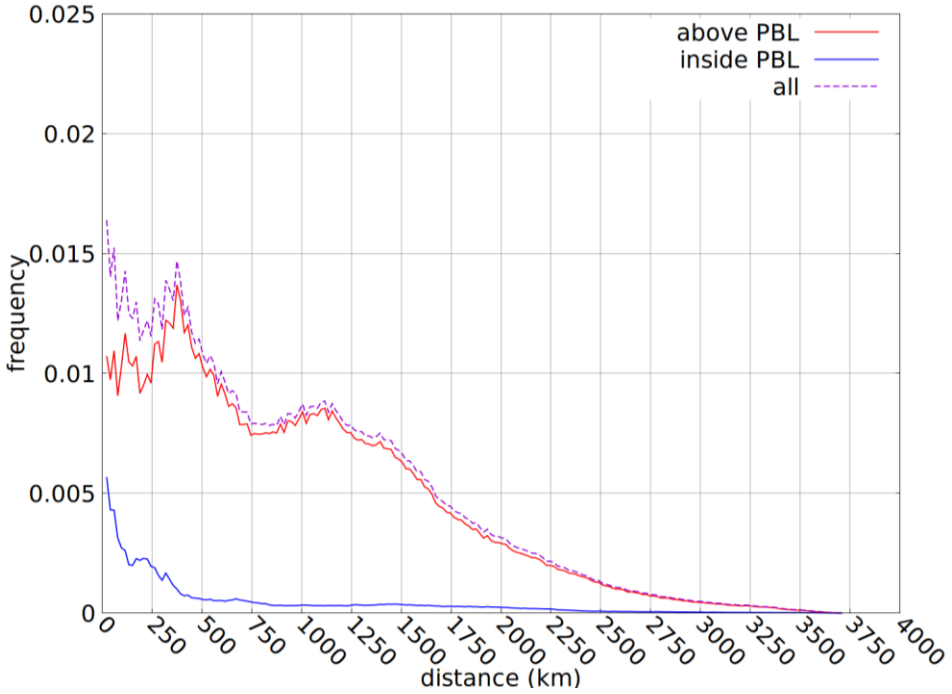

Figure 5.28 KQGR glacier: distribution graph of the trajectories relative frequency (June 2021).

The contour plots of KQGR glacier for June 2021 (Figure 5.25, Figure 5.26, Figure 5.27) show that the signal has a South-South-East direction, while in the reference article the main signal comes from the South direction. In the distribution graph (Figure 5.28) it is shown that the travelled distance of the particles inside the PBL is below 500 km, where most of the particles travelled up to 300-400 km, coming across to different populated areas of Nepal, India and Bhutan, and particularly meeting the capital and most populated city of Bhutan, Thimphu, with a population density of about 4390 inhabitants/km^2[7]. All these regions represent an area for the research of possible short-range sources (Figure 5.35a). The particles above the PBL travel for about 2500 – 2750 km and a peak as regards this curve can be noticed between 300 and 400 km from the receptor. This increase in the relative frequency can be seen also on the contour plot when changing the intervals of representation and obtaining the following output (Figure 5.29) that suggests an accumulation area for the particles travelling above the PBL that can be explained with the meteorological data already presented for the passage area from Nepal to the TP, from Figure 5.14 to Figure 5.19. For the long-range transport, from Figure 5.26 the main part of the trajectories travel in the range of 1000 km, and over a part of India, Nepal and Myanmar (Figure 5.35b).

[7] Thimphu - Wikipedia

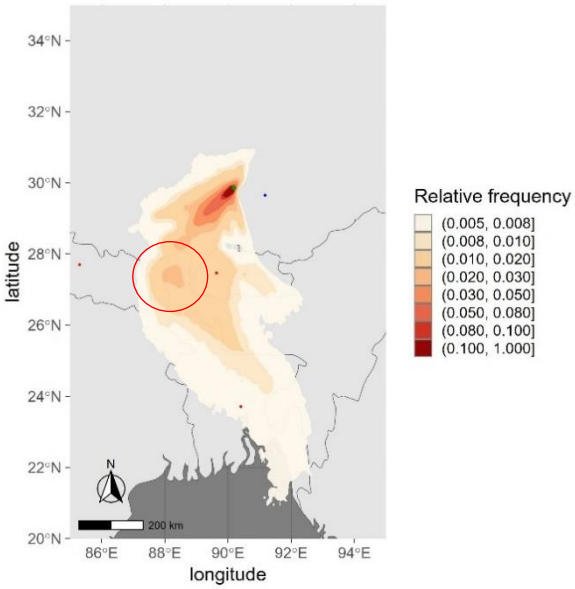

Figure 5.29 Visualisation of the spike on the contour plot.

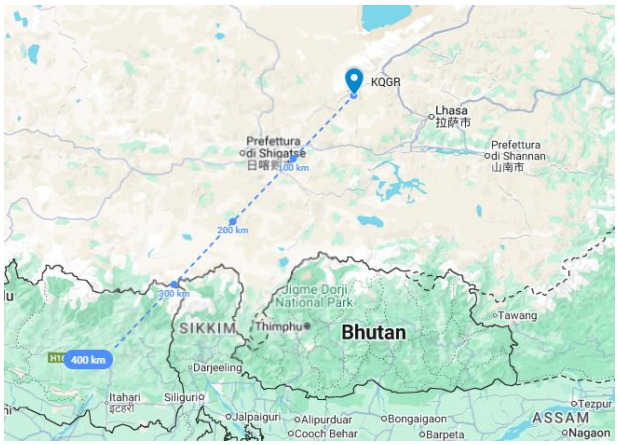

Figure 5.30 Distance of the area of the spike from KQGR glacier.

KQGR glacier, April 2022

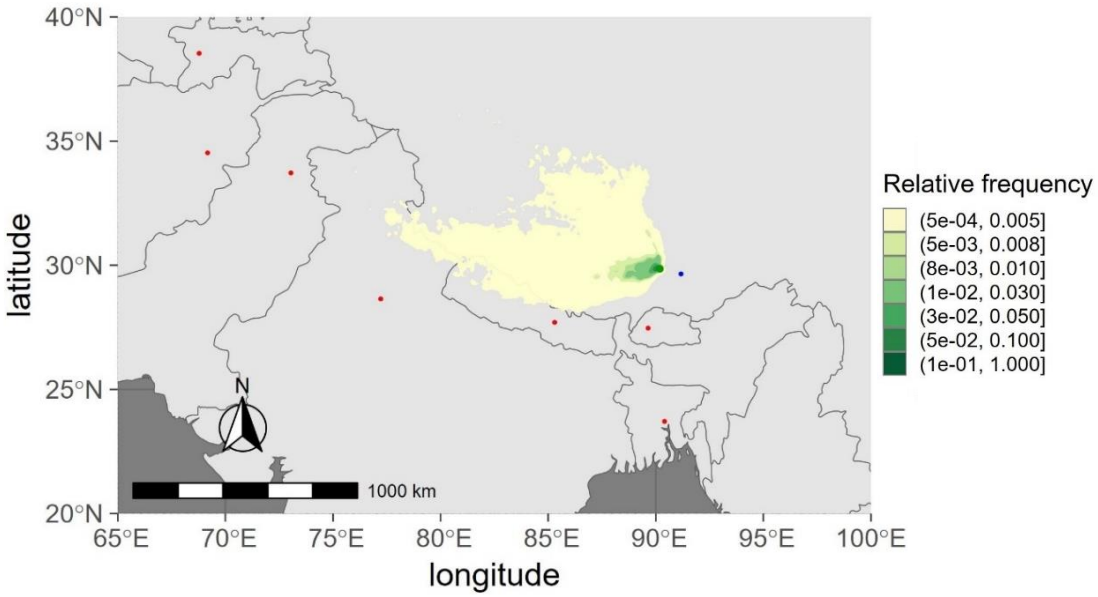

Figure 5.31 KQGR glacier contour plot of the trajectories relative frequency: particles travelling inside the PBL (April 2022). The green point represents the receptor, the blue point represents the city of Lhasa, the red points represent the capitals of the States of the area. Zoomed image with respect the simulation domain.

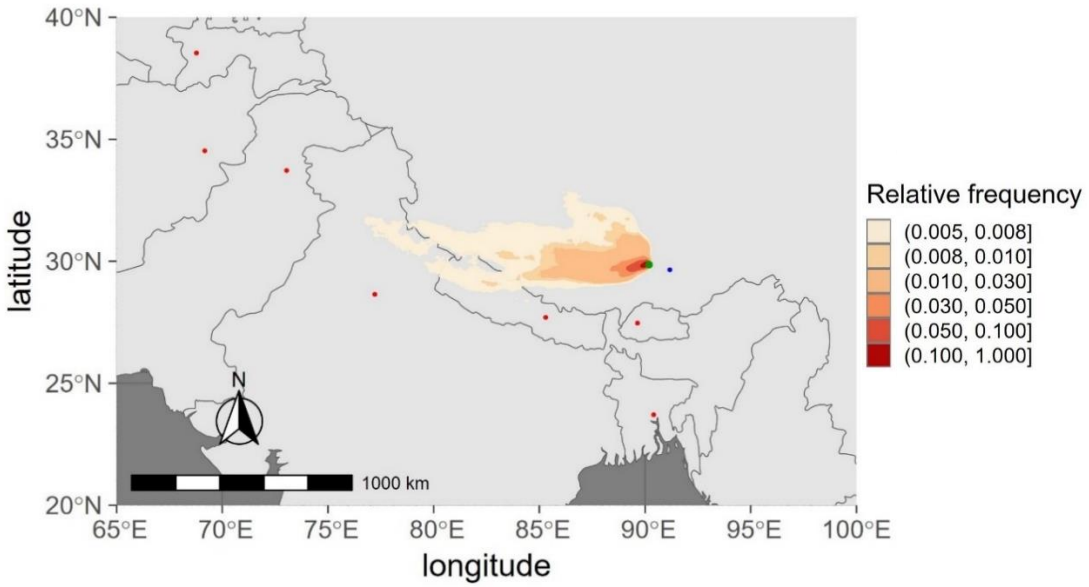

Figure 5.32 KQGR glacier contour plot of the trajectories relative frequency: particles travelling above the PBL (April 2022). The green point represents the receptor, the blue point represents the city of Lhasa, the red points represent the capitals of the States of the area. Zoomed image with respect the simulation domain.

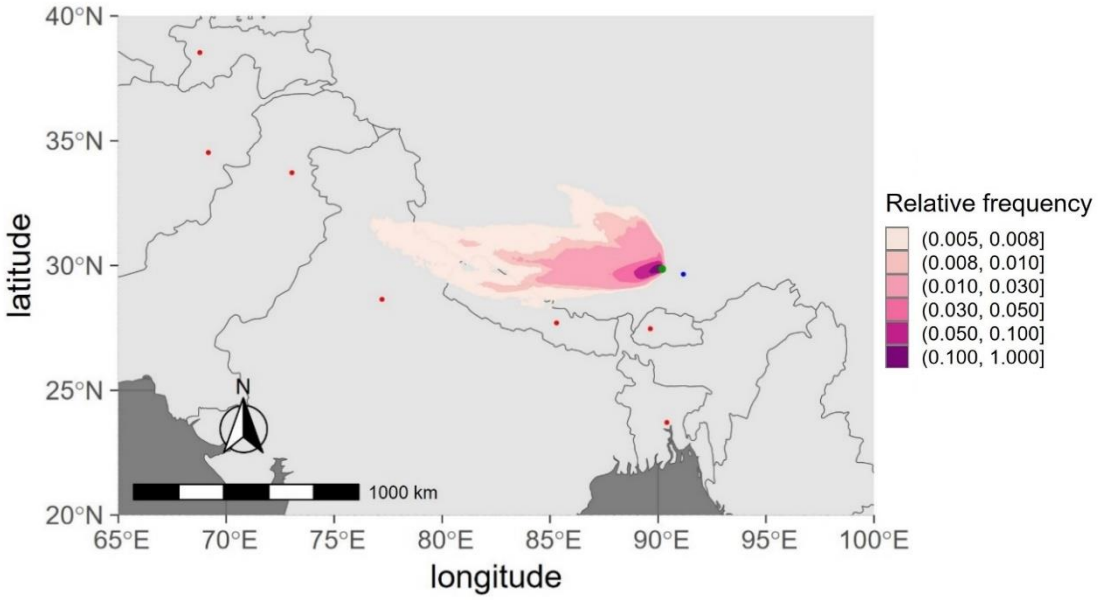

Figure 5.33 KQGR glacier contour plot of the trajectories relative frequency: all particles (April 2022). The green point represents the receptor, the blue point represents the city of Lhasa, the red points represent the capitals of the States of the area. Zoomed image with respect the simulation domain.

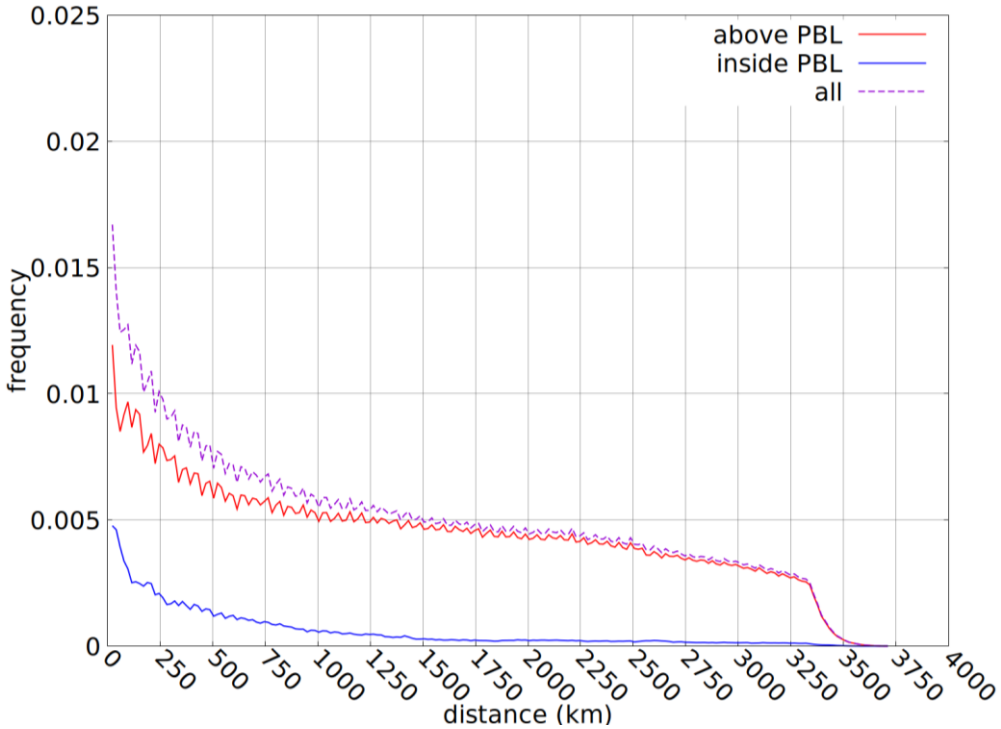

Figure 5.34 KQGR glacier: distribution graph of the trajectories relative frequency (April 2022).

For April 2022, and about the KQGR glacier, it can be seen in the contour plots (Figure 5.31, Figure 5.32, Figure 5.33) that the air masses come mainly from the West direction (same result as the reference article). The travelled distance for most of the particles inside the PBL is about 500 km and the particles above the PBL travel for about 3250 km (Figure 5.34). As regards possible short-range sources, in the reference article the city of Lhasa is mentioned as possible source of MPs for the glacier in exam for its distance of about 100 km from it. From the obtained results with the simulations of this work, it can be noticed that, even if the travel distance of the particles inside the PBL is higher than the distance between Lhasa and the glacier, the signal does not intercept the city since it comes from the west, while Lhasa is found eastward. For this reason, the city of Lhasa could not be identified as a possible short-range source for this specific case. In the same area of interest, only the prefecture of Shigatse, that is less than 150 km far from the glacier, can be indicated as possible source of MPs, but given its minimal density population of about 4 ab./km^2[8] it is reasonable to think that it would play a limited role as MP source (Figure 5.35aFigure 5.35). Apart from that, no other significant short-range source could be identified in this region. For the long-range transport, from Figure 5.32, the main part of the trajectories travel in the range of 1000 km coming from India and Nepal (Figure 5.35b).

[8] Prefettura di Shigatse - Wikipedia

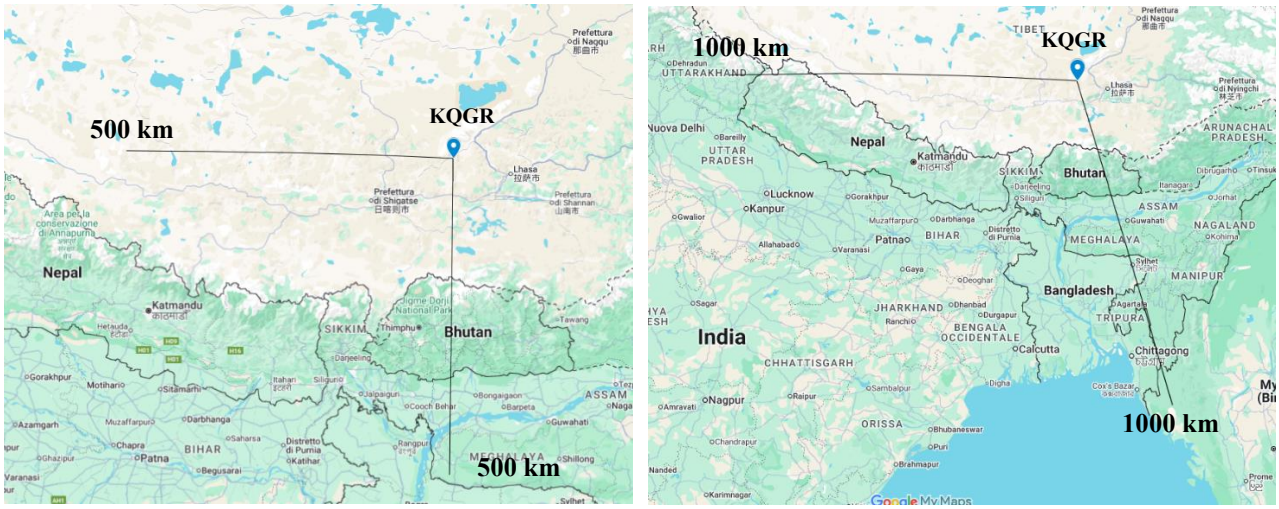

Figure 5.35 KQGR glacier: a) Area of impact of a possible short-range source given a travelling distance for the particles travelling inside the PBL the direction of provenience read in the relative contour plot, b) area of provenience of the particles travelling above the PBL in the range of 1000 km (Source: Google – My Maps).

AL glacier

AL glacier, June 2021

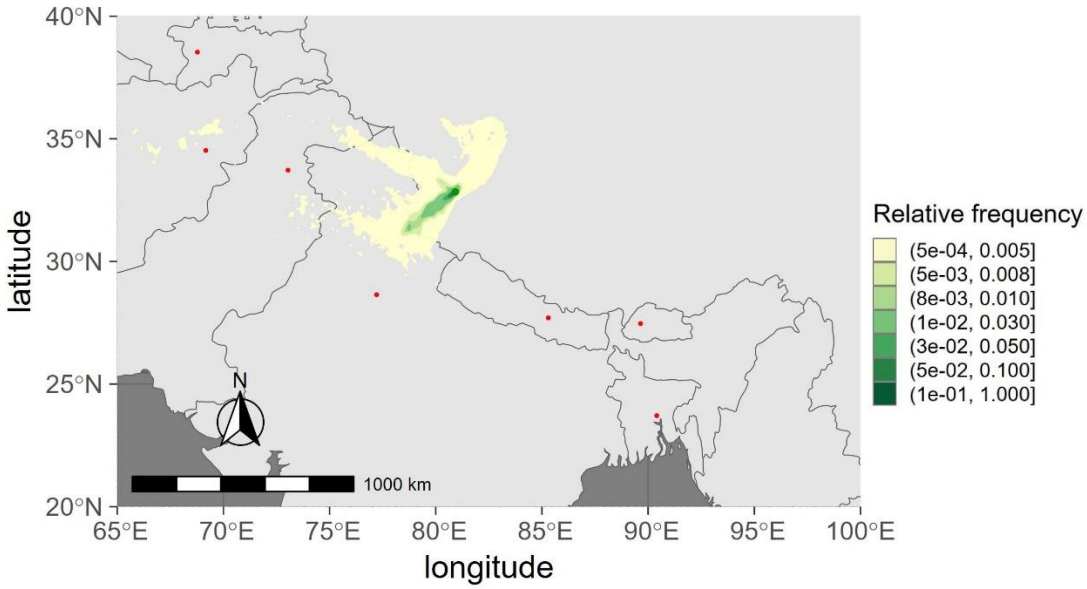

Figure 5.36 AL glacier contour plot of the trajectories relative frequency: particles travelling inside the PBL (June 2021). The green point represents the receptor, the red points represent the capitals of the States of the area. Zoomed image with respect the simulation domain.

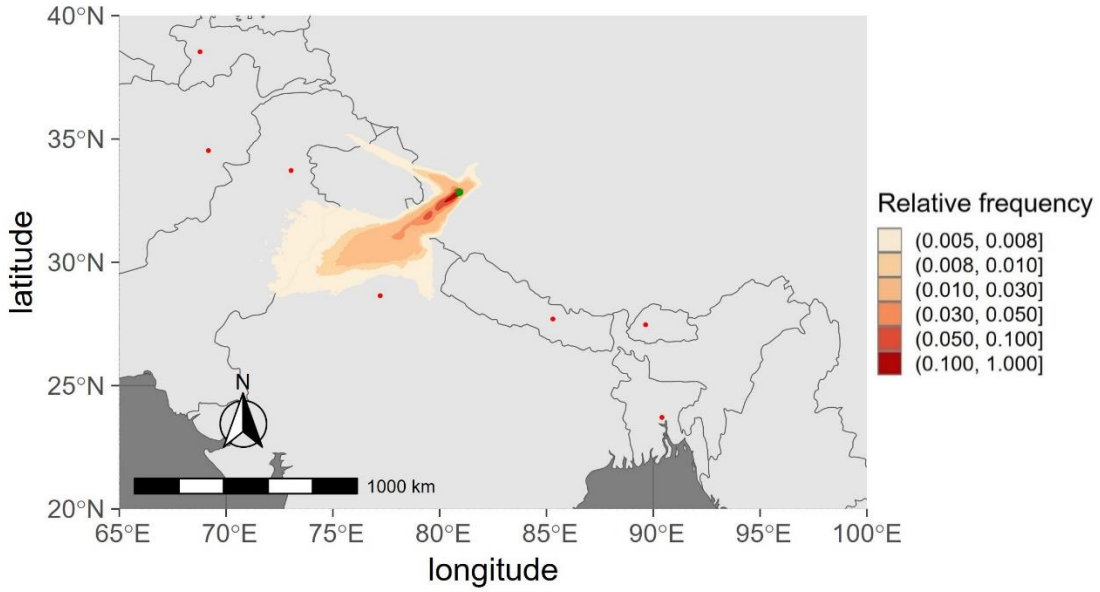

Figure 5.37 AL glacier contour plot of the trajectories relative frequency: particles travelling above the PBL (June 2021). The green point represents the receptor, the red points represent the capitals of the States of the area. Zoomed image with respect the simulation domain.

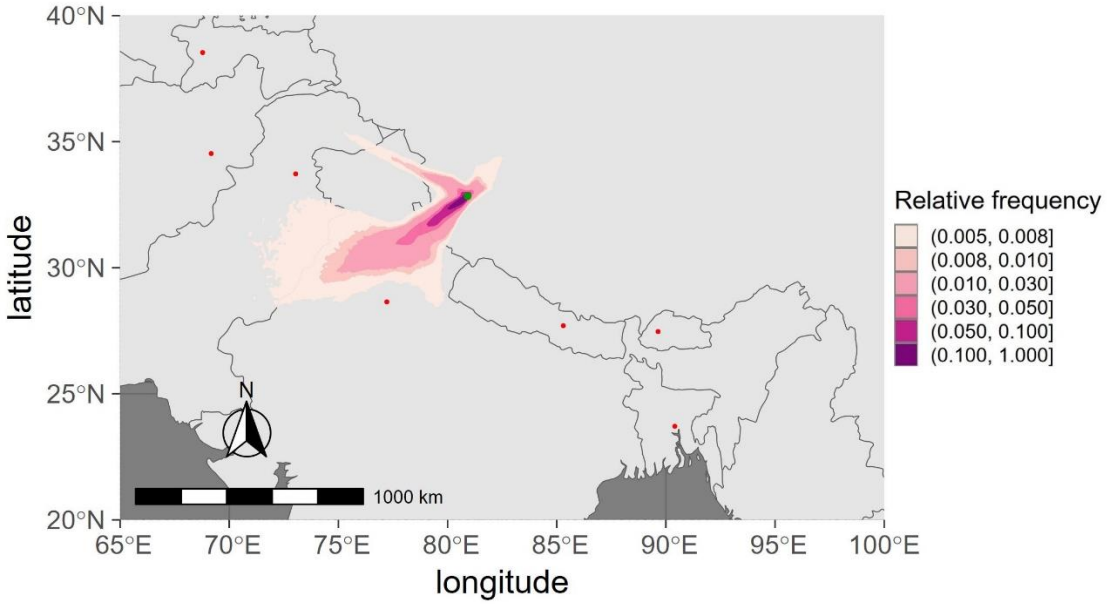

Figure 5.38 AL glacier contour plot of the trajectories relative frequency: all particles (June 2021). The green point represents the receptor, the red points represent the capitals of the States of the area. Zoomed image with respect the simulation domain.

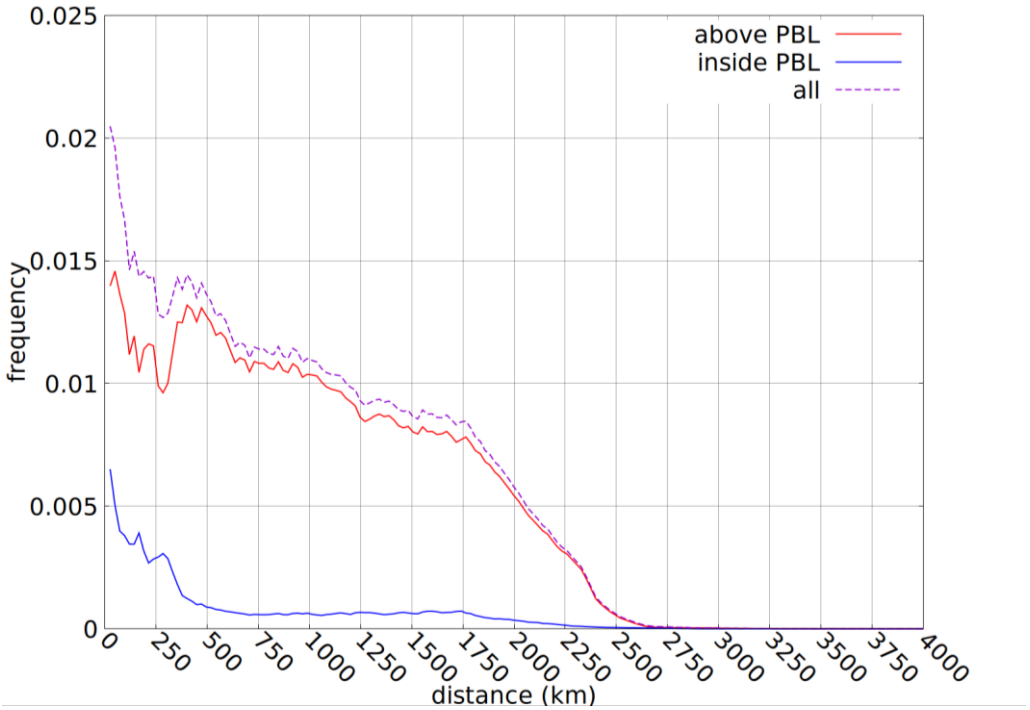

Figure 5.39 AL glacier: distribution graph of the trajectories relative frequency (June 2021).

For AL glacier, in June 2021 a main signal is seen from the South-West direction in accordance with the article, and in addition, a smaller signal is seen coming also from the North-West direction (Figure 5.36, Figure 5.37, Figure 5.38). The travelled distance of particles inside the PBL is about 250-500 km, the distance of the particles travelling above the PBL is between 2250 and 2500 km (Figure 5.39). For the research of possible short-range sources of MPs, it is noticed that the signal of the particles travelling inside the PBL passes the boundary of North India and meets different populated areas that are consequently to be kept into account as potential contributing MP source (Figure 5.44a). As regards the long-range transport, from Figure 5.37 it is noticed that the main part of the trajectories travel in the range of 1000 km mostly coming from India (see Figure 5.44b).

AL glacier, April 2022

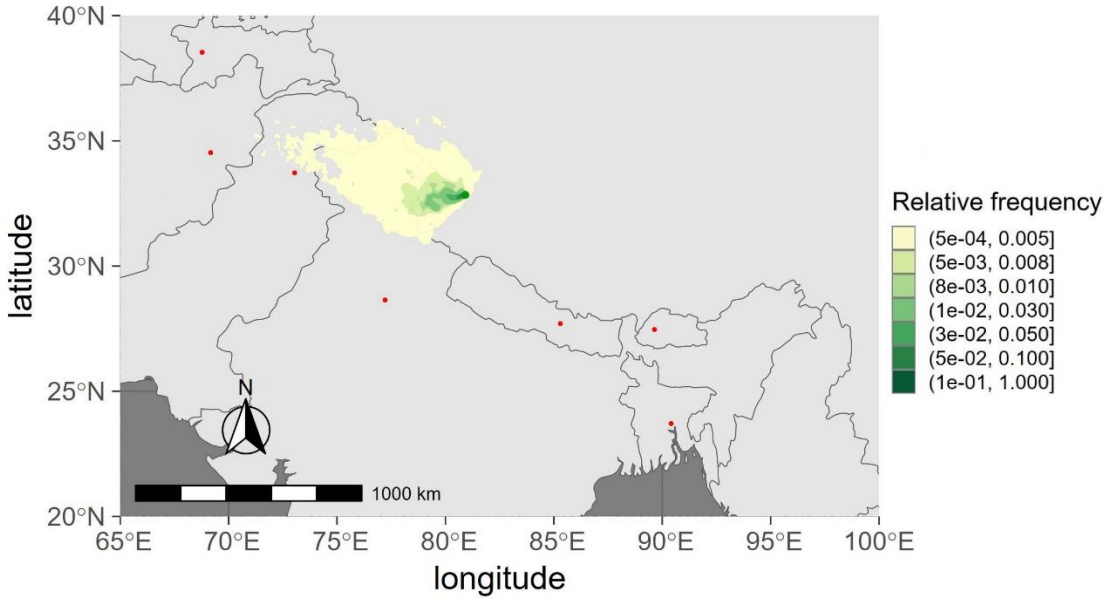

Figure 5.40 AL glacier contour plot of the trajectories relative frequency: particles travelling inside the PBL (April 2022). The green point represents the receptor, the red points represent the capitals of the States of the area. Zoomed image with respect the simulation domain.

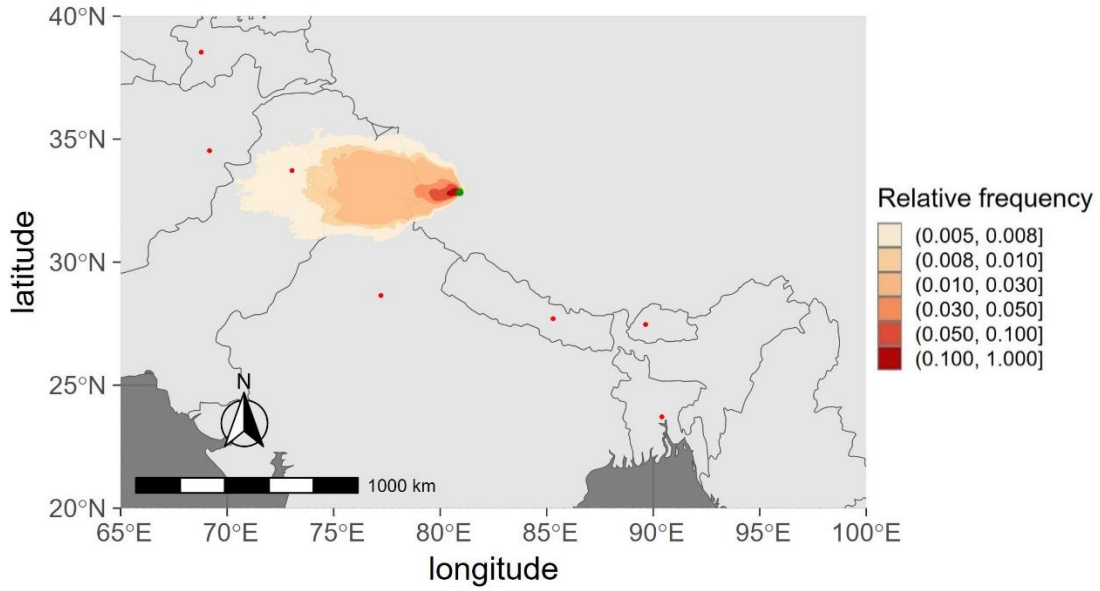

Figure 5.41 AL glacier contour plot of the trajectories relative frequency: particles travelling above the PBL (April 2022). The green point represents the receptor, the red points represent the capitals of the States of the area. Zoomed image with respect the simulation domain.

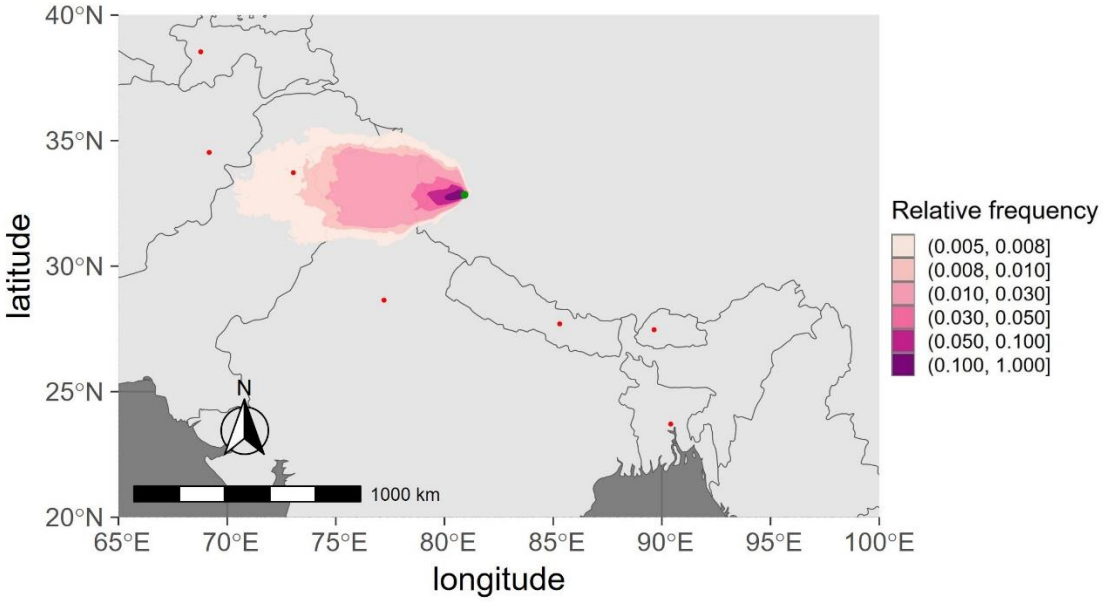

Figure 5.42 AL glacier contour plot of the trajectories relative frequency: all particles (June 2021). The green point represents the receptor, the red points represent the capitals of the States of the area. Zoomed image with respect the simulation domain.

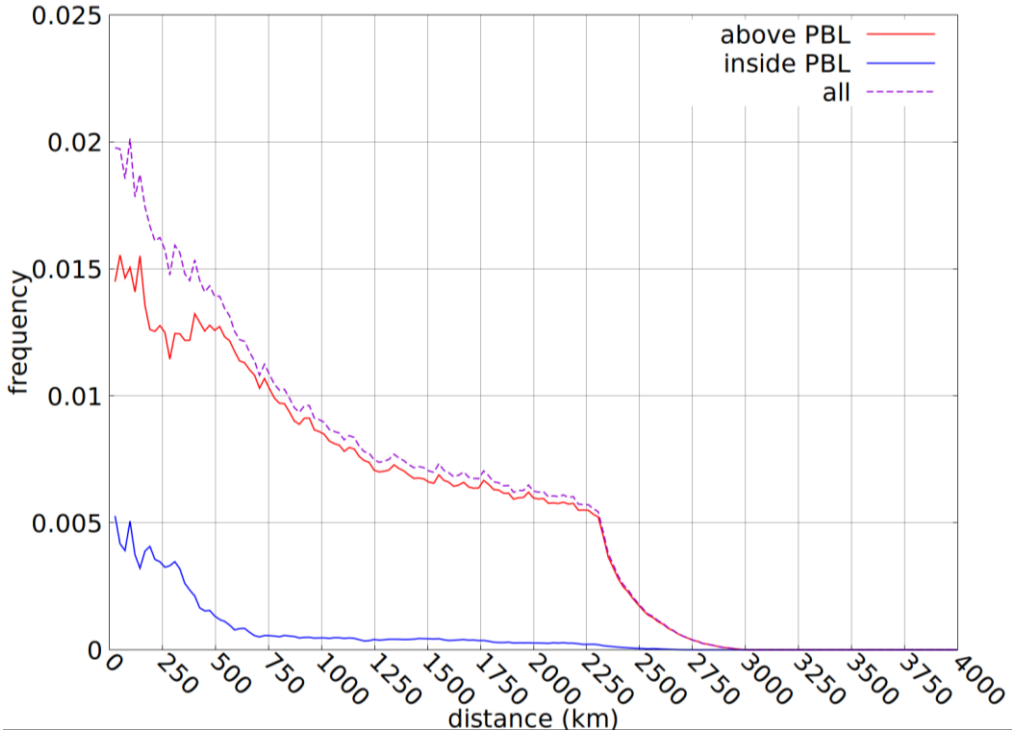

Figure 5.43 AL glacier: distribution graph of the trajectories relative frequency (April 2022).

In April 2022, the masses of air travelling towards AL glacier come from the West (Figure 5.40, Figure 5.41, Figure 5.42). In the article, for the same months a similar signal was seen coming from the West and South-West. Most of the particles inside the PBL travel for 250-500 km, most of the particles above the PBL travel for about 2250-2500 km (Figure 5.43). For the research of possible short-range sources of MPs, in this case the cross of the boundary of North India of particles travelling inside the PBL is less marked than the one of the previous month. Anyway, the influence of populated areas of North India is still to be kept into account (Figure 5.44a). As regards the long-range transport, it is noticed that the main part of the trajectories travel in the range of 1000 km, mostly coming from India and Pakistan (Figure 5.41 and see Figure 5.44b).

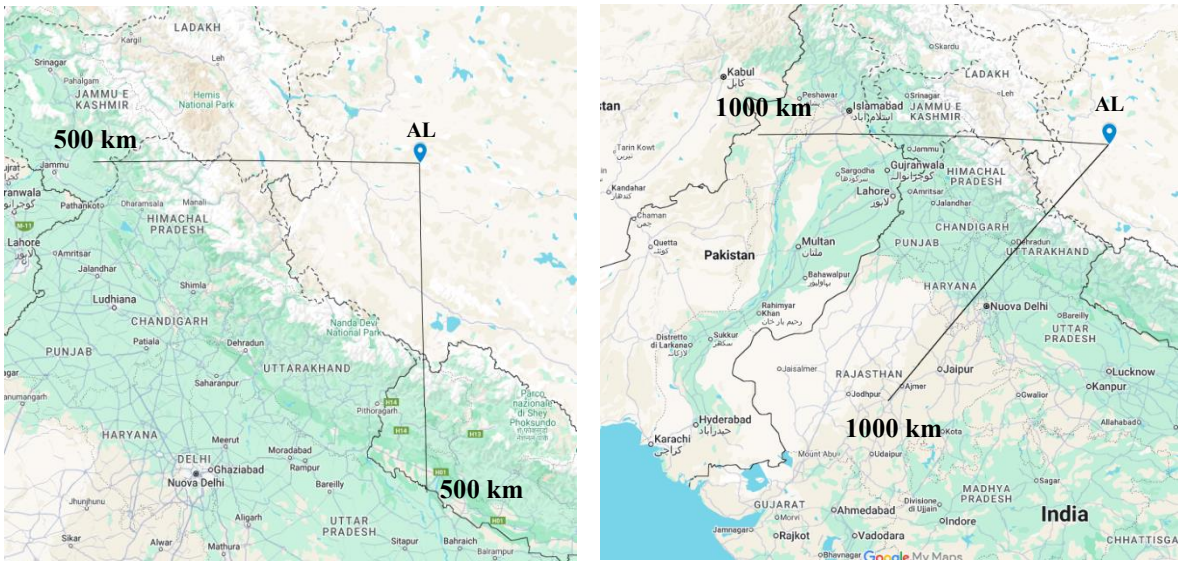

Figure 5.44 AL glacier: a) Area of impact of a possible short-range source given a travelling distance for the particles travelling inside the PBL the direction of provenience read in the relative contour plot, b) area of provenience of the particles travelling above the PBL in the range of 1000 km (Source: Google – My Maps).

Comments

The study of the area of the Tibetan Plateau in different periods of the year and in different regions of it allows to make some considerations about the possible provenience of the MPs found in the studied glaciers. The first aspect that can be noticed evaluating the output of these simulations is the general correspondence and match between our results, derived with MILORD model, and the ones of the reference article (Wang et al., 2024), attained with HYSPLIT model, as regards the direction of provenience of the air masses in the areas of the three glaciers studied. This, despite the differences and uncertainties regarding how the simulations were set by the authors of the reference article, as introduced in Section 3. As regards the distinction between the pre-monsoon and monsoon period, represented respectively by the month of April and June, it is possible to notice that during the pre-monsoon period the signal mostly comes from the West direction, while during the monsoon period the signal comes mostly from the South-West direction. For all the three studied glaciers it turned out that, for a simulation of the duration of one month, most of the particles travelling inside the PBL comes from distances up to 500-750 km, and in most cases the majority of them remains under the 250-500 km of distance from the receptor. The research of possible short-range sources of MPs must be done in this range, and if no significant sources can be indicated, it means that for the glacier in exam the long-range transport of MPs can be considered the main responsible for the MPs found on it. From the output obtained, it results that for DKMD and KQGR glaciers, the long-range transport could play a significant role on MP atmospheric transport, while for the AL glacier also the short-range one has to be kept into account. In particular, for DKMD and KQGR glaciers, and for the pre-monsoon period, the one assessed in the reference article as the more relevant for the pollutant transport in the atmosphere, it can be noticed that the only possible source of MPs could be the National Highway 109. Apart from it, the particles travelling inside the PBL do not meet any possible significant source for even more than 500 km, the estimated travel distance. In addition, considering the relative distribution graphs, in these two cases, the output indicates that for the particles travelling above the PBL, thus indicative of the long-range transport, there is a constant trend of the values of the relative frequencies in the range between 250 km and 3500 km. Consequently, it can be stated that, for these two glaciers and for the pre-monsoon period, eventual MPs found in the area can have travelled up to 3500 km. A similar behaviour is found for the DKMD glacier in the monsoon period, while the signal of the same period for KQGR glacier leads to consider that the presence of some short-range sources is possible since it meets some populated area of India, Nepal and Bhutan, within a distance of 500 km. As regards the AL glacier, both the signals of the month of April and June find populated areas of India within the estimated travel distance of the particles inside the PBL. So, in this case, the information emerging from the contour plots and from the distribution graphs help to identify the area of research of a short-range source. Regarding the long-range transport specifically, it is noticed that the contour plots of the relative frequency for the particles travelling above the PBL describe their main spatial resolution, within a distance of 1000 km, starting from the minimum value in the considered ranges. However, the distribution graphs show that the totality of those particles travel for longer distances (mentioned also in this paragraph). For this reason, a further investigation about the number of trajectories is done to study also the provenience of those particles that are not represented in the previous plots. The resulting images are reported in Appendix 2. They enable identifying the long-range pathways followed by the air masses before arriving to the receptor sites, capturing the effect of the circulation at the detected longer distances, in the simulation domain.

5.2. Pacific Ocean

In this paragraph the output obtained with the backward simulations done for the area of the North Pacific Ocean is reported. Three areas of the Ocean are investigated, each one represented by a starting point for the model simulations as described in chapter 3.2. All the simulations performed for this geographical area are done using ECMWF data resolution of 0.25°x0.25° and a number of 80 time steps per day (corresponding to 1080 *s* each time step). The simulations are performed for periods of time of 2 days, 1 week, 1 month for the nearshore, pelagic and remote areas. For each zone of investigation, and for each period of simulation, the three relative contour plots and the frequency distribution graphs are elaborated. The images about all the particles travelling are reported followed by the images of the particles travelling inside the PBL coupled with the images of the particles travelling above the PBL, for the three time intervals of the simulations. Then, also the distribution graphs are reported.

Nearshore area

All particles travelling both above and inside the PBL:

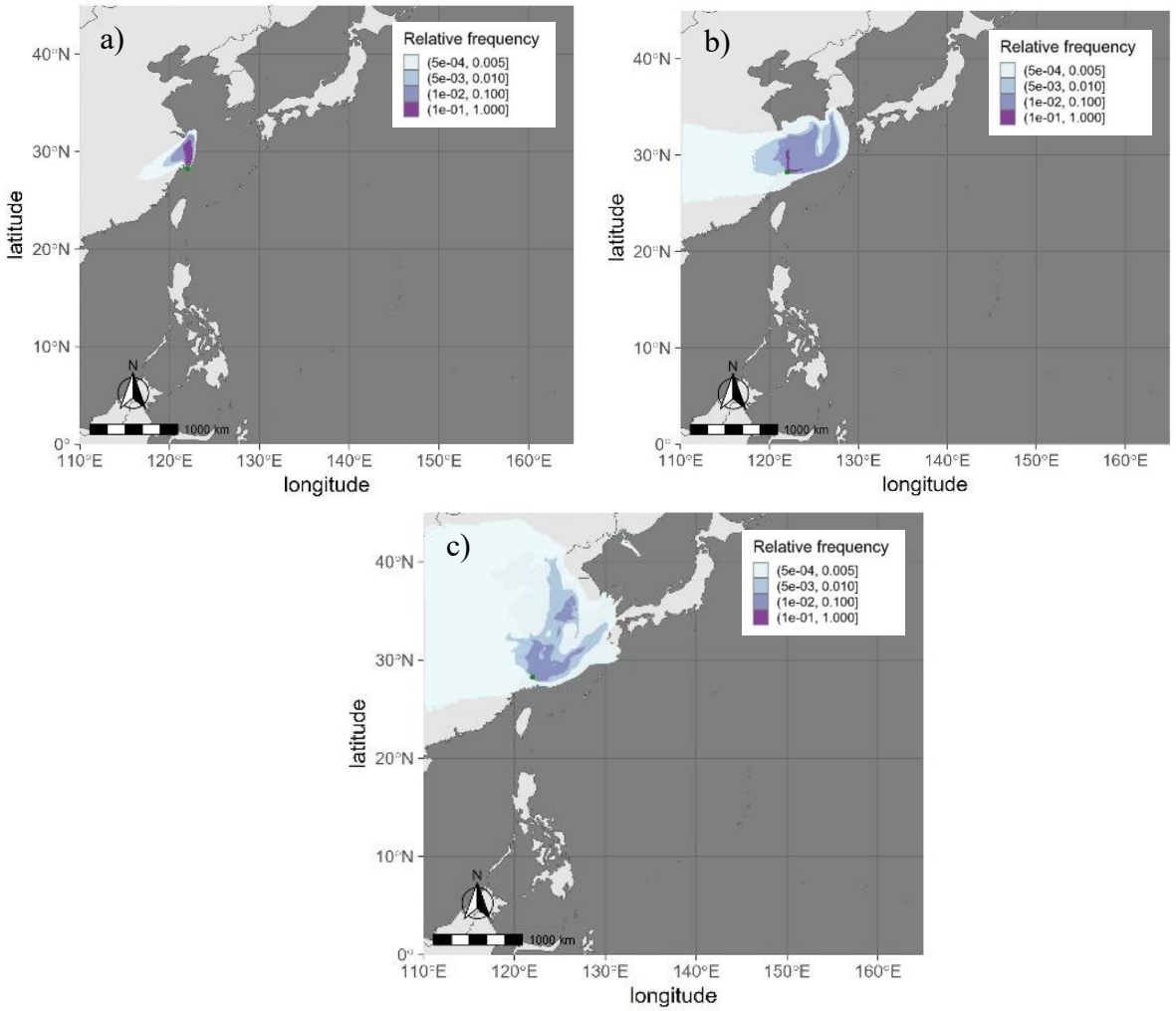

Figure 5.45 Simulation about all particles travelling both above and inside the PBL for the nearshore area. The green point represents the receptor point. a) two days simulation, b) one week simulation, c) one month simulation.

The images about all particles travelling (Figure 5.45) show for the three periods of simulation that the masses of air mainly come from the West, and so from the continent.

Particles travelling inside and above the PBL:

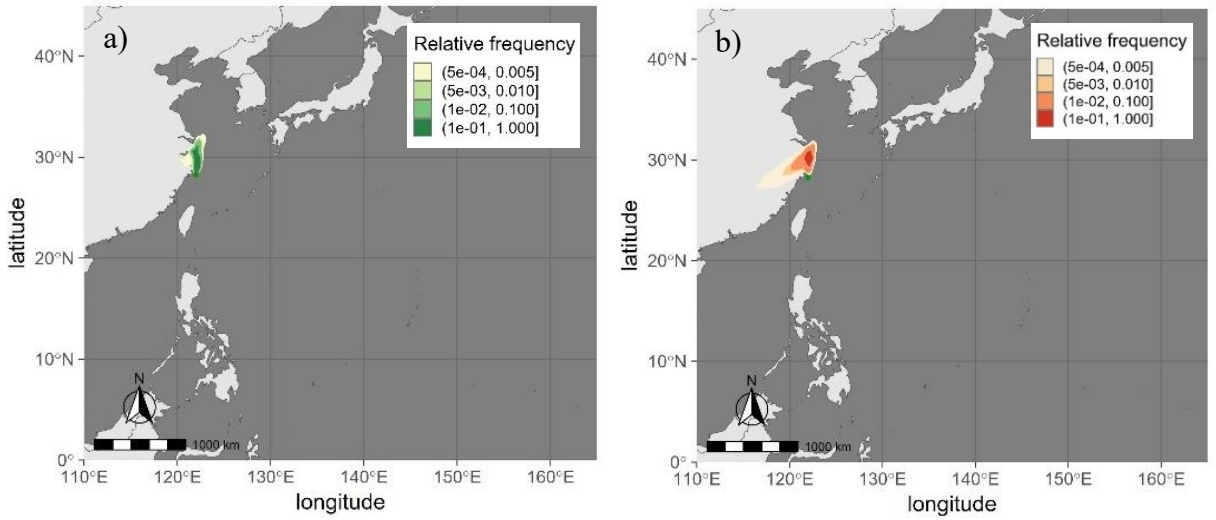

Figure 5.46. Two days simulation about the nearshore area. The green point represents the receptor point. a) Particles travelling inside the PBL, b) particles travelling above the PBL.

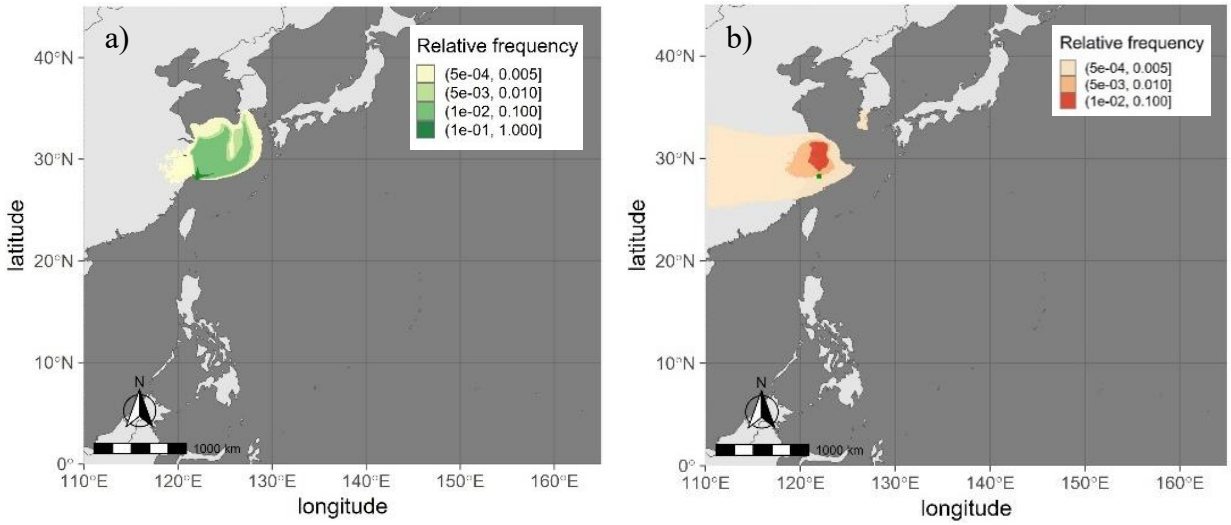

Figure 5.47 One week simulation about the nearshore area. The green point represents the receptor point. a) Particles travelling inside the PBL, b) particles travelling above the PBL.

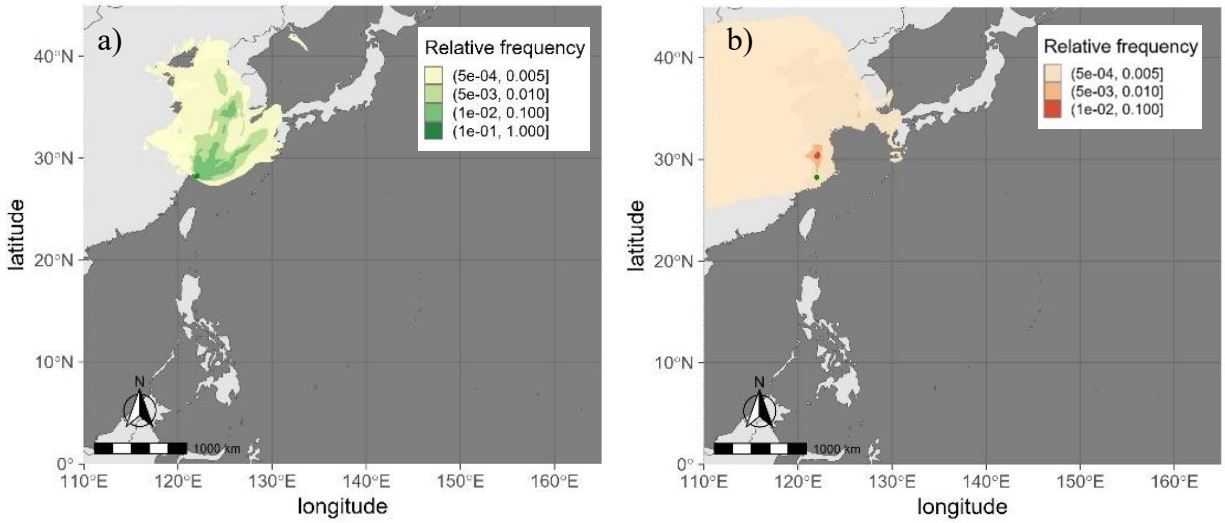

Figure 5.48 One month simulation about the nearshore area. The green point represents the receptor point. a) Particles travelling inside the PBL, b) particles travelling above the PBL.

The output of the simulations about the particles travelling inside the PBL shows that the masses of air mostly come from the North direction, while the output about the particles travelling above the PBL shows a predominant West direction. In both cases the particles get to the receptor from the continental area (Figure 5.46, Figure 5.47, Figure 5.48).

Distribution graphs:

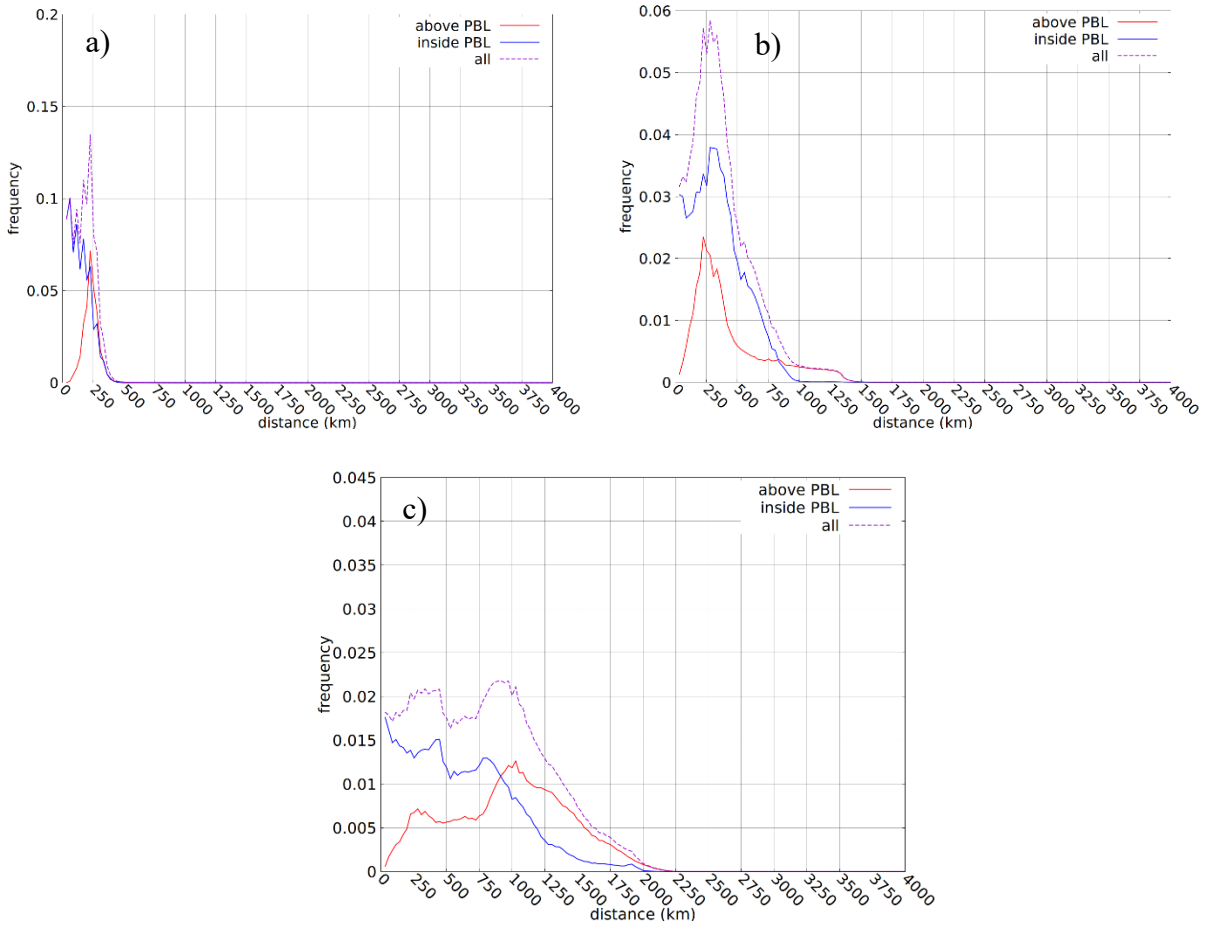

Figure 5.49 Distribuiton graphs for the nershore area. a) two days simulation, b) one week simulation, c) one month simulation.

From the distribution graphs about the relative frequency of the trajectories (Figure 5.49), it can be noticed that longer times of simulation allow the particles to be displaced for longer distances. Specifically, the graphs show that when travelling for two days, both the particles travelling inside the PBL and the particles travelling above it can reach around 250-500 km (Figure 5.49a). For the simulation of a week, it can be seen that the particles traveling inside the PBL cover around 1000 km, while the particles above it arrive at the receptor from up to 1250-1500 km (Figure 5.49b). At last, for the simulation of one month, the particles inside the PBL travel for around 2000 km, and the ones above it for around 2000-2250 km (Figure 5.49c). However, given that the area of provenience extends western to the boundary of the simulation domain, the distance travelled by the air masses may be longer than represented in the present simulation.

Pelagic area

All particles travelling both above and inside the PBL:

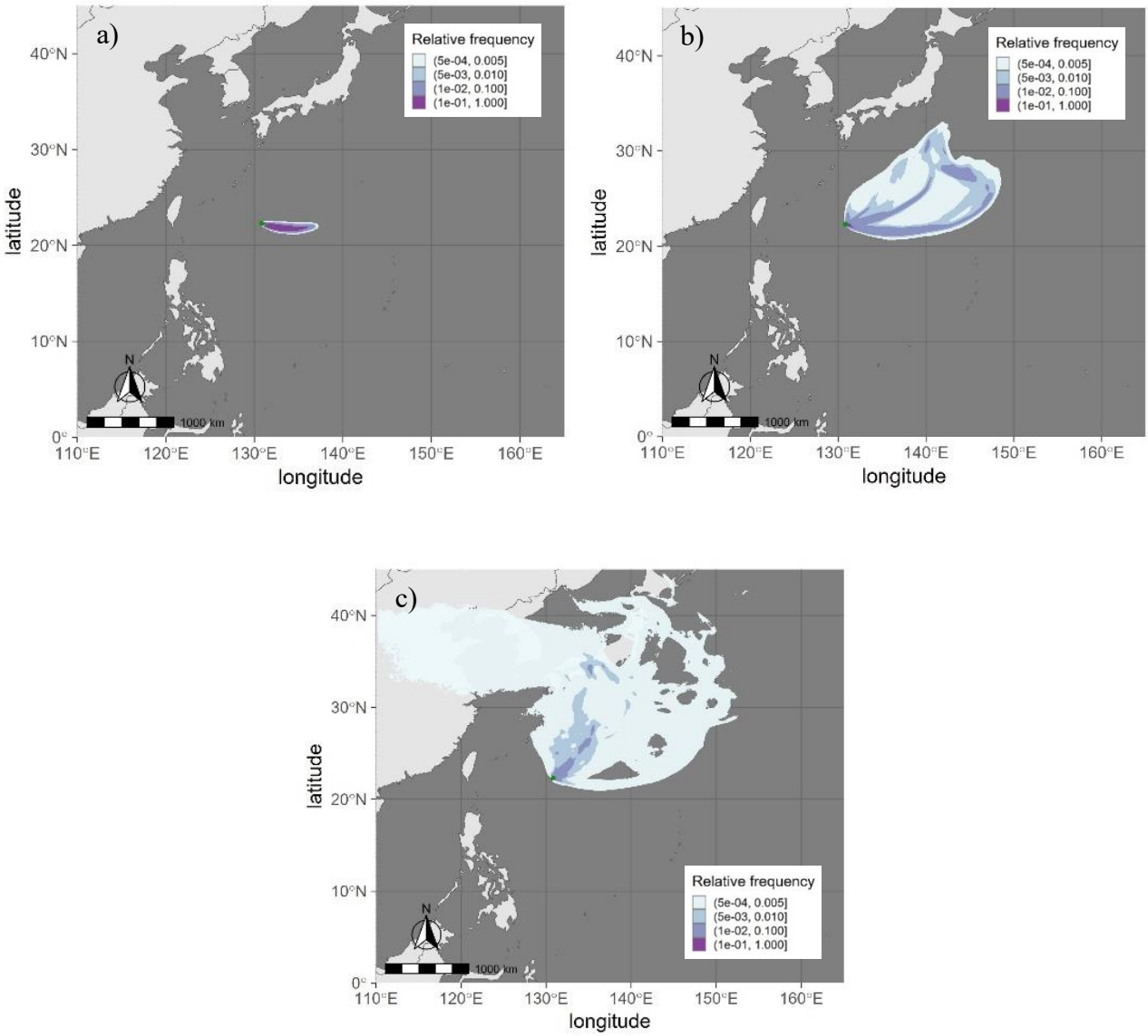

Figure 5.50 Simulation about all particles travelling both above and inside the PBL for the pelagic area. The green point represents the receptor point. a) two days simulation, b) one week simulation, c) one month simulation.

The images about all particles travelling (Figure 5.50) show that for the two-days simulation the masses of air come from the East direction, for the one-week simulation come from the East direction and from the North direction, and for the simulation of one month, the masses of air come from both the North direction and West direction, in particular highlighting the continental provenience for this last case.

Particles travelling inside and above the PBL:

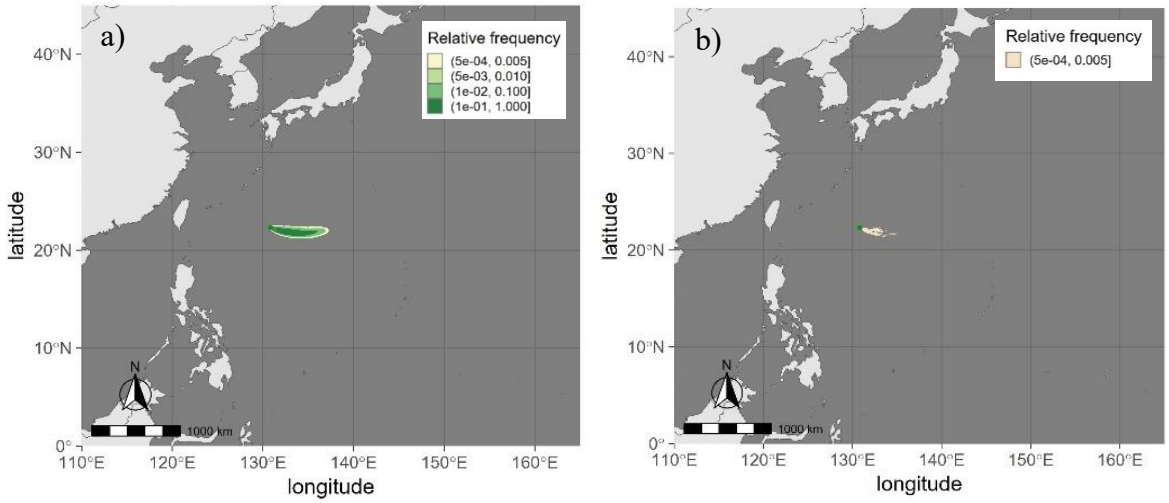

Figure 5.51 Two days simulation about the pelagic area. The green point represents the receptor point. a) Particles travelling inside the PBL, b) particles travelling above the PBL.

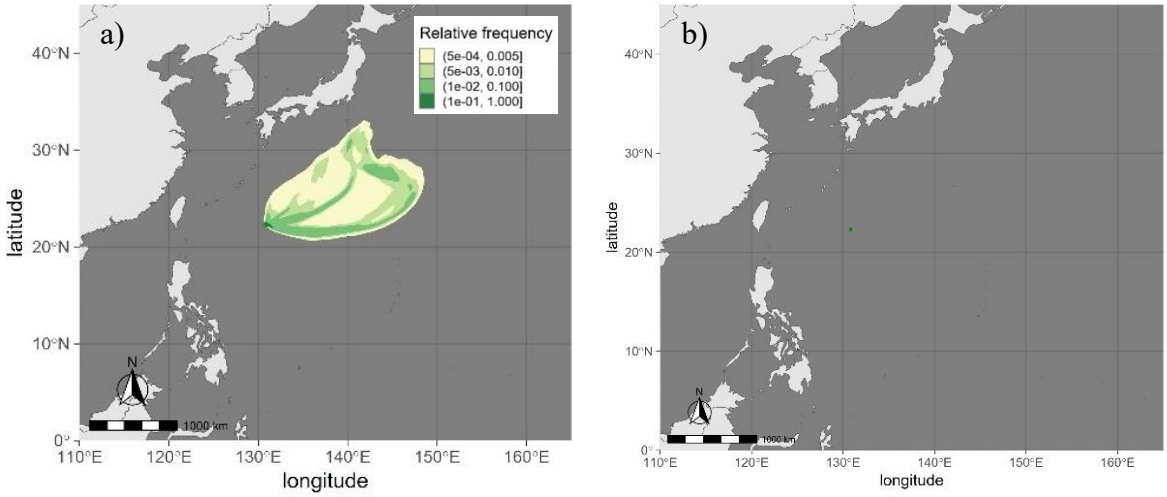

Figure 5.52 One week simulation about the pelagic area. The green point represents the receptor point. a) Particles travelling inside the PBL, b) particles travelling above the PBL.

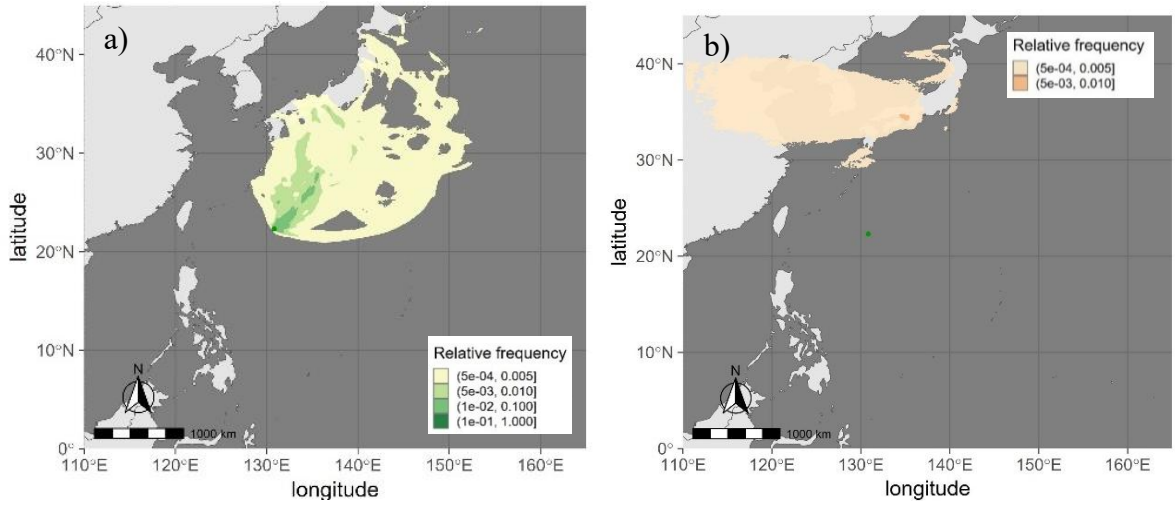

Figure 5.53 One month simulation about the pelagic area. The green point represents the receptor point. a) Particles travelling inside the PBL, b) particles travelling above the PBL.

For the pelagic area, and for the two-days and one-week simulations, the provenience of the particles inside the PBL is oceanic and coming from the East direction. Only in the one-month simulation also a continental provenience is seen from North and North-East directions, since at longest distances the air masses arrive from Japan, thus from land environment where anthropic activities play an important role in pollution release. The signal of the particles travelling above the PBL is very low, it can be noticed only in the one-month simulation where it has a continental provenience from the West direction, and does not meet the receptor. The particles above the PBL travel from the continent to Japan, where the signal ends up. So, it can be assumed that those particles travel up to Japan and in correspondence of its area they enter the PBL for the daily variations on its height, and reach the receptor travelling inside it. This particular behaviour can also be noticed in the following distribution graphs (Figure 5.54c).

Distribution graphs:

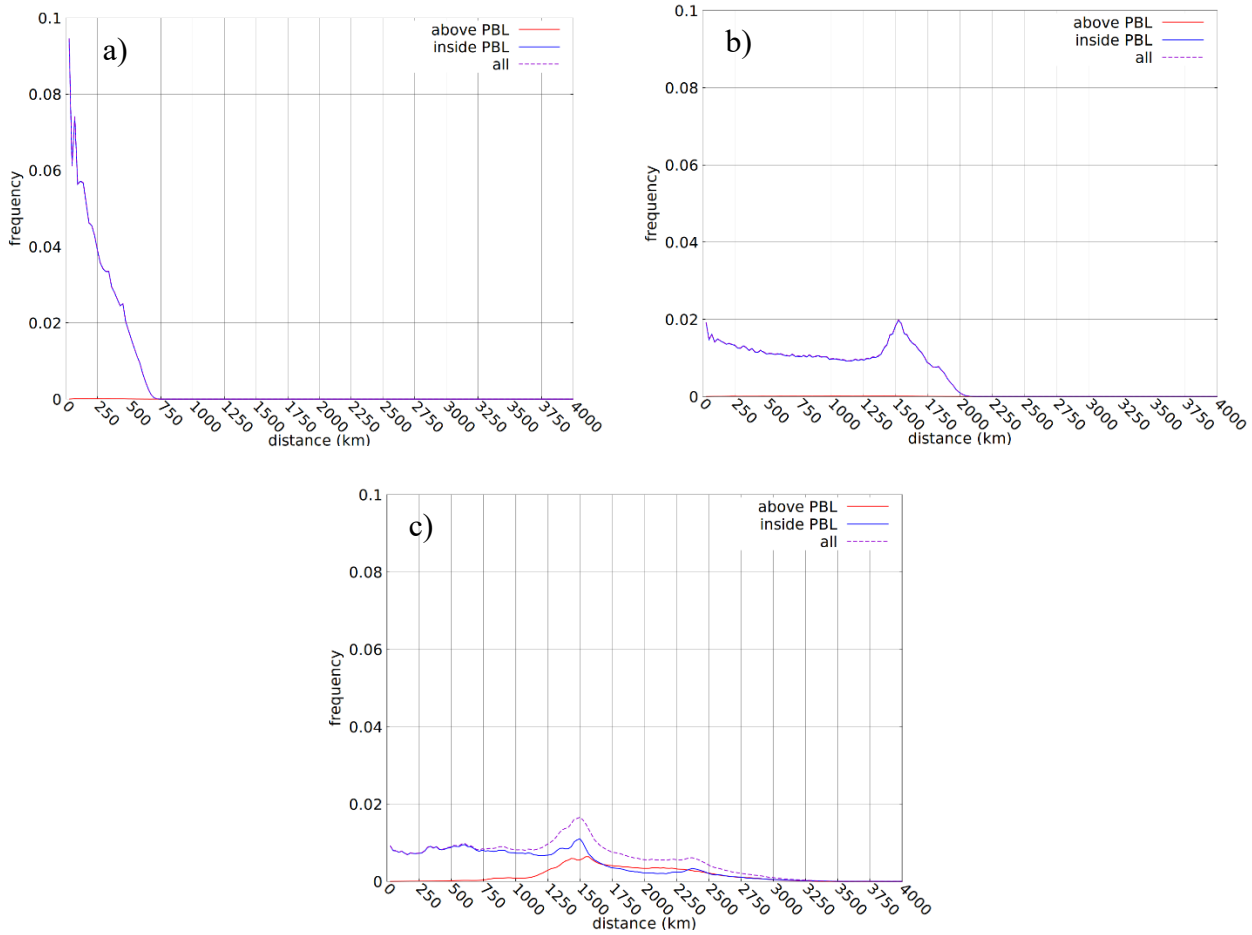

Figure 5.54 Distribuiton graphs for the pelagic area. a) two days simulation, b) one week simulation, c) one month simulation.

The relative frequency distribution graphs show that in the pelagic area the particles inside the PBL travel for around 750 km in the simulation of two days (Figure 5.54a), for around 2000 km for the simulation of one week (Figure 5.54b) and for around 3000 km for the simulation of one month (Figure 5.54c). As regards the particles travelling above the PBL, as already shown in the previous contour plots (from Figure 5.51 to Figure 5.53), also in these last graphs it is noticeable that the number of particles travelling above the PBL is relevant only in the case of the one month simulation in which they are detected between a minimum distance of 750 and a maximum of 2750-3000 km (Figure 5.54c). This result means that the particles that reach the receptor arrive at most from 3000 km and that they travel above the PBL up to 750 km from it. After that distance, no particles above

the PBL are seen, suggesting their passage from the free atmosphere to the PBL around that distance from the receptor.

Remote area

<u>All particles travelling both above and inside the PBL:</u>

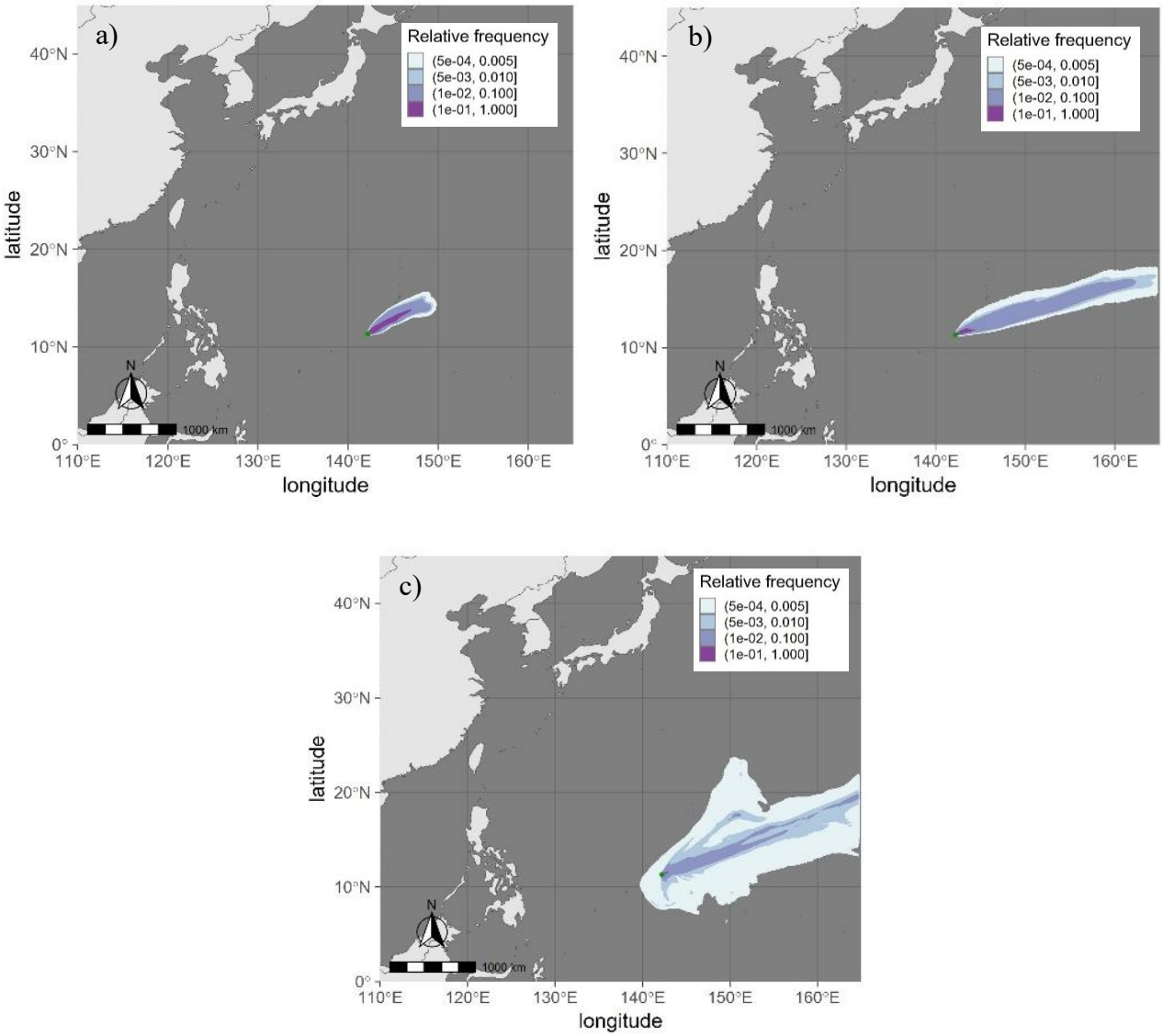

Figure 5.55 Simulation about all particles travelling both above and inside the PBL for the remote area. The green point represents the receptor point. a) two days simulation, b) one week simulation, c) one month simulation.

The images about all particles travelling (Figure 5.55) show for the three periods of simulation that the masses of air mainly come from the East direction, and so from the Ocean.

Particles travelling inside and above the PBL:

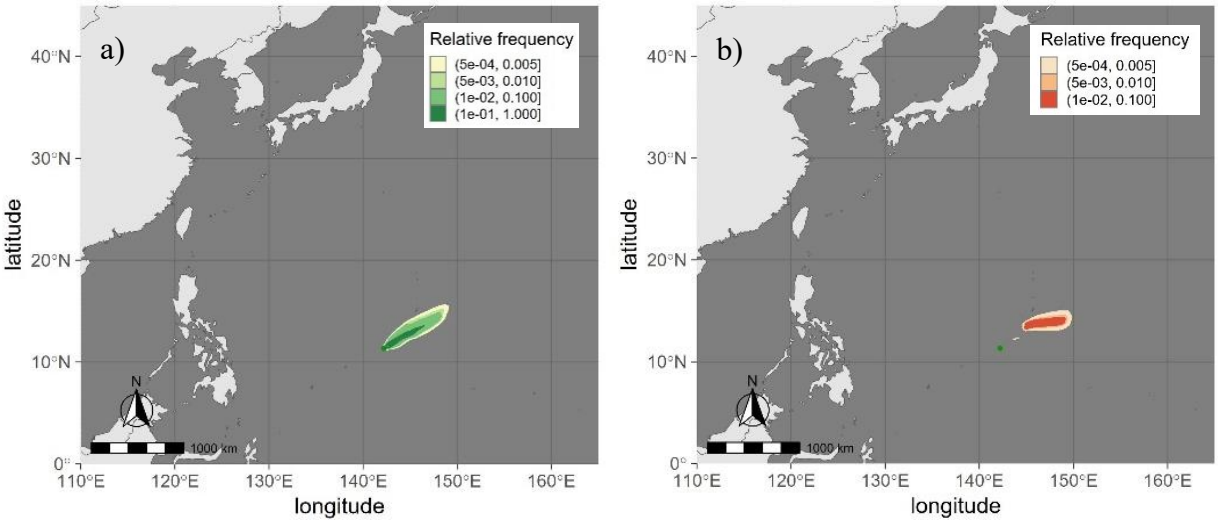

Figure 5.56 Two days simulation about the remote area. The green point represents the receptor point. a) Particles travelling inside the PBL, b) particles travelling above the PBL.

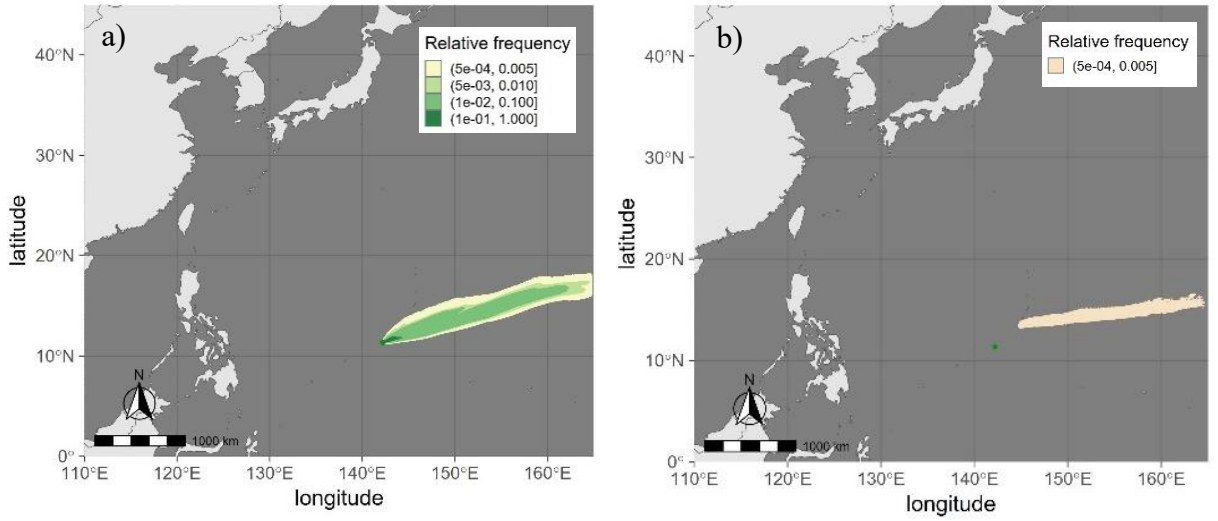

Figure 5.57 One week simulation about the remote area. The green point represents the receptor point. a) Particles travelling inside the PBL, b) particles travelling above the PBL.

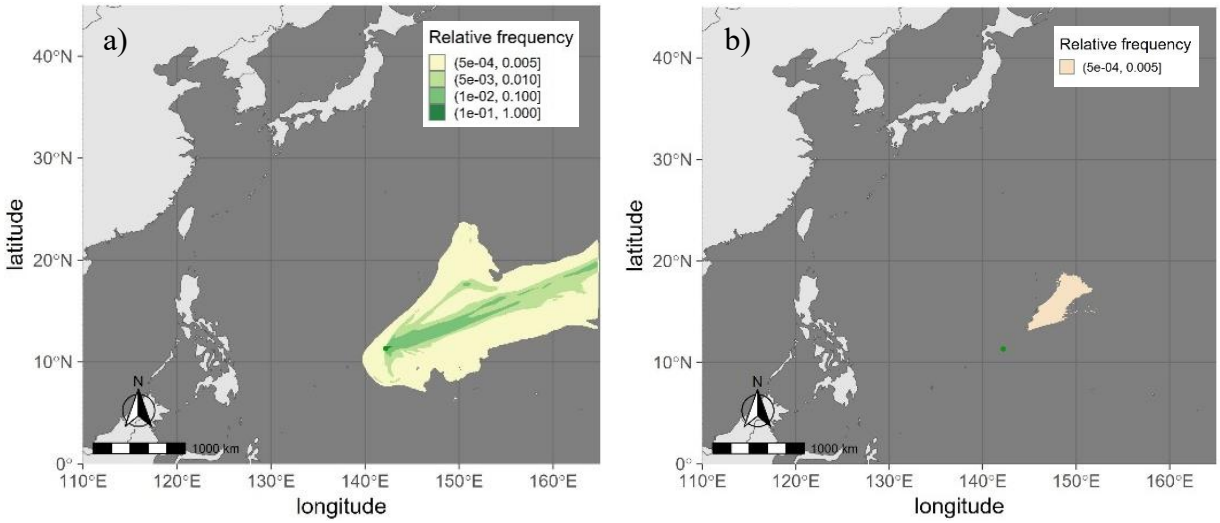

Figure 5.58 One month simulation about the remote area. The green point represents the receptor point. a) Particles travelling inside the PBL, b) particles travelling above the PBL.

For the remote area it is evident that the signal about the particles travelling inside the PBL is only related to the atmospheric transport over the Ocean since it comes from the East and North-East direction, thus travelling only over the North Pacific Ocean. The graphs show that in this case, given the lower and generally constant height of the PBL, which are characteristic of the marine boundary layer, the particles that arrive at the receptor have been travelling for much longer distances inside the PBL than in the other cases studied in this work (i.e. Tibet case study). For the particles travelling above the PBL instead, the signal is found to be very low and at a certain distance from the receptor, indicating some weak entrainment between the free atmosphere and the PBL (from Figure 5.56 to Figure 5.58).

Distribution graphs:

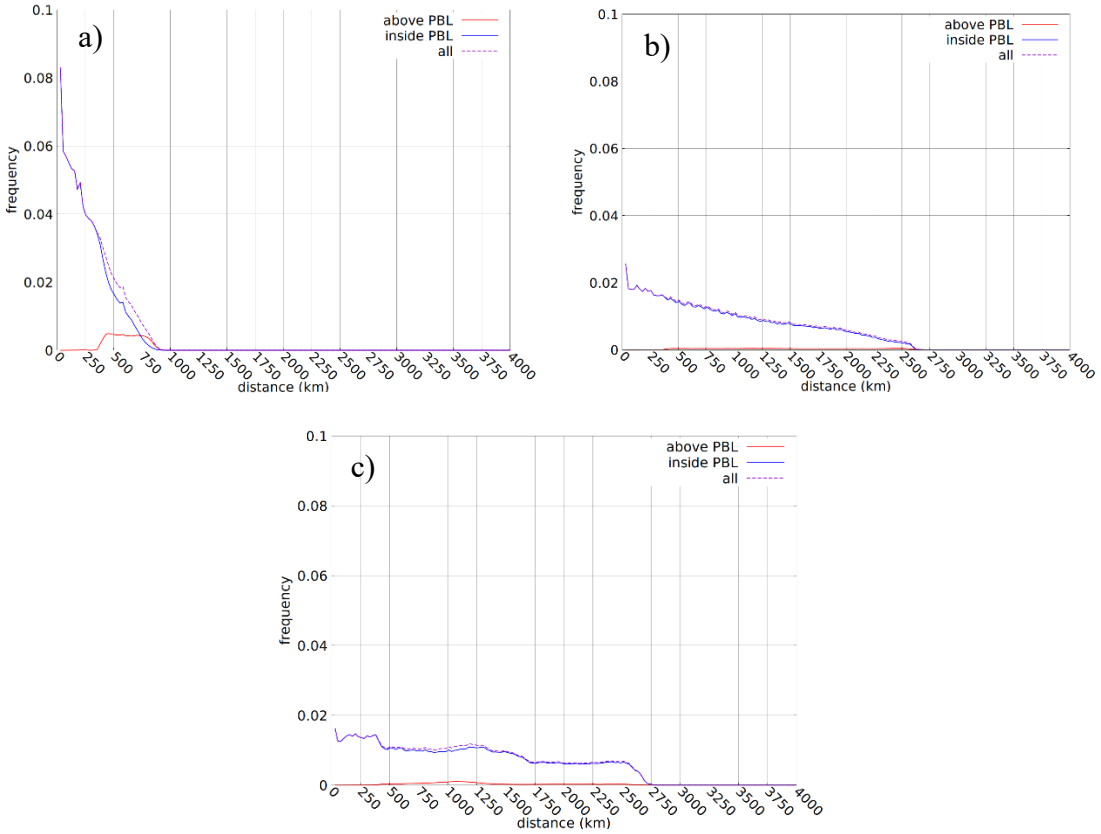

Figure 5.59 Distribuiton graphs for the remote area. a) two days simulation, b) one week simulation, c) one month simulation.

The distribution graphs of the relative frequency of the trajectory number as regards the remote area show that for the two-days simulation (Figure 5.59a) the particles travelling inside the PBL can reach around 750 km, while for the two-weeks (Figure 5.59b) and one-month (Figure 5.59c) simulations the travelled distance is around 2500 and 2750 km. For the particles travelling above the PBL the distribution graphs confirm the weak signal already noticed in the contour plots.

Comments

The reference article of Liu et al. (2019) wanted to study the continental atmospheric transport to the Ocean. With the simulations done in this work, it is found that the continental influence for the transport of pollutants is relevant in the investigation of the coastal area. For the pelagic area, represented with a starting point for the backward simulations that is about 1200 km far from the point indicating the coastal area, and even more for the remote area, represented with a starting point for the backward simulations that is about 1700 km far from the point representing the pelagic area, it is found that the signal comes mainly or totally from the Pacific Ocean and following an East and North-East direction. This is particularly interesting since in the preliminary study of the scientific

articles about MP atmospheric transport described in Section 3, an article about the possibility of considering the Pacific Ocean as a source of atmospheric MPs was examined (Shaw et al., 2023). In this article the emission of MPs from the Ocean to the atmosphere is estimated and from their results two areas of the Pacific Ocean can be identified as characterised by particularly high emissions. One of these two zones is in the same direction of provenience of the signal found for the particles travelling inside the PBL in the remote area simulation. This suggests that MPs emitted from the Ocean to the atmosphere in the East part of the North Pacific Ocean could be transported by the masses of air travelling over it in the south-western direction and possibly reaching and being deposited in the mentioned areas of this paragraph indicated as pelagic and remote one. From a larger perspective this consideration leads to think that a possible cycle of MPs from the Ocean and to the Ocean itself is possible.

5.3. Pacific Ocean (forward simulation)

The simulations performed in this paragraph aim to investigate a possible circulation of masses of air over the Ocean, in particularly focusing on the possibility of the transport of MPs emitted by the Ocean itself. A backward and a forward simulation are performed with a duration of a month and a half between the month of November and December (Section 3.2). As output, for each of the two simulations, the three contour plots and the distribution graphs are obtained. Considering the wide area chosen for the domain of the simulation and the topographical homogeneity of the Ocean, it is chosen to use the 0.5°x0.5° for the spatial resolution of the input data, and a number of 40 time steps, corresponding to 2160 *s* each one.

Backward simulation

The backward simulation as regards the remote area of the previous paragraph is here performed again in a wider domain to see the complete signal and also extending the simulation time from one month to about a month and a half. The resulting contour plots are reported in Figure 5.60, Figure 5.61, Figure 5.62, and the resulting distribution graph in Figure 5.63.

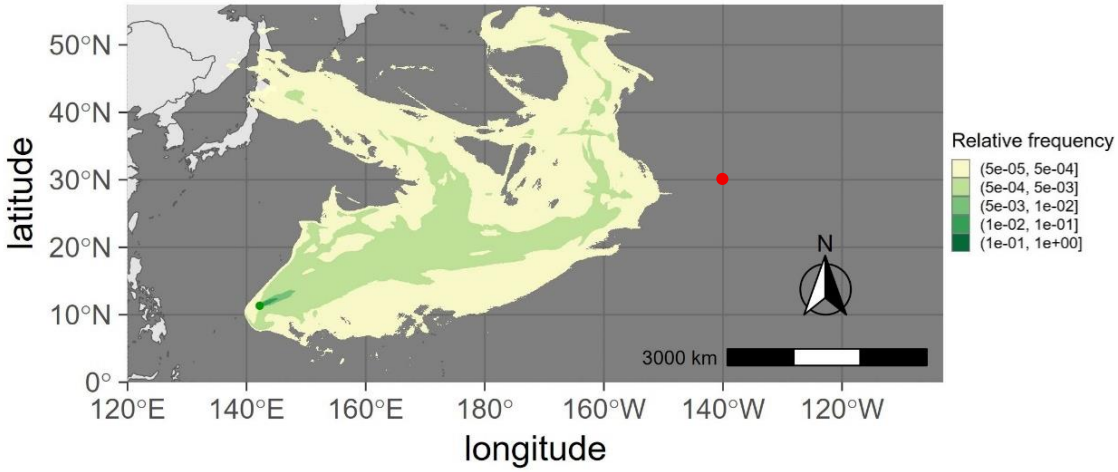

Figure 5.60 Backward simulation about the particles travelling inside the PBL performed from the point belonging to the remote area described in the previous paragraph. The green point represents the receptor, and the red point represents the possible source point of MPs.

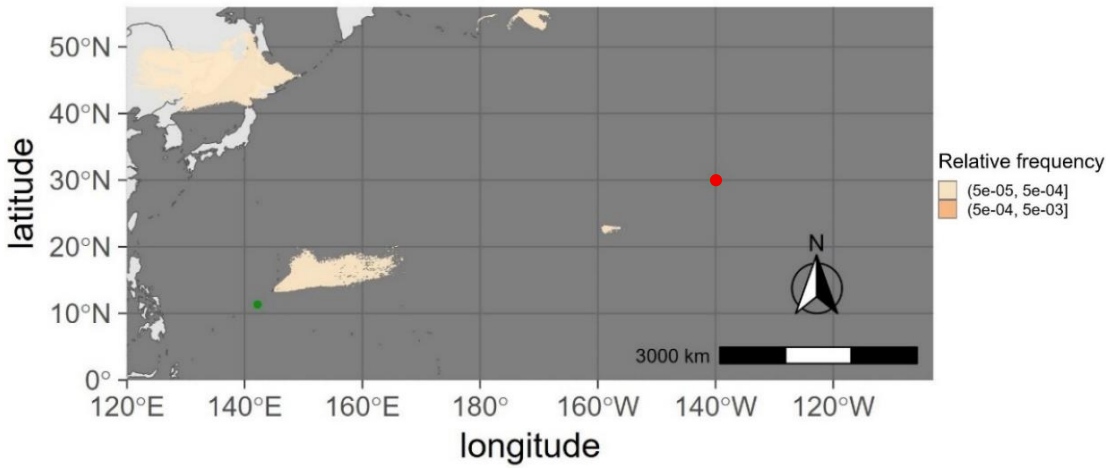

Figure 5.61 Same of Figure 5.60 for particles travelling above the PBL.

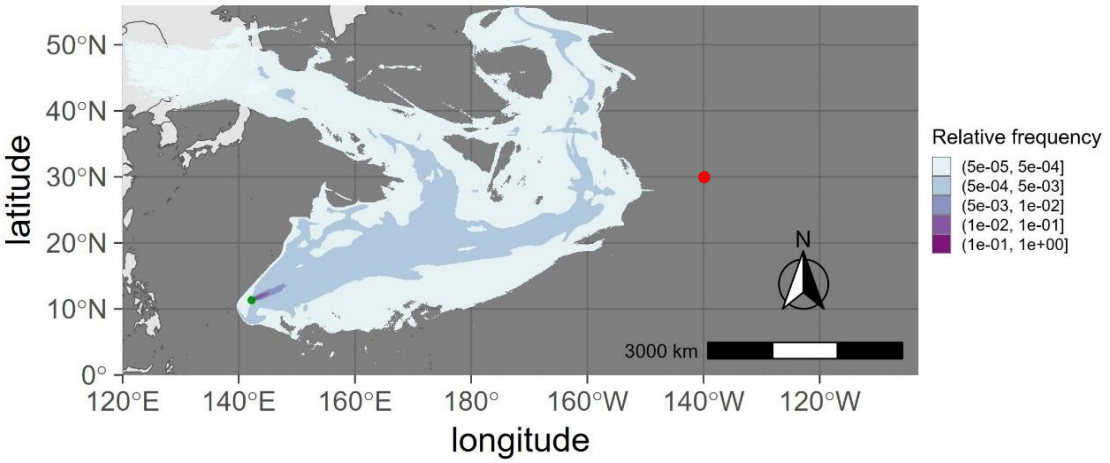

Figure 5.62 Same of Figure 5.60 for all particles travelling both above and inside the PBL

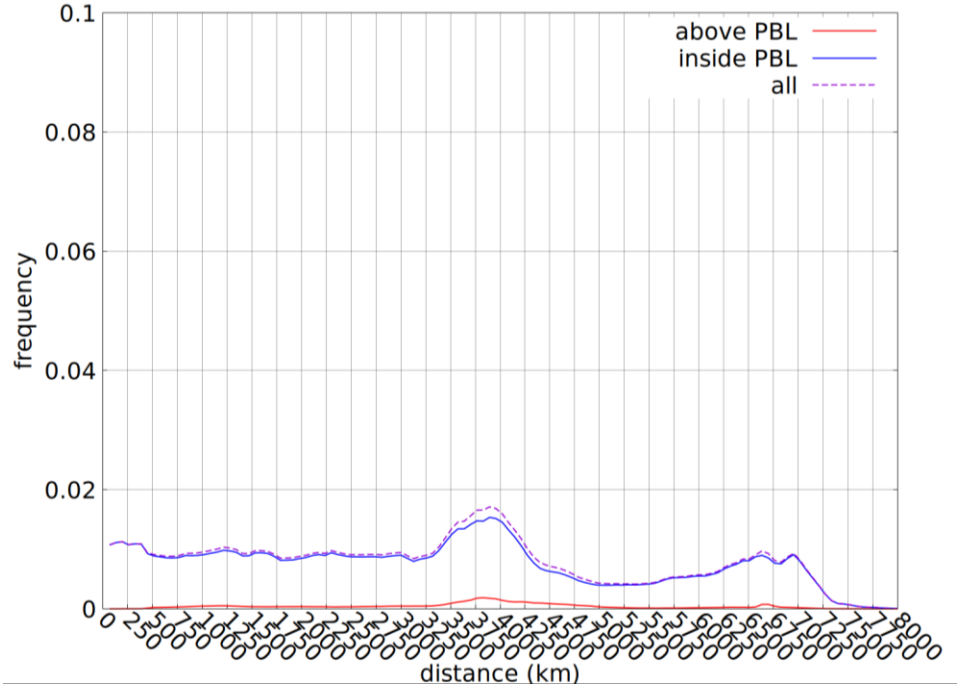

Figure 5.63 Distribution graph of the backward simulation performed from the point belonging to the remote area described in the previous paragraph.

Forward simulation

The forward simulation is now performed to verify if the signal found in this case is consistent with the one of the previous backward simulation, and also to verify if the source and the receptor points can be linked from the atmospheric transport as suggested previously. The resulting contour plots are reported in Figure 5.64, Figure 5.65, Figure 5.66, and the resulting distribution graph in Figure 5.67.

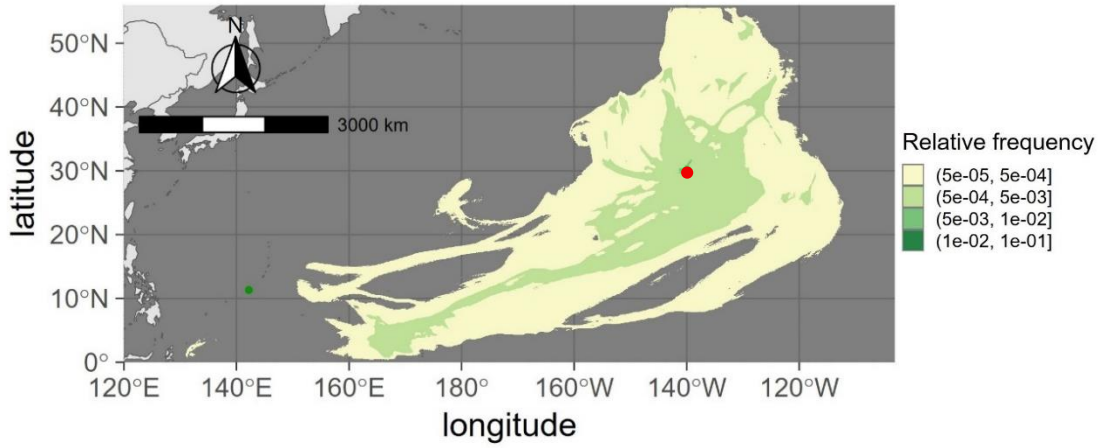

Figure 5.64 Forward simulation about the particles travelling inside the PBL performed from the point assumed as possible source of MPs. The red point represents the possible source, the green point represents the receptor.

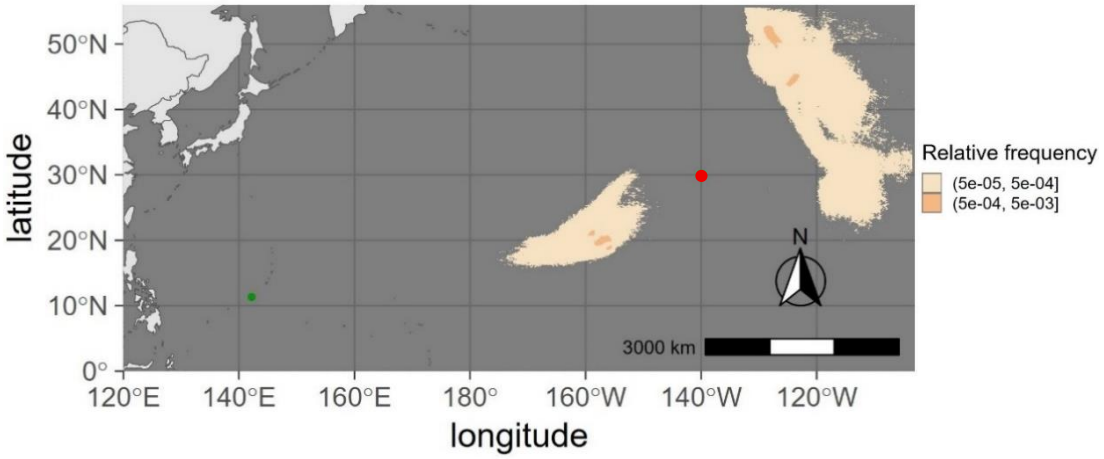

Figure 5.65 Forward simulation about the particles travelling above the PBL performed from the point assumed as possible source of MPs. The red point represents the possible source, the green point represents the receptor.

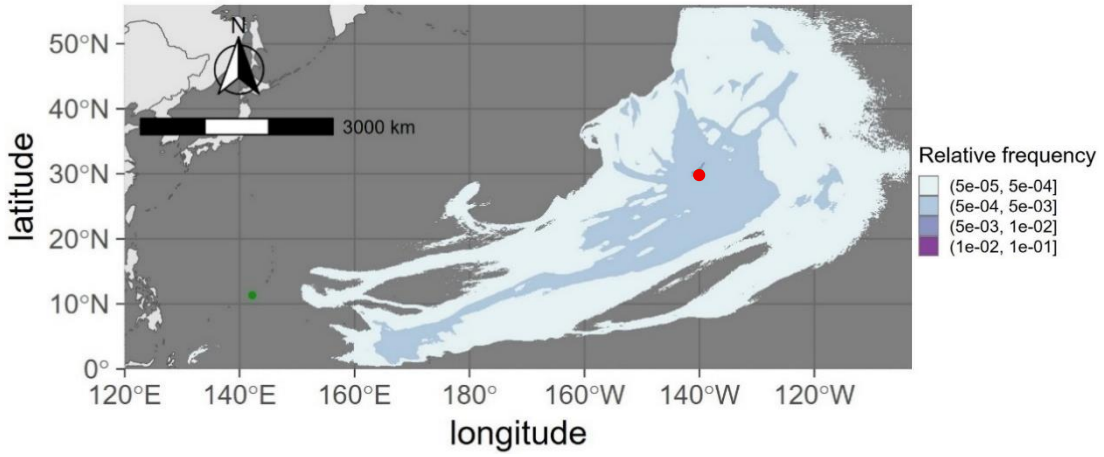

Figure 5.66 Forward simulation about all the particles travelling both above and inside the PBL performed from the point assumed as possible source of MPs. The red point represents the possible source, the green point represents the receptor.

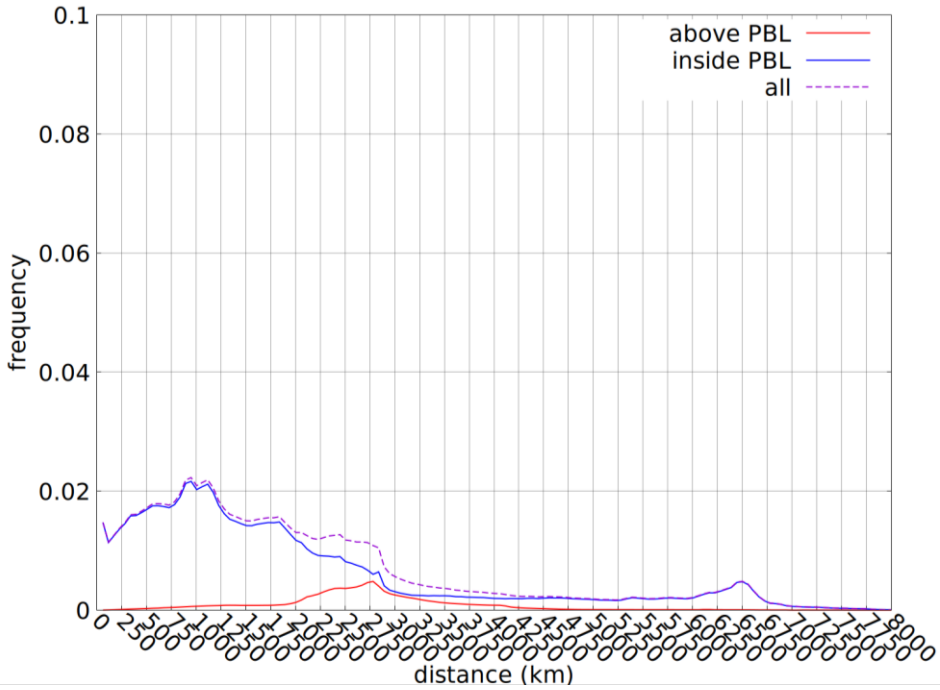

Figure 5.67 Distribution graph of the forward simulation performed from the point in the North Pacific Ocean assumed as possible source of MPs.

Comments

Considering the output of the contour plots, it can be seen that in the one month and a half period of the backward and forward simulations, most of the trajectories do not reach the source in the first case (from Figure 5.60 to Figure 5.62) and do not reach the receptor in the second one (from Figure 5.64 to Figure 5.66). This, even if the direction of transport emerging from these images confirms that the masses of air travelling over the Ocean follow a path that could link the two points, or at least the areas represented by them. From the distribution graphs (Figure 5.63 and Figure 5.67), it is shown that the maximum travelled distance in both cases is about 7000-7500 km, and the distance between the two points in exam is within about 7700 km (Figure 5.68).

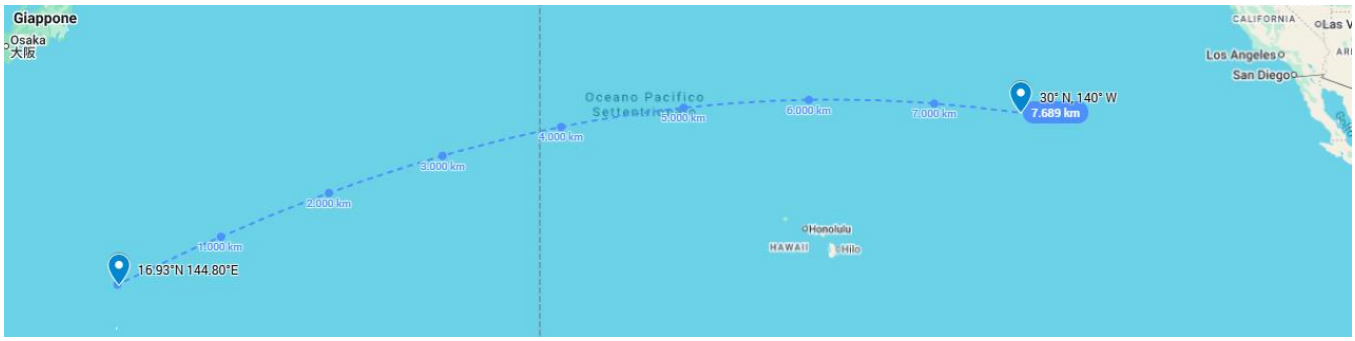

Figure 5.68 Representation of the distance of the source and receptor points (Source: Google – My maps).

However, even if from these results it seems that the masses of air travelling over the investigated area of the North Pacific Ocean do not precisely link the two points, the distance travelled over it results to be long enough to validate the assumption for which there could be a circulation of MPs emitted by the North Pacific Ocean in its East side, that are transported westwards over it, and maybe deposited on its West side. So, these results may support the hypothesis for which the Ocean could represent a source of MPs for itself. A last investigation can be done to further deepen the possibility of the masses of air travelling over the Ocean to connect the source and receptor points. From the output of the MILORD model simulations of this paragraph, it is possible to obtain the images of the particle plume development, representing in this way the distribution of the particles in the

investigated area, and not the normalized number of trajectories. Below are reported some frames of the forward simulation about the particles travelling over the area of investigation (from Figure 5.69 to Figure 5.75), and in particular Figure 5.73 and Figure 5.74 show as a certain number of the particles emitted from the source point in the Ocean travel over it and can actually reach the receptor point. With these images, that are in this case obtained every 12 hours and for the whole period of the simulation, but that can be generated with a minimal frequency equal to the time step, it is also possible to realize an animation to visualize the development of the particle plume over time.

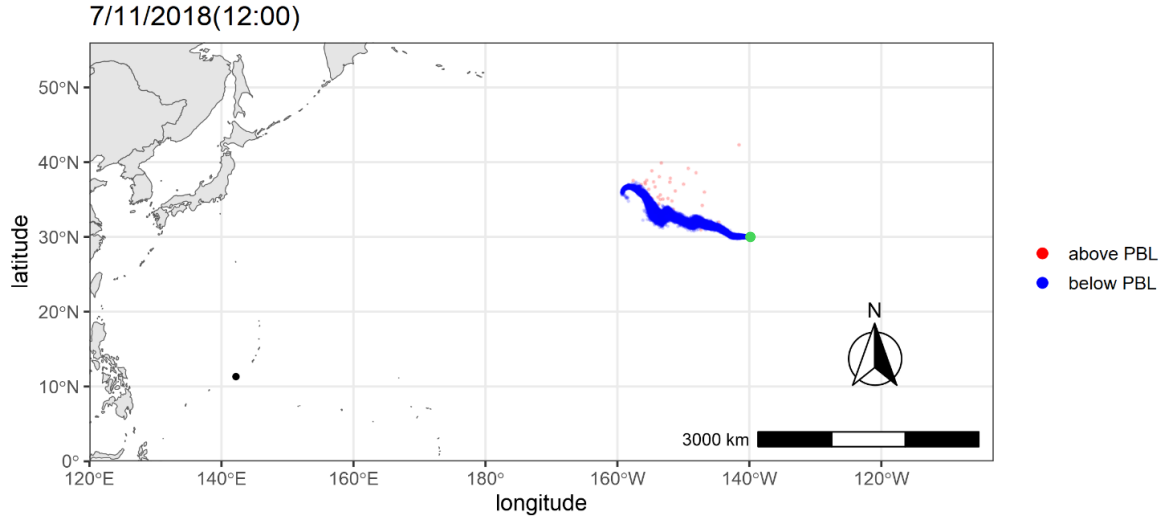

Figure 5.69 Image representing the particles distribution over the Ocean for the 7^{th} of November at 12:00 a.m., the black point represent the receptor point, the green point represents the source point.

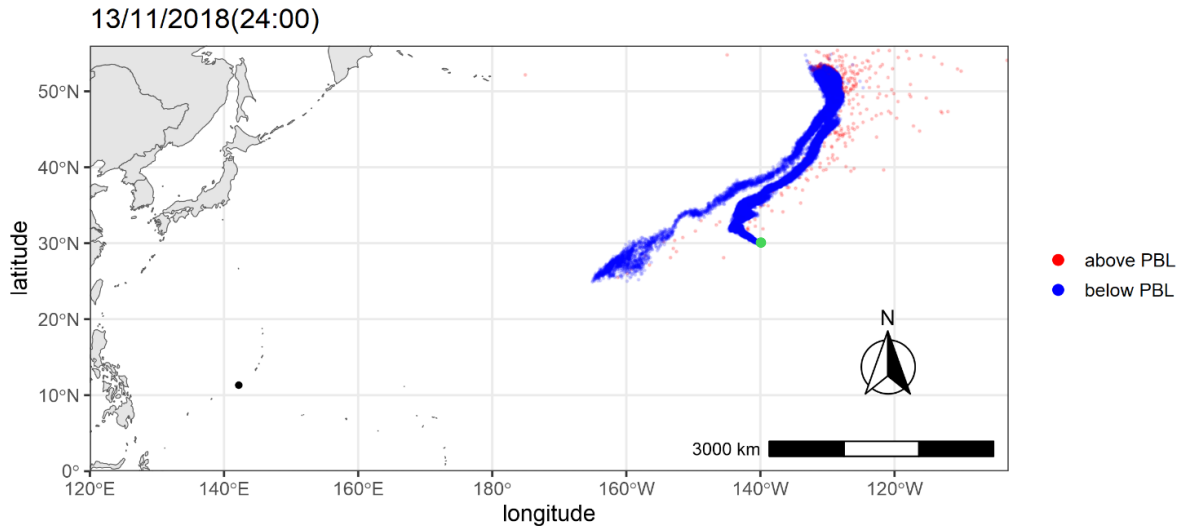

Figure 5.70 Image representing the particles distribution over the Ocean for the 13^{th} of November at 00:00 a.m., the black point represent the receptor point, the green point represents the source point.

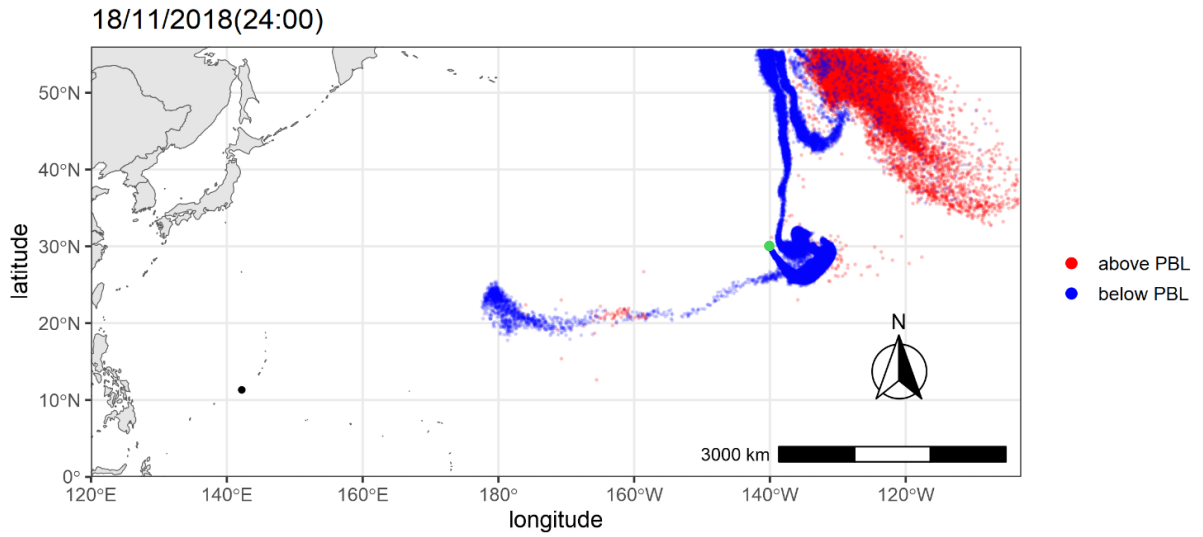

Figure 5.71 Image representing the particles distribution over the Ocean for the 18^{th} of November at 00:00 a.m., the black point represent the receptor point, the green point represents the source point.

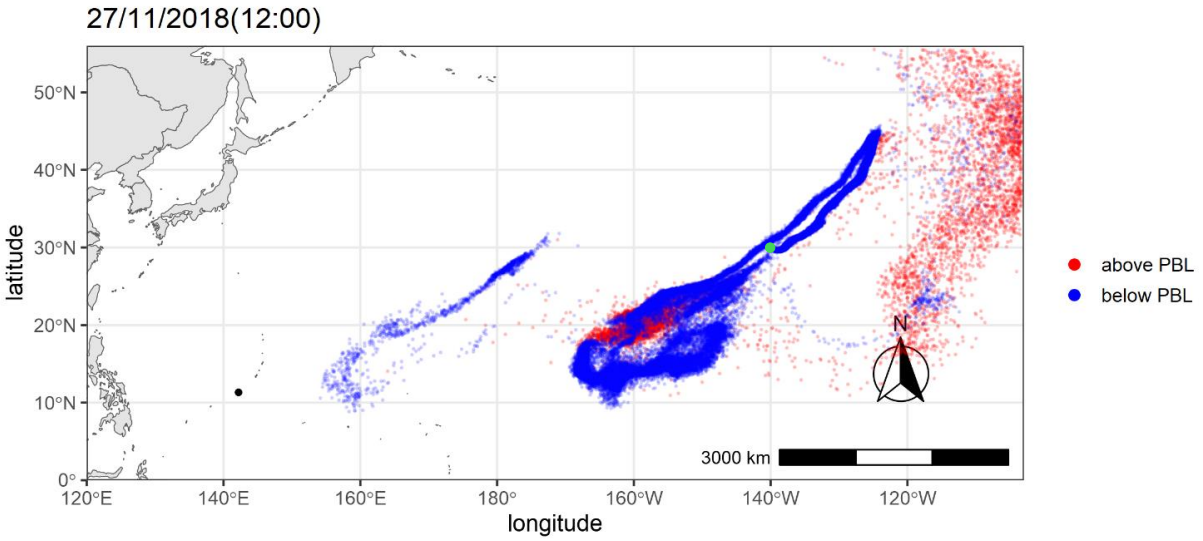

Figure 5.72 Image representing the particles distribution over the Ocean for the 27^{th} of November at 12:00 a.m., the black point represent the receptor point, the green point represents the source point.

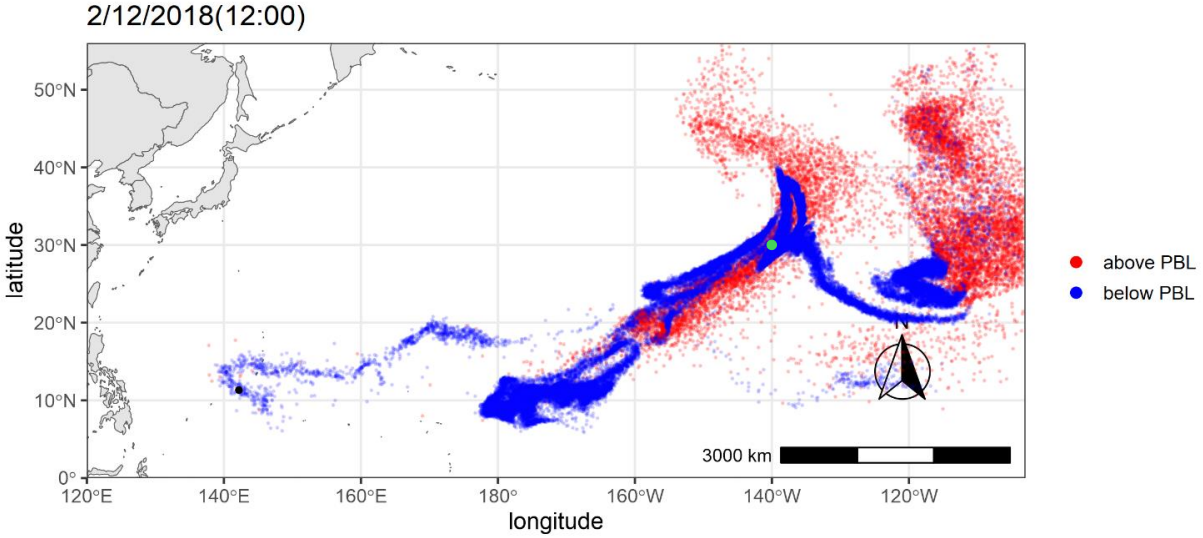

Figure 5.73 Image representing the particles distribution over the Ocean for the 2^{nd} of December at 12:00 a.m., the black point represent the receptor point, the green point represents the source point.

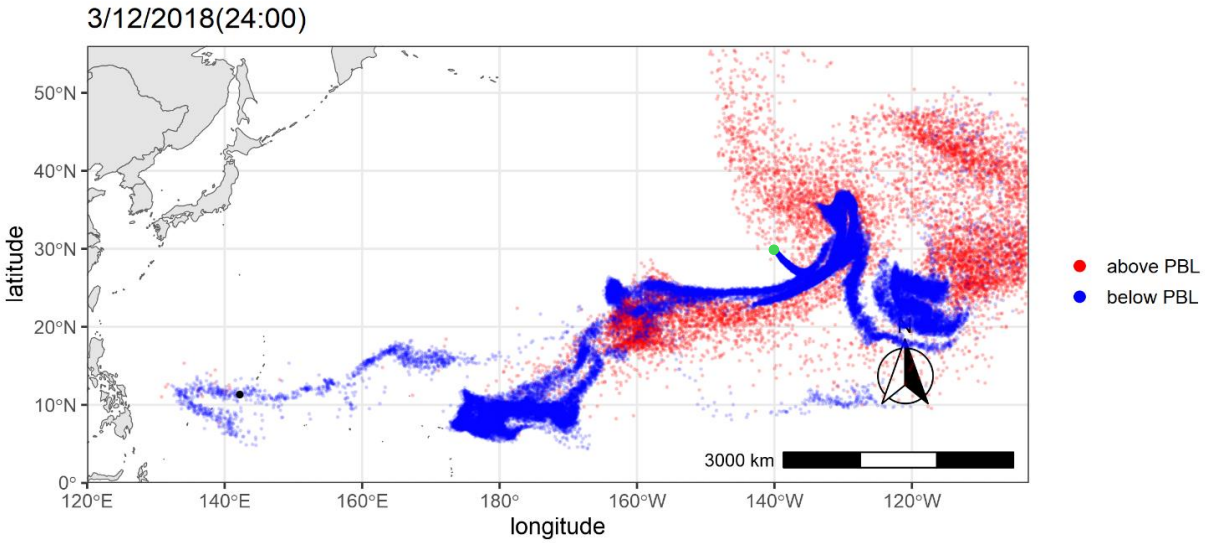

Figure 5.74 Image representing the particles distribution over the Ocean for the 3^{rd} of December at 00:00 a.m., the black point represent the receptor point, the green point represents the source point.

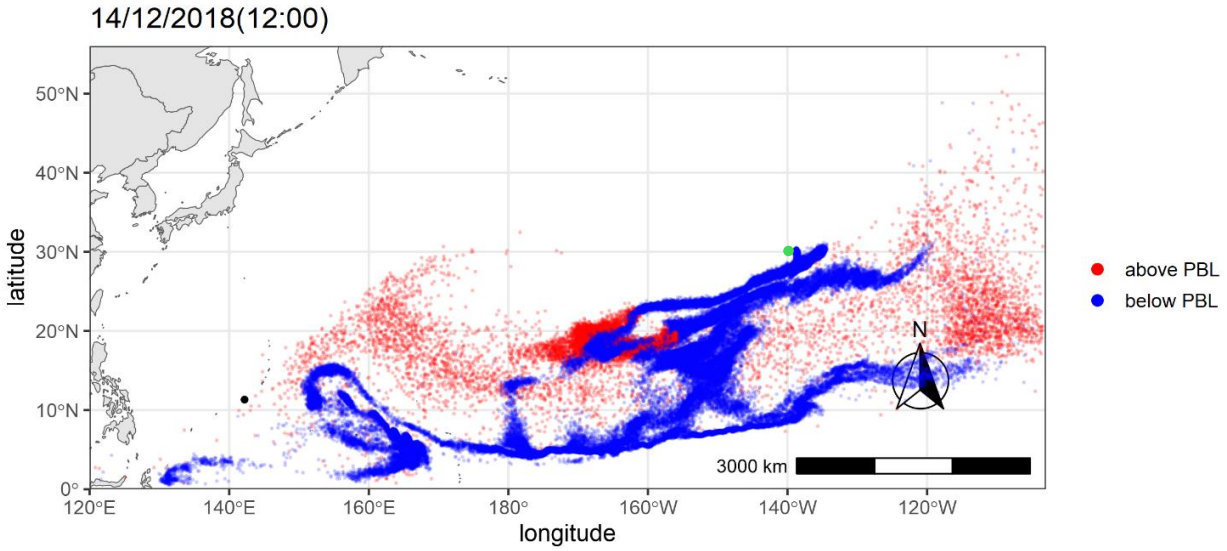

Figure 5.75 Image representing the particles distribution over the Ocean for the 14^{th} of December at 12:00 a.m., the black point represent the receptor point, the green point represents the source point.

6. Final considerations

The use of the MILORD model enabled the study of the transport and dispersion of microplastics in the atmosphere, and specifically, in the present work, it has been applied for the study of more remote regions than those previously investigated with this model. The considered areas are the Tibetan Plateau and the North Pacific Ocean, two regions that are topographically very different from each other, very complex and heterogeneous in the first case and homogeneous in the second one. In such remote places, it has been possible to investigate the provenience of the air masses and the travelled distance of the microplastics, represented by the model with computational Lagrangian particles, by performing backward trajectories simulations in different periods of the year and for different durations of simulations. Besides the long-range transport, it has been possible to study the dispersion also at short-range, thanks to the grid-free approach in the Lagrangian modelling.

The study of two areas characterised by such topographical differences allows for some general comparisons. In the case of the Tibetan Plateau, for all three studied glaciers and the duration of the simulation of one month, most of the particles travelling inside the PBL come from less than 500 km. In the case of the Ocean, instead, for the same duration of the simulation, the particles travel for distances that are much longer (over 2000 km), and that increase moving from the coast to the open ocean. Even the results about the particles travelling above the PBL in the two areas are very different. In the Tibetan Plateau area, the trajectory number of the particles above the PBL is always higher than the one of the particles inside it, and the distances travelled by these particles is always more than 2500 km, reaching maximum values of about 3500-37500 km, always given the duration of the simulation of one month and the extension of the simulation domain. For the Ocean, the contribution of these particles is significant when close to the coast, and it is mostly connected to air masses coming from the continent. When farther from the coast, the signal is weak and in almost all cases it does not directly reach the receptor, and if some particles above the PBL are detected, they enter the PBL before reaching it. So here, the situation is the opposite, given that the relative frequency of the trajectory number, and so the trajectory number itself, is higher for the particles travelling inside the PBL for almost all the simulations done in this area. In general, it can be stated that the PBL over the Ocean generally maintains a constant value of its height, and so, the particles emitted in it, scarcely pass to the free atmosphere, since for that it is necessary that the PBL height changes during the motion of the particles along their path. Instead, over land, and in this particular case over the Tibetan Plateau area, the PBL height changes following the orography and the diurnal variation. Therefore, the exchange of particles between the PBL and the free atmosphere is more efficient. These behaviours depend of course on how the model handles the particle dispersion, even in its simplified parameterisation of the PBL structure. The backward simulations are thus able to reproduce what can be expected for the exchange of air masses, and their tracer content, between the PBL and the free atmosphere, more effective in case of convective conditions, which are typical over land. This, also considering that the pollutant collected at the surface (and retro-released from the receptor in case of backward simulations) resides inside the PBL and can hardly be arriving there directly from the free atmosphere, unless strong vertical convection occurs or when precipitation (not considered here) plays a role.

Another interesting aspect deepened in this study is the fact that the Ocean could represent a source of microplastic emission for itself, since previous studies indicated that it can be responsible of the release of microplastics to the above atmosphere. From the simulations of this work, it has been seen that the masses of air travel over the North Pacific Ocean from its north-eastern part to its south-western one. The results support the potential of the identified areas of microplastic emission (Shaw et al., 2023) to be a source of the microplastic concentration.

As for the elaboration of the outputs, notice that the values of the relative frequency reported in the graphs provide useful information about the provenience and distance travelled by most of the particles, also allowing for comparisons between different areas of the Earth. At the same time, a way to supply on the plots more quantitative information about the number of particles travelling, and

without losing the comparability between the different investigated areas, has not yet been found. To date, work is being done to improve this aspect.
The study of the atmospheric transport of microplastics is an emerging topic, and for this reason, there is still a lack of quantitative measurements of established quality. Deposition measurements to detect the presence of microplastics and their concentration have been done in different studies (as in Wang et al., 2024), but the problem of this kind of sample collection is that it is difficult to know exactly when the collected microplastics have been deposited, and so to investigate their provenience. This, unless the samples are taken during or soon after a deposition event, as it was done in the sampling campaign in Aves et al. (2022). In addition, also measurements of microplastic concentrations in air have been done (as in Liu et al., 2019), with the advantage in this case that there is the certainty of studying particles that have arrived close to the sampling time. For this reason, and to have the possibility of doing more detailed studies also from the quantitative point of view, further studies and the collection of further data would be valuable.
In this context, the numerical models are proved to be useful, when not essential, to advance the understanding of the presence and dispersion of microplastics in the atmosphere, and the role of this last in the exchange between the other environmental compartments, land and seas.

7. Bibliography

Anfossi, D., Sacchetti, D. (1994). Transport of volcano Etna emissions towards the alpine region using ECMWF data. *Il Nuovo Cimento*, 17 C, 473-484. https://doi.org/10.1007/BF02506732.

Anfossi, D., Sacchetti, D., Trini Castelli, S. (1995). Development and sensitivity analysis of a Lagrangian particle model for long range dispersion. *Environmental Software*, Vol. 10, No. 4, pp. 263-287. https://doi.org/10.1016/0266-9838(95)00001-1.

Anfossi, D., Trini Castelli, S. (2009). An Outline of Lagrangian Stochastic Dispersion Models. In *Air Pollution and Turbulence* (pp 203-231). CRC Press.

Anfossi, D., Physick, W. (2004). Lagrangian Particle Models. Chapter 11 of *AIR QUALITY MODELING – Theories, Methodologies, Computational Techniques, and Available Databases and Software*. Vol. II – Advanced Topics (P. Zannetti, Editor). Published by The EnviroComp Institute (http://www.envirocomp.org/) and the Air & Waste Management Association (http://www.awma.org/).

Aves, A. R., Revell, L. E., Gaw, S., Ruffell, H., Schuddeboom, A., Wotherspoon, N. E., LaRue, M., and McDonald, A. J. (2022). First evidence of microplastics in Antarctic snow, *The Cryosphere*, 16, 2127–2145. https://doi.org/10.5194/tc-16-2127-2022.

Bergmann, M., Mützel, S., Primpke, S., Tekman, M. B., Trachsel, J., Gerdts, G. (2019). White and wonderful? Microplastics prevail in snow from the Alps to the Arctic. *Sci. Adv*. 5, eaax1157. https://doi.org/10.1126/sciadv.aax1157.

Bergmann, M., Collard, F., Fabres, J., Gabrielsen, W. G., Provencher, J. F., Rochman, C. M., van Sebille, E., Tekman, M. B. (2022). Plastic pollution in the Arctic. *Nat Rev Earth Environ* 3, 323–337. https://doi.org/10.1038/s43017-022-00279-8.

Boetti, M., Castelli, S. T., Ferrero, E. (2018). Reviving MILORD Long-Range Model for Simulating the Dispersion of the Release during Fukushima Nuclear Power Plant Accident. In: Mensink, C., Kallos, G. (eds) Air Pollution Modeling and its Application XXV. ITM 2016. *Springer Proceedings in Complexity*. Springer, Cham. https://doi.org/10.1007/978-3-319-57645-9_61.

Chen, P., Kang, S., Tripathee, L., Ram, K., Rupakheti, M., Panday, A. K., Zhang, Q., Guo, J., Wang, X., Pu, T., & Li, C. (2020). Light absorption properties of elemental carbon (EC) and water-soluble brown carbon (WS–BrC) in the Kathmandu Valley, Nepal: A 5-year study. *Environmental Pollution*, 261. https://doi.org/10.1016/j.envpol.2020.114239.

Deike, L., Reichl, B. G., Paulot, F. (2022). A mechanistic sea spray generation function based on the sea state and the physics of bubble bursting. *AGU Advances*, 3, e2022AV000750. https://doi.org/10.1029/2022AV000750.

Desiato, F. (1992). A long-range dispersion model evaluation study with chernobyl data. *Atmospheric Environment*. Part A. General Topics 26, 2805–2820.

Draxler, R. R., Hess, G. D. (1998): An overview of the HYSPLIT_4 modeling system for trajectories, dispersion, and deposition. *Aust. Meteor. Mag*., 47, 295–308.

Ferrarese, S., Trini Castelli, S. (2019). Detection of CO2 source areas using two Lagrangian particle dispersion models, at regional scale and long range. Proceedings of the 19th International Conference on Harmonisation Within Atmospheric Dispersion Modelling for Regulatory Purposes, *Harmo 2019*, p. 5. https://www.harmo.org/Conferences/Proceedings/_Bruges/publishedSections/H19-038 Silvia Trini Castelli.pdf.

Kaandorp, M. L. A., Lobelle, D., Kehl, C., Dijkstra, H. A., van Sebille, E. (2023). Global mass of buoyant marine plastics dominated by large long-lived debris. *Nat. Geosci.* 16, 689–694. https://doi.org/10.1038/s41561-023-01216-0.

Lin, J. C. (2012). Lagrangian modeling of the atmosphre: An introduction. Geophysical Monograph Series, 200, 1–11. https://doi.org/10.1029/2012GM001376.

Liu, K., Wu, T., Wang, X., Song, Z., Zong, C., Wei, N., Li, D. (2019). Consistent transport of terrestrial microplastics to the ocean through atmosphere, *Environ. Sci. Technol*., 53, 10612–10619. https://doi.org/10.1021/acs.est.9b03427.

Martina, M., Trini Castelli, S. (2023). Modelling the potential long-range dispersion of atmospheric microplastics reaching a remote site. *Atmospheric Environment* 312, 120044. https://doi.org/10.1016/j.atmosenv.2023.120044.

Musso, M. M. (2025). *Study and assessment of the dispersion of microplastics in the atmosphere through numerical modelling* [Tesi di dottorato]. Università di Torino, Torino, Italia.

Obukhov, A. M. (1959). Description of turbulence in terms of Lagrangian variables. *Adv. Geophys.*, 6, 113-116. https://doi.org/10.1016/S0065-2687(08)60098-9.

Reap, R. M. (1972). An operational three-dimensional trajectory model. Journal of Applied Meteorology and Climatology 11, 1193–1202.

Rosal, R. (2021). Morphological description of microplastic particles for environmental fate studies. In Marine Pollution Bulletin (Vol. 171). Elsevier Ltd. https://doi.org/10.1016/j.marpolbul.2021.112716.

Seifried, T. M., Nikkho, S., Morales Murillo, A., Andrew, L. J., Grant, E. R., & Bertram, A. K. (2024). Microplastic Particles Contain Ice Nucleation Sites That Can Be Inhibited by Atmospheric Aging. Environmental Science and Technology. https://doi.org/10.1021/acs.est.4c02639.

Shaw, D. B., Li, Q., Nunes, J. K., & Deike, L. (2023). Ocean emission of microplastic. *PNAS Nexus*, 2(10). https://doi.org/10.1093/pnasnexus/pgad296.

Smith, F.B. (1968). Conditional particle motion in a homogeneous turbulent field. *Atmospheric Environment*, 2, 491-508. https://doi.org/10.1016/0004-6981(68)90042-5.

Stein, A. F., Draxler, R. R., Rolph, G. D., Stunder, B. J. B., Cohen, M. D., Ngan, F., Stein, A. (2015). NOAA's HYSPLIT atmospheric transport and dispersion modeling system. *Bulletin of the American Meteorological Society* 96, 2059–2077. https://doi.org/10.1175/BAMS-D-14-00110.1.

Thomson, D. J. (1987). Criteria for the selection of stochastic models of particle trajectories in turbulent flows. *J. Fluid Mech.*, 180, 529-556. https://doi.org/10.1017/S0022112087001940.

Trini Castelli, S. (2021). The Lagrangian Approach to Dispersion Modeling: Why We Like It (and What We Did with It). In: Mensink, C., Matthias, V. (eds) Air Pollution Modeling and its Application XXVII. ITM 2019. *Springer Proceedings in Complexity*. Springer, Berlin, Heidelberg. https://doi.org/10.1007/978-3-662-63760-9_31.

Trini Castelli, S. (2012). MILORD - reload. Model for the Investigation of Long Range Dispersion. Internal Report ISAC-TO/02-2012, 10 September 2012, pages 28.

Wang, Z., Kang, S., Zhang, Y., Luo, X., Kang, Q., Chen, P., Guo, J., Hu, Z., Yang, Z., Zheng, H., Gao, T., Yang, W. (2024). Microplastics in glaciers of Tibetan Plateau: Characteristics and potential sources. *Science of The Total Environment* 954, 176370. https://doi.org/10.1016/j.scitotenv.2024.176370.

Ziero, S. (2025). *Study of the dispersion of microplastics in the atmosphere with Lagrangian models* [Tesi di laurea magistrale]. Università di Torino, Torino, Italia.

Zhang, Y., Gao, T., Kang, S., Allen, S., Luo, X., Allen, D. (2021). Microplastics in glaciers of the tibetan plateau: evidence for the long-range transport of microplastics. *Science of The Total Environment* 758, 143634. https://doi.org/10.1016/j.scitotenv.2020.143634.

8. Acknowledgments

A final acknowledgment is due to the CNR – ISAC of Turin for hosting me during the period of my thesis work and for providing me with the computational resources used for this study.

Appendix 1

Plastic and microplastic polymers

Following the recycling codes, plastic materials are classified in seven typologies.

Table 6. Name and common application of the seven tipologies of plastic for the recycle

Class Code	Name	Most common application
1	Polyethylene Terephtalate (PETE)	Water bottles, containers for food, fibers for clothing
2	High-Density Polyethylene (HDPE)	Detergent containers, plastic bottles, piping for water
3	Polyvinyl Chloride (PVC)	Window frames, electric cable insulation
4	Low-Density Polyethylene (LDPE)	Shopping bags, clear food containers
5	Polypropylene (PP)	Food containers, medical devices
6	Polystyrene or Styrofoam (PS)	CD and DVD cases, single-use disposable cutlery
7	Others	-

List of the typologies of microplastic found in the sampling done in the articles studied in this work. Varnish and rubber are considered even if they are not plastic materials, but since they can release MPs.

Table 7. Tipologies of microplastic found in the sampling done in the articles studied in this work

Typology	Abbreviation
Polyethylene	PE
Polypropylene	PP
Polystyrene	PS
Polyesters	PET
Polyamide	PA
Polyimide	PI
Expanded Polyethylene	EP
Polytetrafluoroethylene	PTFE
Cellulose Propionate	CP
Polymethyl Methacrylate	PMMA
Polyvinyl Chloride	PVC
Polyurethane	PU
Varnish	-
Rubber	-

Microplastic morphologies

MPs can be classified starting from three basic morphologies of MPs: sphere (3D), plate (2D) and rod (1D), (Rosal, 2021). Here are reported the most common types of microplastics morphologies.

Table 8. Classification of microplastics based on their morphology

Morphology	Geometry
Fibers	1D
Filaments	1D
Films	2D

Fragments	3D (irregular shape)
Pellet	3D (irregular shape)
Microbeads	3D (spherical)
Granules	3D (spherical)

Appendix 2

DKMD glacier, June 2021

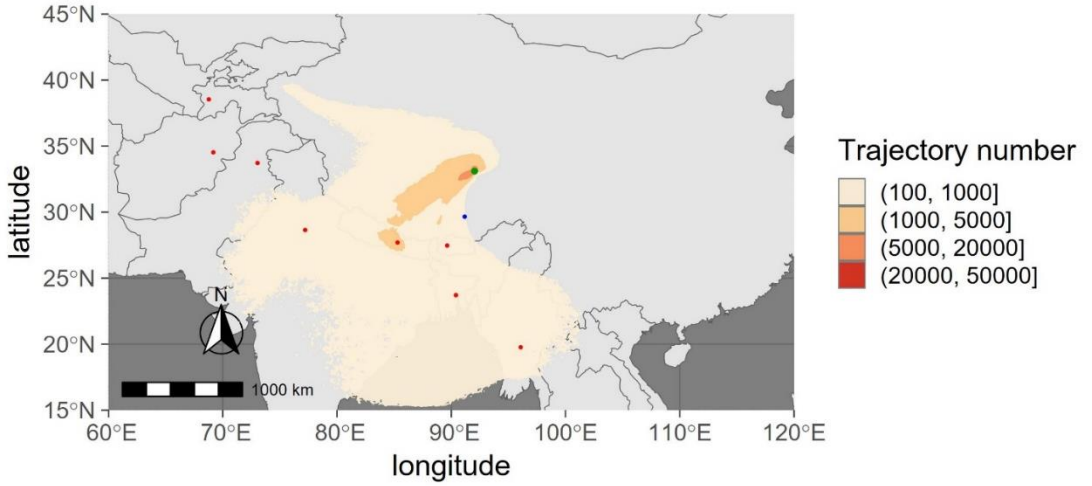

Appendix image 1. Trajectory number of the particles travelling above the PBL for DKMD glacier and June 2021.

DKMD glacier, April 2022

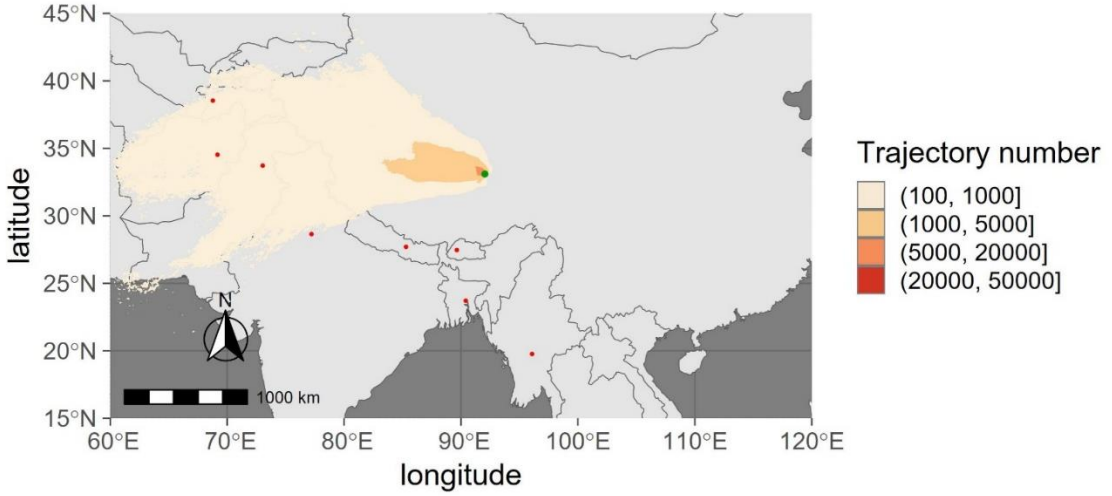

Appendix image 2. Trajectory number of the particles travelling above the PBL for DKMD glacier and April 2022.

KQGR glacier, June 2021

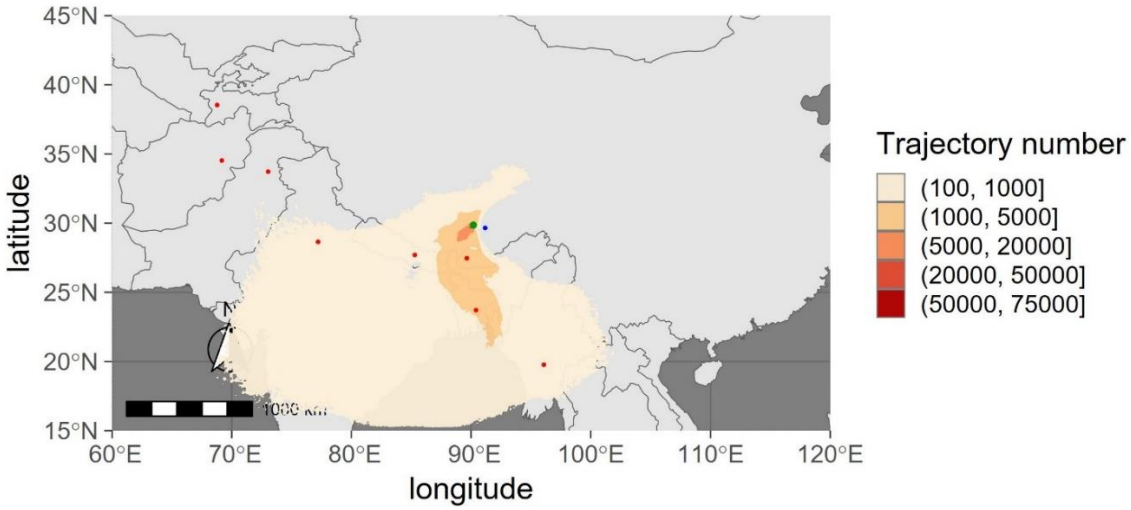

Appendix image 3. Trajectory number of the particles travelling above the PBL for KQGR glacier and June 2021.

KQGR glacier, April 2022

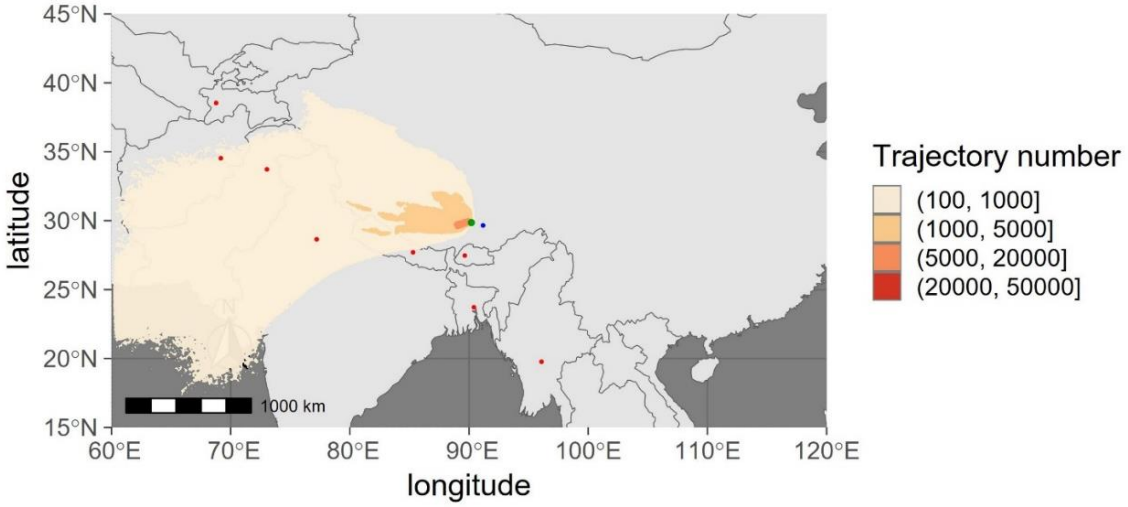

Appendix image 4. Trajectory number of the particles travelling above the PBL for KQGR glacier and April 2022.

AL glacier, June 2021

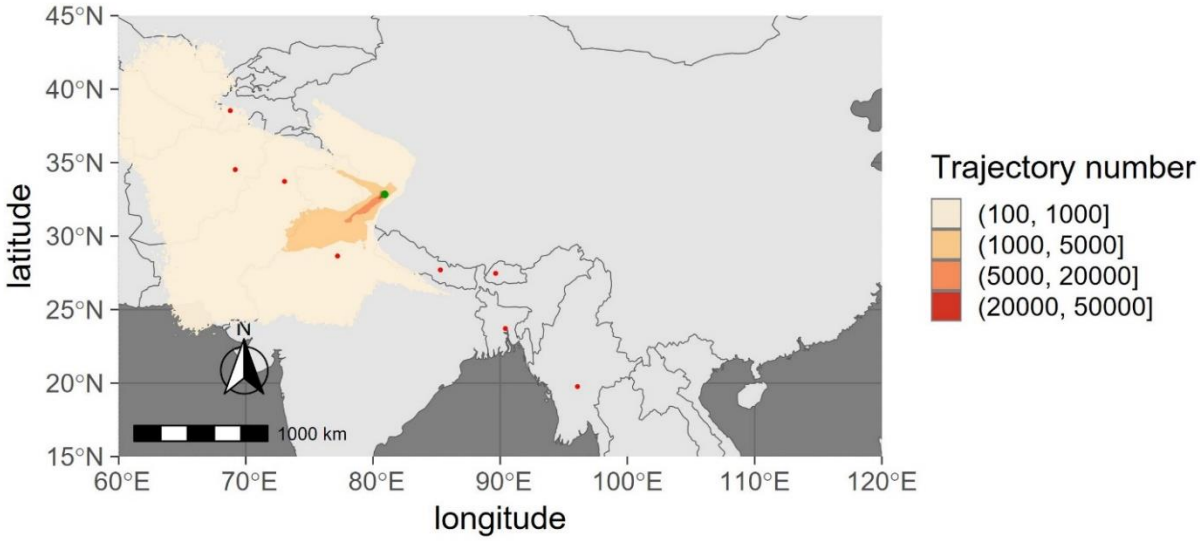

Appendix image 5. Trajectory number of the particles travelling above the PBL for AL glacier and June 2021.

AL glacier, April 2022

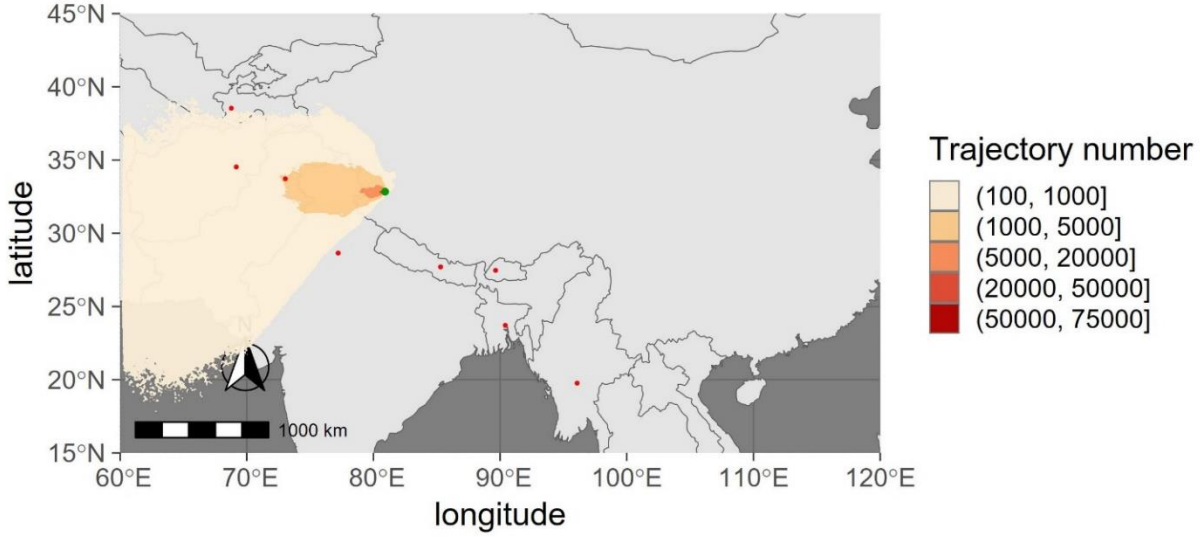

Appendix image 6. Trajectory number of the particles travelling above the PBL for AL glacier and April 2022.

Dichiarazione in merito all'utilizzo di strumenti IA nella redazione delle tesi

Supporto editoriale:
Gli strumenti di IA generativa sono stati utilizzati esclusivamente per il supporto editoriale, come la correzione grammaticale, le traduzioni, i suggerimenti per la parafrasi o il miglioramento della leggibilità.
Perfezionamento delle idee:
Gli strumenti di IA generativa non sono stati utilizzati per il perfezionamento delle idee e il supporto editoriale.
Generazione di contenuti e supporto analitico:
Gli strumenti di IA generativa non sono stati utilizzati per la generazione di contenuti o il supporto analitico.

Indipendentemente dal livello di coinvolgimento dell'IA, tutti i contenuti generati dall'IA sono stati rivisti criticamente, verificati e modificati per allinearsi al rigore accademico. Le citazioni e le argomentazioni sono state verificate in modo indipendente. L'autore si assume la piena responsabilità dell'accuratezza, dell'originalità e dell'integrità del lavoro finale.